DOPAMINERGIC REGULATION OF INSULIN SECRETION FROM THE

PANCREATIC ISLET

By

Alessandro Ustione

Dissertation

Submitted to the Faculty of the

Graduate School of Vanderbilt University

in partial fulfillment of the requirements

for the degree of

DOCTOR OF PHILOSOPHY

in

Molecular Physiology and Biophysics

December, 2012

Nashville, Tennessee

Approved:

Professor Roger Colbran

Professor Kevin Currie

Professor Aurelio Galli

Professor Anne Kenworthy

ACKNOWLEDGMENT

I have always been surrounded by supportive people, in every aspect of my life. My deepest acknowledgment goes to all of them, who contributed to this achievement each one in its own unique way. I could not have been able to earn this doctoral degree if any of them had not been part of this journey.

I thank my mentor Dave Piston, for having always pushed me forward during this scientific endeavor. Whenever I thought I was facing an insurmountable obstacle, he never doubted that I could do it instead. Somehow he knew my potential better than me. He is an exemplar scientist who I deeply admire. Also I am grateful to Roger Colbran, Aurelio Galli, Kevin Currie and Anne Kenworthy for being such a helpful thesis committee.

For all that I learnt in the lab, I thank all the current and previous lab members. Steve Head welcomed me every day with a smile and taught me the very basic of lab-work since the first day I joined the Piston lab. And everyone else made life in the lab such a positive experience: Sylvain, John, Mingming, Suba, Richard, Gert, Chris Easley, Tara, Kurt, JP, Brittany, thanks to all of you. I save a special place for Troy, Chris and Amy as we shared the experience of being graduate student in the Piston lab: we rock!

During these years in Nashville I was lucky to meet so many friends that enriched my life beyond any imagination. Lucia, Concetta, Rita, Tommaso, Stefania, Marco, Francesca, Greg, Michael, Tim, David, Kenny, Zach: you have contributed so much to make these past years in Nashville unforgettable.

And of course I thank my family: my loving parents, Ferdinando and Francesca, and my dearest siblings, Claudia and Sergio. They are the most precious part of me.

ACKNOWLEDGMENT OF SUPPORT

PRIOR PUBLICATIONS

Some of the material included in this thesis has been published. The material described in Chapter II and III was published in *Molecular Endocrinology* (Ustione A, Piston DW 2012, 26(11), 1928-1940). In addition, the material in Chapter IV was published in *The Journal of Neuroscience* (Chang JC *et al.* 2012, 32(26), 8919-8929).

TABLE OF CONTENTS

Chapter

LIST OF TABLES

LIST OF FIGURES

CHAPTER

1. INTRODUCTION

The goal of this work has been to understand the function of dopamine in the context of glucose stimulated insulin secretion (GSIS). Insulin secretion is the natural response of the body to hyperglycemia (1). The secretion of the antagonist hormone glucagon is the response to hypoglycemia (1). The regulated secretion of these two hormones is necessary to maintain glucose homeostasis in healthy individuals. Any impairment in this regulation results in poor glycemic control. Type-2 diabetes is characterized by the loss of glycemic control, and the resulting chronic hyperglycemia damages the capillaries in the body. Untreated type-2 diabetes leads to damages in the retina, in the kidneys, in the peripheral tissues, and in the heart (2).

As a consequence of increased obesity in the population, an increased number of people are expected to develop type-2 diabetes in the next decades. Thus, a big effort is being made at developing new drugs that can better re-establish euglycemia during the early phase of the disease, when insulin replacement is not yet required. From this perspective, it is fundamental to investigate what stimuli other than glucose which can regulate insulin secretion. I focused my study on dopamine. Previous literature showed its role as an inhibitor of insulin secretion, although there was no consensus over its physiological relevance (3, 4). I investigated dopamine synthesis, secretion, and its action on

its specific receptor. The ensemble of results depicts a dopaminergic negative feedback loop acting on insulin secretion. Blocking this dopaminergic feedback increases GSIS. Therefore, it is a potential target for new drugs to improve treatment of type-2 diabetes.

In this chapter I present the background information about the pancreatic islets, insulin secretion and its regulation by G-protein coupled receptors (GPCRs), in particular by dopamine and its receptors.

1.1   The endocrine pancreas and the islets of Langerhans

The pancreas is identified as a single organ in the mammalian abdominal cavity, but in fact it is composed of two parts with distinct functions: the endocrine pancreas and the exocrine pancreas. The exocrine pancreas is a digestive organ: it produces digestive enzymes that are secreted into the small intestine via the pancreatic duct (5). The endocrine pancreas is an endocrine gland that produces several hormones that function to regulate glucose concentration in the bloodstream. The most abundant and important pancreatic hormones are: insulin, glucagon, and somatostatin. These hormones are secreted directly into the blood vessels that perfuse the endocrine pancreas. For this reason the endocrine pancreas that constitutes approximately 1-2% of the pancreatic mass, receives about 10-15 % of the total blood supply for the whole pancreas (6, 7). The endocrine pancreas is organized in spheroidal clusters of endocrine cells, the islets of Langerhans, scattered across the volume of the exocrine pancreas.

1.1.1 The islets of Langerhans

The islets of Langerhans, which were discovered by a medical student and first described in his dissertation in 1869 (8, 9), constitute the functional unit of the endocrine pancreas. Five major cell types can be identified in an islet: the insulin producing β-cells, the glucagon producing α-cells, the somatostatin producing δ-cells (1, 10, 11), the pancreatic polypeptide producing PP-cells (12, 13), and the ghrelin producing ε-cells (14, 15). The cytoarchitecture of the islets varies in between different species, and so does the relative abundance of each cell type in the islet of different species (16). Mouse islets have a characteristic structure with a core of β-cells surrounded by a mantle of α-cells on the surface, which is interspersed with the δ-cells. β-cells represent 60-80% of the cells, α-cells constitutes 15 -20% of the cells, and δ-cells, PP cells, and ε-cells collectively are less than 10% of the cells (16, 17). With regard to their size, there is again variability across species, with mouse islets following a log-normal distribution, and having an average size of ∼ 100 µm (18). The islet size and the β-cells/islet cells ratio for various species are summarized in Table 1.

The cytoarchitecture of the islets of Langerhans is crucial to their function. In fact, dispersed islet cells display a reduced dynamic range of hormone secretion in response to glucose (19, 20). In the islet environment, the endocrine cells interact reciprocally via surface receptors, cell adhesion and junctional molecules (21-23).

Table 1: Islet size and β-cell ratio for different species. (from (18)).

Species	Islet size (μm)	β-cell ratio
Human	50 +/- 29	0.64 +/- 0.21
Monkey	67 +/- 38	0.79 +/- 0.14
Pig	49 +/- 15	0.89 +/- 0.11
Rabbit	64 +/- 28	0.79 +/- 0.17
Bird	24 +/- 6	0.46 +/- 0.24
Wild-type mouse	116 +/- 80	0.85 +/- 0.14
ob/ob mouse	86 +/- 76	0.92 +/- 0.11
db/db mouse	47 +/- 24	0.53 +/- 0.24
Pregnant mouse	112 +/- 94	0.84 +/- 0.22

Gap junctions are protein complexes that form channels in the cell membrane of adjacent cells, and allow for low molecular weight molecules and ions to diffuse among the cells (23). The exchange of ions contributes to the equilibration of the membrane potential of the connected cells, while the diffusion of second messenger contributes to unify the downstream response of the connected cells. More than 20 different connexin isoform are expressed in vertebrates cells, but connnexin-36 is the isoform that is expressed in mouse islets and has been shown to be relevant for proper insulin secretion (24-26).

In addition to the gap junction mediated chemical and electrical connection, the cells in the islet exchange paracrine signals in the intercellular space, and in the bloodstream. The islets are highly vascularized, and the capillaries that perfuse them are highly fenestrated, which facilitates the exchange of chemicals (27). Also, the islets are highly innervated by sympathetic, parasympathetic, and sensory nerves (21). This innervation provides an additional level of coordination both in the islet, and between the

islets. This interconnection and coordination result in tight regulation of hormone secretion by the islets, which is necessary to maintain proper blood glucose concentrations, even under the most extreme conditions.

1.1.2 Glucose homeostasis and type-2 diabetes

Glucose is the main variable controlling hormone secretion by the islet. Under fasting conditions, the concentration of glucose in the blood is ~ 5 mM. Any increase in glucose concentration (e.g. after a meal) triggers insulin secretion. Insulin acts on the liver, the adipose tissue, and the muscles to stimulate glucose uptake and storage (1). When glucose concentration decreases below 5 mM (e. g. after intense exercise) insulin secretion is halted and glucagon is secreted. Glucagon acts mainly on the liver to increase the hepatic glucose output by stimulating glycogenolysis and gluconeogenesis (1). Glucose homeostasis is maintained by the counteracting effects of both hormones. The different secretion profiles of insulin, glucagon, and somatostatin for a healthy human and a healthy mouse in response to glucose can be seen in Figure 1.
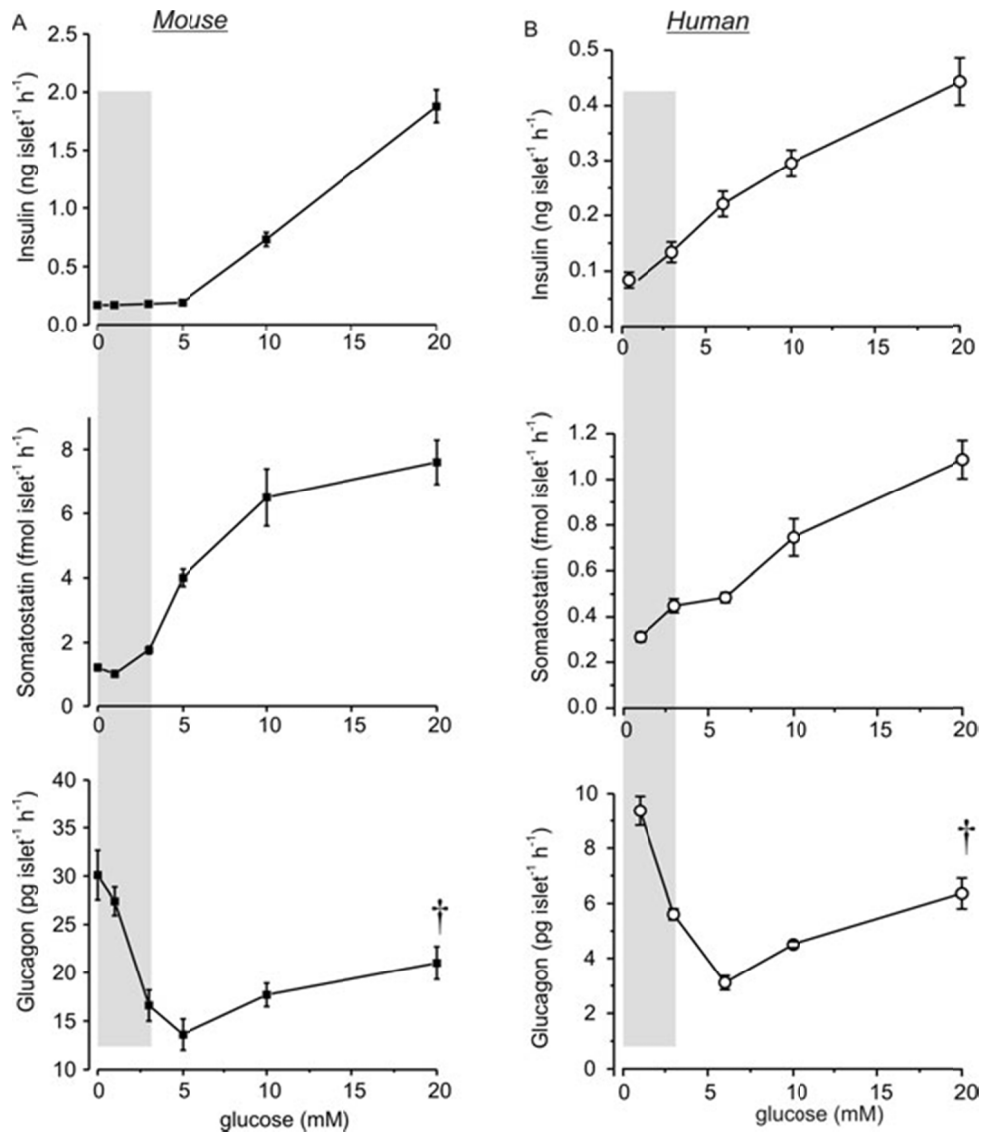
Figure 1: Glucose dependence of pancreatic hormone secretion from mouse (A) and human (B) pancreatic islets (from (28)).

Islet dysfunction, characterized by insufficient insulin secretion and impaired regulation of glucagon secretion, is a key trait of type-2 diabetes (29, 30). This type of diabetes is a complex disease that has multiple causes both genetic and environmental (31). In the majority of cases, type-2 diabetes is associated with obesity, thus linking this disease with a hypercaloric diet and lack

6

of physical activity (32). The normal values for a healthy individual are: a fasting plasma glucose concentration (FPG) of 5.6 mM, and a plasma glucose concentration comprised between 5.6 mM and 6.9 mM two hours after a 75 g oral glucose tolerance test (2h-PG) (33). There is a consensus model that describes the early stage of type-2 diabetes and its progressive development. The elevated caloric intake and the lack of exercise produce obesity and insulin resistance in an individual with the polygenic predisposition to develop type-2 diabetes. When this happens more insulin is necessary to clear the same amount of glucose from the bloodstream. At this stage the individual has normal fasting glucose levels, but shows hyperinsulinemia and impaired glucose tolerance, that is 2h-PG between 7.8 mM and 11.0 mM. With the progression of the disease, β-cell function starts deteriorating and postprandial hyperglycemia appears. When β-cell function decreases to 50% type-2 diabetes becomes full-blown, showing mild fasting hyperglycemia. Later stages show fasting hyperglycemia (FPG > 7.0 mM, 2h-PG >11.1 mM) and then finally a total loss of β-cell function. The progression of type-2 diabetes is illustrated in Figure 2. If left untreated, hyperglycemia causes macrovascular and microvascular complications due to glucose toxicity (34). The damage to capillaries targets the kidneys, the retina, the heart, the brain, and the peripheral circulation. Thus, type-2 diabetes causes elevation in the risk of developing heart disease and stroke, hypertension, blindness, kidney failure, neuropathies and amputations (2).
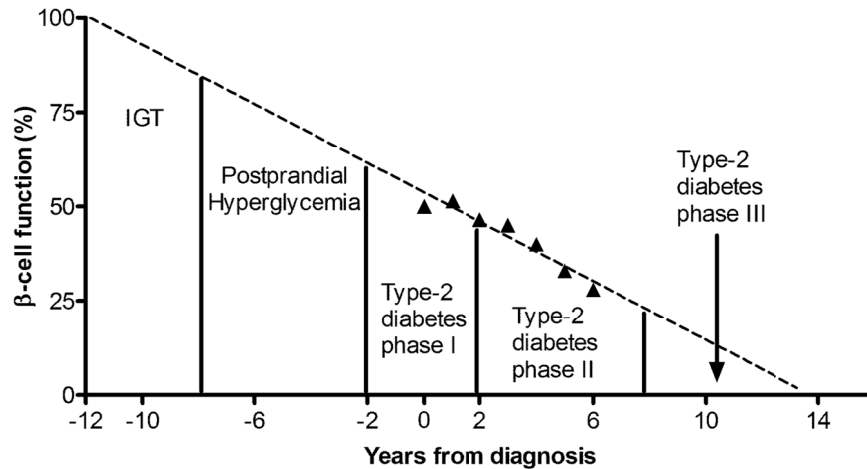
Figure 2: The progression from normal glucose tolerance to type-2 diabetes with complete absence of insulin secretion. The dashed line indicates the extrapolation based on 6 years of data for β-cell function. IGT = impaired glucose tolerance. (35, 36).

The current pharmacological treatments for type-2 diabetes provide four ways to restore euglycemia or at least manage the hyperglycemia. The insulin sensitizer drugs (thiazolidinediones) improve the efficacy of the available insulin on the target tissues to increase glucose uptake and storage. The insulin secretagogue drugs (sulfonylureas, glinides, glucagon-like peptide agonists) act on β-cells to increase insulin secretion, while the inhibitors of dipeptidyl peptidase 4 (sitagliptin, vidagliptin) produce the same effect by extending the half-life of naturally occurring peptides (glucagon-like peptide 1 and glucose-dependent insulinotropic peptide) that subsequently potentiate glucose stimulated insulin secretion (GSIS). The glucose output inhibitor drugs reduce glucose production by the liver (metformin). The last form of intervention is insulin replacement by injections that provides the body with an external source of insulin (37).

8

With type-2 diabetes being a disease that has such a slow progression (spanning almost 30 years to go from 100% to 0% β-cell function (36)), the development of better drugs to treat the early stages can significantly delay the late stage of the disease with its onset of the microvascular complications, improving the quality of life for patients. For this reason, expanding our knowledge on the mechanisms that regulate insulin secretion is important, as it increases the number of targets for new possible drugs.

1.1.3 The mechanism of glucose stimulated insulin secretion

β-cells secrete insulin in response to elevated glucose, as is shown in Figure 1. The cascade of intracellular events that produces this response has been studied in great detail and can be summarized as follows. Extracellular glucose enters the β-cell cytoplasm through the facilitative glucose transporter GLUT2 (38-40). This high capacity transporter equilibrates extra- and intra-cellular glucose within seconds. In the cytoplasm, glucose is phosphorylated by the enzyme glucokinase, and the resulting glucose-6 phosphate enters the glycolytic pathway (41-43). The complete oxidative metabolism of one molecule of glucose-6 phosphate produces 36 molecules of ATP, thus the cytosolic [ATP]/[ADP] ratio increases. β-cells express ATP-sensitive potassium channels (K_{ATP}) that close in response to this elevated [ATP]/[ADP] ratio (44-46). The closure of K_{ATP} channels increases the concentration of intracellular K^+ depolarizing the cell membrane, which leads to the opening of L-type voltage gated calcium channels. The influx of Ca^{2+} triggers conformational changes in

the exocytotic machinery causing the fusion of the insulin secretory granules with the plasma membrane, and insulin is secreted in the extracellular space (47-50). Secretion continues until the membrane repolarizes. Multiple processes are responsible for the repolarization of the β-cell membrane. The elevated concentration of intracellular Ca^{2+} ($[Ca^{2+}]_i$) stimulates the activity of Ca^{2+}ATPase that transports Ca^{2+} in the endoplasmic reticulum. This process diminishes both $[Ca^{2+}]_i$ and the [ATP]/[ADP] ratio (51). Additionally the opening of Ca^{2+} activated K^+ channels (52) and voltage dependent K^+ channels (53) generates an efflux of K^+. These three processes cause a temporary cessation of insulin secretion, until more glucose is metabolized and the full chain of events starts again. So the overall response to glucose of a β-cell is a sequence of action potentials eliciting insulin secretion.

1.1.4   The coordinate response of β-cells

Isolated β-cells respond to an increase in glucose concentration with a sequence of action potentials, but the action potentials of two β-cells will not be synchronous, due to the stochastic nature of the molecular processes. Nonetheless, in the islets, β-cells show a coordinated response to glucose. Thanks to the presence of gap junctions providing electrical coupling, the β-cells excitability is synchronized, and so are the changes in $[Ca^{2+}]_i$, and insulin secretion (25). As a result of the β-cell synchronization GSIS from an islet is pulsatile. In detail, the membrane potential of a β-cell in an intact islet experiences burst of action potentials interspersed between silent phases, with a

10

periodicity of 8-27 s. These fast oscillations are superimposed to slow oscillations that have a periodicity of 5-10 min. Both $[Ca^{2+}]_i$, and insulin follow the same periodicity (54). While the fast oscillations are dependent on the changes to the electrical properties of the membrane, the slow oscillation are currently attributed to changes in the metabolic processes that affect the [ATP]/[ADP] ratio (55, 56). Hence the specific architecture of an islet contributes to produce the characteristic insulin secretion profile that is biphasic and pulsatile. The first phase is a strong secretory response occurring 5-10 minutes after the glucose stimulation. After a short decrease in secretion, the second phase follows, which is characterized by a slow increase in insulin secretion and the insulin pulses (57). Pulsatile secretion of insulin is observed *in vivo* too, in the portal vein of mice and humans (57-59). Interestingly, during type-2 diabetes, the strong first phase secretory response is lost (60, 61), and similarly the pulsatile response is altered (62, 63). This suggests that the pulsatile secretion is important for proper insulin signaling. In fact pulsatile insulin therapy seems to significantly reduce the progression of diabetic complications in patients, when compared with non-pulsatile insulin treatment (64). The current model to explain the advantages of pulsatile insulin administration, points at its positive effects on the insulin receptor sensitivity both in the liver and in adipose tissue (65, 66).

1.2 GPCR regulation of insulin secretion

1.2.1 <u>The GPCR family of receptors</u>

G-protein coupled receptors (GPCRs) constitute the largest family of cell surface receptors, with more than 800 members encoded by the human genome (67). The basic function of these membrane-spanning proteins is to translate an extracellular stimulus into an intracellular signal. The variety of stimuli that target GPCRs is similarly wide, and includes photons, ions, amines, fatty acids, amino-acids, nucleotides, peptides, proteins, and steroids. In addition, there are more than 100 orphan GPCRs for which neither the ligand nor the function is yet known (68). The ensemble of these receptors regulates embryonic development and organism homeostasis, and they are involved in vision, smell, taste, memory, and learning. For this reason they are an important target for drug design. It has been estimated that almost 50% of the drug targets in the pharmaceutical industry are GPCRs (69), and 46 GPCRs have been successfully targeted by drugs (70).

The first primary structure of a GPCR was published 30 years ago (71-73). Since then, we have learned that despite the necessary structural diversity that allows GPCRs to carry such variety of functions, these receptors share a similar topology. They have a core of 7 transmembrane α-helices with 3 hydrophilic intracellular loops, 3 hydrophilic extracellular loops, an extracellular N-terminus, and an intracellular C-terminus (Figure 3).
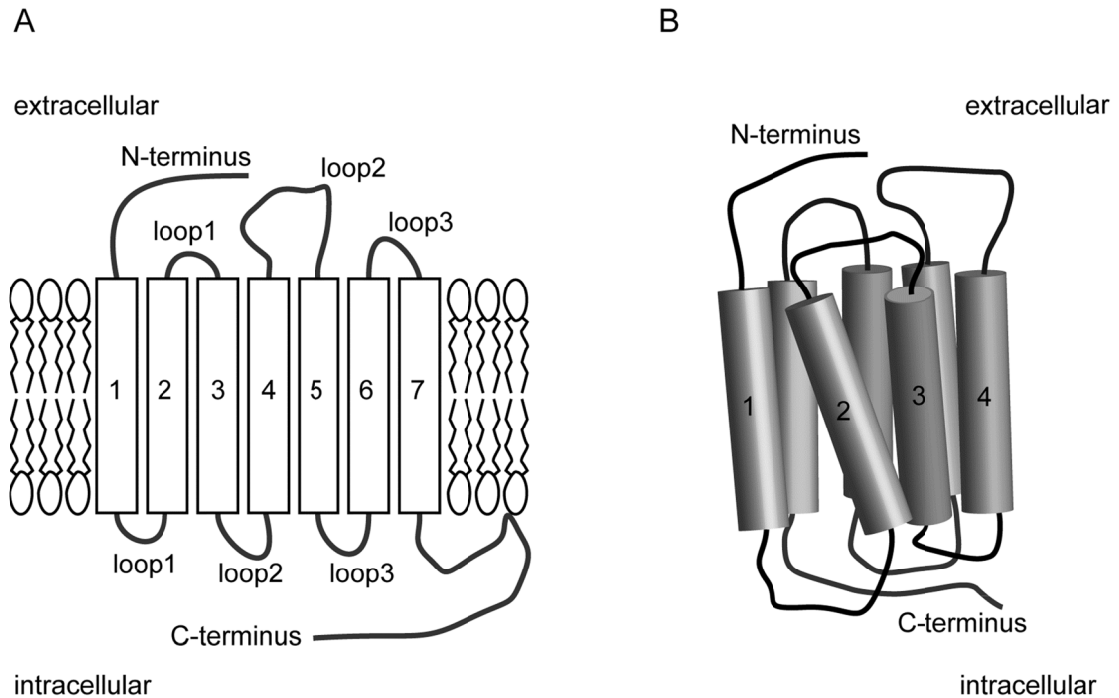
Figure 3: Schematic representation of a GPCR. A: Transmembrane topology of a GPCR. The seven transmembrane α-helices are numbered 1 to 7; the three intracellular loops and the three extracellular loops are numbered 1 to 3. B: Simplified representation of the three-dimensional arrangement of the 7 α-helices of a GPCR.

Based on phylogenetic properties, the GPCRs can be classifieds in 5 families: *glutamate*, *rhodopsin*, *adhesion*, *frizzled/taste2*, and *secretin* (Table 2) (74). More than 80% of all GPCRs belong to the *rhodopsin* family. When a ligand binds to the extracellular side of a GPCR, the receptor undergoes conformational changes that expose previously hidden amino-acids at its intracellular face. These conformational changes allow dissociation of the heterotrimeric G-protein from the receptor (75). The heterotrimeric G-protein in turn activates the intracellular signaling cascade. Several G-proteins exist and they are differentially expressed in different cell types. The different combinations

between GPCR and G-protein explain the variety of downstream effects and how

the same ligand can have opposite effects on different cell types.

Table 2: Summary of properties for the GPCR families. ORs = olfactory receptors. (reprinted by permission from Mcmillan Publishers Ltd: Nature Reviews Drug Discovery (67), copyright (2008).

Property	Rhodopsin	Secretin	Adhesion	Glutamate	Frizzled	Taste2
Number of full-length receptor proteins	672 (388 ORs)	15	33	22	11	25
Number of identified major drug targets	>39	4	0	3	0	0
Number of orphans	63 (not including ORs)	0	30	7	0	21
Type of ligand	Peptides, proteins (including enzymes), small organic compounds, lipid-like substances, nucleotides	Peptides, proteins	Proteins, glycosaminoglycan	Amino acids, cations, small organic compounds, carbohydrates	Proteins	Small organic compounds

1.2.2 The multiplicity of G proteins and downstream effectors

Heterotrimeric guanine nucleotide-binding proteins (G proteins) are the

signal transducers that couple GPCRs to several intracellular signaling pathways

(76). The heterotrimer consists of the subunits α, β,and γ. Currently there are 35

known genes encoding G protein subunits. 16 genes encode α subunits, 5 genes

encode β subunits, and 14 genes encode γ subunits (77). When a GPCR

activates the heterotrimeric G protein, this dissociates the G_α subunit and the $G_{\beta\gamma}$

complex. Both the G_α subunit and the $G_{\beta\gamma}$ complex are relevant in communicating

the signal downstream. G proteins can be grouped in 4 families, based on the

sequence similarity of their G_α subunit: G_s, $G_{i/o}$, $G_{q/11}$, and $G_{12/13}$ (77, 78). Yet, this

system does not describe the effects that are mediated by the $G_{\beta\gamma}$ complex. Each

of the 4 families is associated to a preferential signaling pathway. The G_s family stimulates adenylyl cyclase (AC) activity, resulting in increased cAMP levels. This leads to activation of protein kinase A (PKA) and the group of exchange protein directly activated by cAMP (Epac), both of which act on multiple downstream targets (78, 79). The $G_{i/o}$ family inhibits AC activity via its G_α subunit, and also it acts on phospholipase C-β (PLC-β), K^+ channels, AC, and phosphoinositide3-kinase (PI3K) via the $G_{\beta\gamma}$ complex (78). The $G_{q/11}$ family activate PLC-β that produces inositol 1,4,5-trisphosphate (IP_3) and diacylglycerol (DAG). In turn IP_3 causes release of Ca^{2+} from the intracellular stores, and DAG activates protein kinase C (PKC) (78). The $G_{12/13}$ is the least characterized of the 4 groups, and it is thought to stimulate phospholipase D, c-Src, PKC. Also it has been reported to interact with GTP-ase-activating protein for Ras, RasGAP, and Bruton's tyrosine kinase (78, 80). A schematic and simplified representation of the complex interactions between the G proteins is shown in Figure 4.

The tuning of insulin secretion to meet the energy demand of an healthy organism, and maintaining glucose homeostasis, is one example of complex large-scale regulation mediated by GPCRs. The fact the β-cells express multiple GPCRs and G proteins allow them to sense the energy status and the energy demand of the body. The network of interactions between GPCRs and G proteins activates multiple second messengers in the β-cells to constantly adjust their function and their output to the external demand. This concept will be described in more detail in the next section.
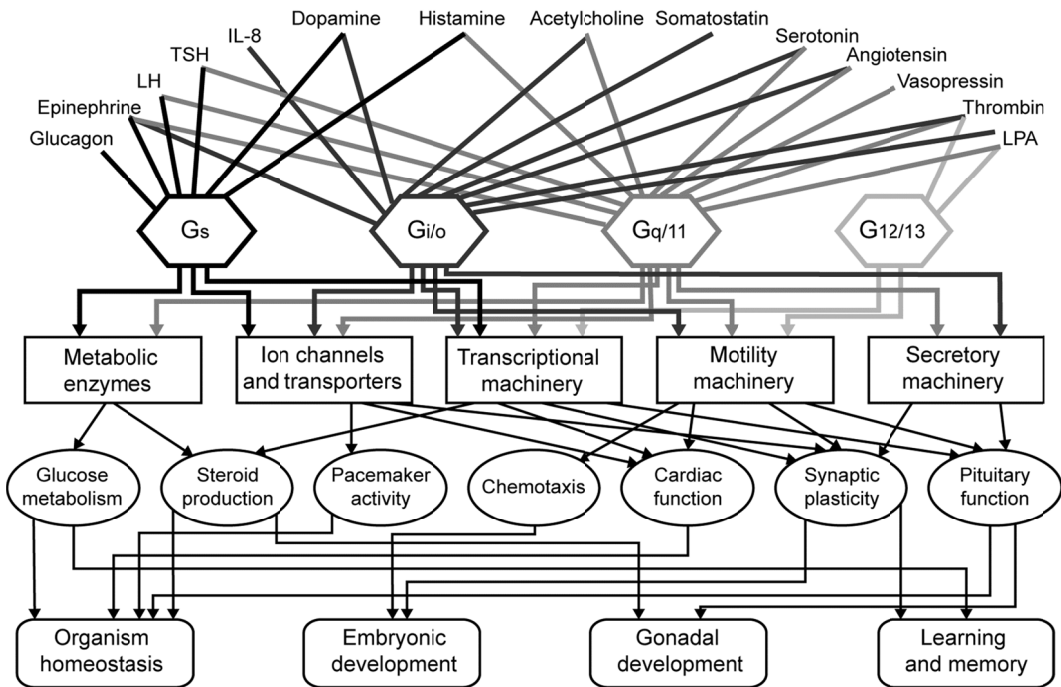
Figure 4: The regulation of systemic functions by the G proteins pathways.Many extracellular ligands signal through the 4 G protein families to regulate cellular components. In turn these change specific cellular functions. The coordination of these changes regulates large-scale systems (78).

1.2.3 The islets of Langerhans integrate many stimuli

We described in section 1.1.3 how the β-cells secrete insulin in response to elevation of glucose concentration in the plasma. This basic mechanism is constantly altered by external stimuli that may come from other cells in the islet (i.e. glucagon coming from the α-cells and stimulating insulin secretion (81)), from nerve fibers (i.e. norepinephrine coming from adrenergic nerve fibers and inhibiting insulin secretion (21)), and from the blood stream (e.g., GLP-1 coming from cells in the intestine and stimulating insulin secretion (82)). Each agent acts on one or more GPCRs expressed by the β-cell. There is an active search for novel therapy to restore euglycemia in type-2 diabetes

patients, so these external stimuli that alter insulin secretion and β-cell function,

make their respective GPCRs potential drug targets. Table 3 presents a list of

some of the most studied receptors in the β-cell and in the α-cell, including the G

proteins mediating the effect.

Table 3: Hormones, neurotransmitter, neuropeptides and nutrients that affect islet hormone secretion via interaction through GPCRs. (from (83)).
Ach = acetylcholine, CCK = cholecystokinin, FFA = free fatty acids,
GLP-1 = glucagon-like peptide, GIP = glucose-dependent insulinotropic peptide,
NPY = neuropeptide Y, PACAP = pituitary adenylyl cyclase-activating peptide,
VIP = vasoactive intestinal polypeptide.

Ligand	Receptor	Effect on insulin secretion	Effect on glucagon secretion	G protein
ACh	M_3	Stimulatory	Stimulatory	G_q
ATP/ADP	P_{2Y}	Stimulatory	Not known	G_s
Cannabinoids	CB_1	Inhibitory	Not known	G_i
CCK	CCK_A	Stimulatory	Stimulatory	G_q
FFA	GPR40	Stimulatory	Stimulatory	G_q
	GPR119	Stimulatory	Not known	G_s
Glucagon	Gcgr	Stimulatory	Stimulatory	G_s, G_q
GLP-1	GLP-1R	Stimulatory	Inhibitory	G_s
GIP	GIPR	Stimulatory	Stimulatory	G_s
Kisspeptin	GPR54	Stimulatory	No effect	G_q
NPY	Y_1	Inhibitory	Stimulatory	G_i
Noradrenaline	β_2	Stimulatory	Stimulatory	G_s
	α_2	Inhibitory	Stimulatory	G_i
Somatostatin	$sstr_2$	Inhibitory	Inhibitory	G_o/G_i
PACAP	PAC_1	Stimulatory	Stimulatory	G_s
Vasopressin	V_{1B}	Stimulatory	Stimulatory	G_q
VIP/PACAP	$VPAC_2$	Stimulatory	Stimulatory	G_s

This list is far from being complete and new GPCRs that can be

potential targets for the treatment of the islet dysfunction in type-2 diabetes are

often added (84). One successful example of this strategy is the introduction of

novel therapies targeting the actions of the incretin hormone GLP-1: GLP-1

mimetics are now available to directly stimulate the GLP-1 receptor. Also there are inhibitors of dipeptidyl-peptidase 4 (DPP4) which increase the concentration of endogenous GLP-1 (85, 86). Since our lab is primarily interested in insulin secretion from the β-cell, I describe the relevant intracellular mechanisms that GPCRs can act on to modulate insulin secretion. First, increasing K^+ conductance causes the hyperpolarization of β-cell membrane, which counterbalances the depolarization that triggers opening of L-type Ca^{2+} channels. The net effect is a reduction of Ca^{2+} dependent exocytosis. In the β-cell, this mechanism is activated by receptor that signals via $G_{i/o}$ (i.e. norepinephrine) (87). This effect can be obtained by G_α acting on the K_{ATP} channels (88). Alternatively, the $G_{\beta\gamma}$ complex can directly activate the G protein-gated inward rectifying potassium channels (GIRK) (89, 90), as these channels are active in β-cells (91). Second, AC activity increases cAMP that potentiates GSIS through PKA and Epac. G_s and $G_{i/o}$ coupled receptor can respectively stimulate or inhibit AC to modulate insulin secretion (88, 92). Additionally the $G_{\beta\gamma}$ complex can differentially stimulate and inhibit 8 of the 9 isoforms of AC (93). Third, GPCRs can modulate insulin secretion by a direct effect on the Ca^{2+} conductance. The β-cell expresses at least 6 isoforms of the pore forming subunit of the voltage gated calcium channel: $Ca_V1.2$, $Ca_V1.3$, $Ca_V2.1$, $Ca_V2.2$, $Ca_V2.3$, $Ca_V3.1$ (that correspond to α_{1C}, α_{1D}, α_{1A}, α_{1B}, α_{1E}, α_{1G} in the previous nomenclature system) (94, 95). They conduct L-, P/Q, N-, R- and T- calcium currents (Table 4). While the L-type calcium current is responsible for the Ca^{2+} influx during the first phase of insulin

secretion, the N- and R- type are important during the second phase of insulin secretion.

Table 4: Biophysical properties of types of Ca^{2+} channels. HVA = high voltage activated, LVA = low voltage activated (94, 96-101).

	LVA	HVA			
Current type	T	L	P/Q	N	R
α_1 subunit	$Ca_V3.1$, $Ca_V3.2$ $Ca_V3.3$	$Ca_V1.1$, $Ca_V1.2$ $Ca_V1.3$, $Ca_V1.4$	$Ca_V2.1$	$Ca_V2.2$	$Ca_V2.3$
Single-channel conductance	8 pS	25 pS	13 pS		
Activation	$\geq$ -70 mV	$\geq$ -30 mV	$\geq$ -20 mV		
Inactivation	Complete $\tau \approx$ 20-50 ms	Very slow $\tau >$ 500 ms	Partial $\tau \approx$ 50-80 ms		

The $G_{\beta\gamma}$ complex binds to $Ca_V2.1$, $Ca_V2.2$ and $Ca_V1.3$ inhibiting the Ca^{2+} conductance (102). Furthermore, there is evidence that $Ca_V1.2$ is also directly regulated by the $G_{\beta\gamma}$ complex (103, 104). In addition, GPCRs modulate Ca^{2+} conductance by the effect on AC, cAMP, PKA or through the PLC, DAG, IP_3, PKC pathway. Finally, GPCRs can modulate insulin secretion downstream of the $[Ca^{2+}]_i$ increase. At this stage, the molecular mechanism can be described as follows: Ca^{2+} binds to synaptotagmin VII and IX (105), the activated synaptotagmins bind to the SNARE complex (it includes SNAP-23, SNAP-25, syntaxin 1A and syntaxin 4, VAMP-2) with Munc18c and other proteins, and together, these permit fusion of the granule membrane with the plasma membrane to complete the exocytosis (88). The $G_{\beta\gamma}$ complex can bind to the

C-terminus of SNAP-25, thus blocking the interaction with the synaptotagmins and inhibiting exocytosis (106-109).

1.3   Dopamine and the dopamine receptors

1.3.1   The neurotransmitter dopamine

Dopamine was first identified as neurotransmitter in brain by Arvid Carlsson almost 50 years ago (110). For this discovery he received the Nobel Prize for medicine in the year 2000. He showed that dopamine was not just an intermediate product in the synthesis of epinephrine and norepinephrine; instead it was a neurotransmitter itself. Dopaminergic neurons were identified in specific regions of the brain: the substantia nigra and the ventral tegmental area. Dopaminergic neurons project fibers to the basal ganglia, to the nucleus accumbens, and to the prefrontal cortex (111, 112). Dopaminergic neurons were also identified in the hypothalamus, where they modulate the secretion of the hormone prolactin from the anterior pituitary gland (113). These neurons control crucial brain functions like motor coordination (114), motivation (115), reward (116), and working memory (117). Dysfunction of the dopaminergic neurons can cause Parkinson's disease (118), and is thought to be the cause of schizophrenia (119) and attention deficit hyperactivity disorder (120). Dopamine, once it has been secreted by the dopaminergic neurons, achieves its effect via binding to dopamine receptors.

1.3.2 The dopamine receptors

Dopamine receptors are members of the *rhodopsin* family of GPCRs, and they include 5 different receptor subtypes named D1, D2, D3, D4, and D5. They are the products of 5 genes from different chromosomal loci, but they display significant homology in their protein structure and function. Table 5 summarizes the main feature of the 5 receptors.

Table 5: Molecular characteristics of human dopamine receptors. (121)

	D1-like		D2-like			
	D1	D5	D2short	D2long	D3	D4
Amino acids	446	467	414	443	400	387-515
3rd cyoplasmic loop	57	50	134	163	120	101-261
Introns	0	0	5	6	5	3
Chromosomal localization	5q35	4p15-16	11q22-23		3q13	11q15

The D1 and D5 receptors have no introns and have 80% homology in their transmembrane domains. They usually display a stimulatory function on AC activity and for this reason they are classified as D1-like receptors (122). The D2, D3, and D4 receptors are encoded by genes which have introns. The D2 and D3 have a 75% homology in their transmembrane domain, while D2 and D4 have 54% homology. These 3 receptors have a long third intracellular loop that is a feature of GPCR interacting with $G_{i/o}$ proteins. They generally show inhibitory

function on AC activity and are classified as D2-like receptors (122). A cartoon

displaying the dopamine receptor topology is shown in Figure 5.
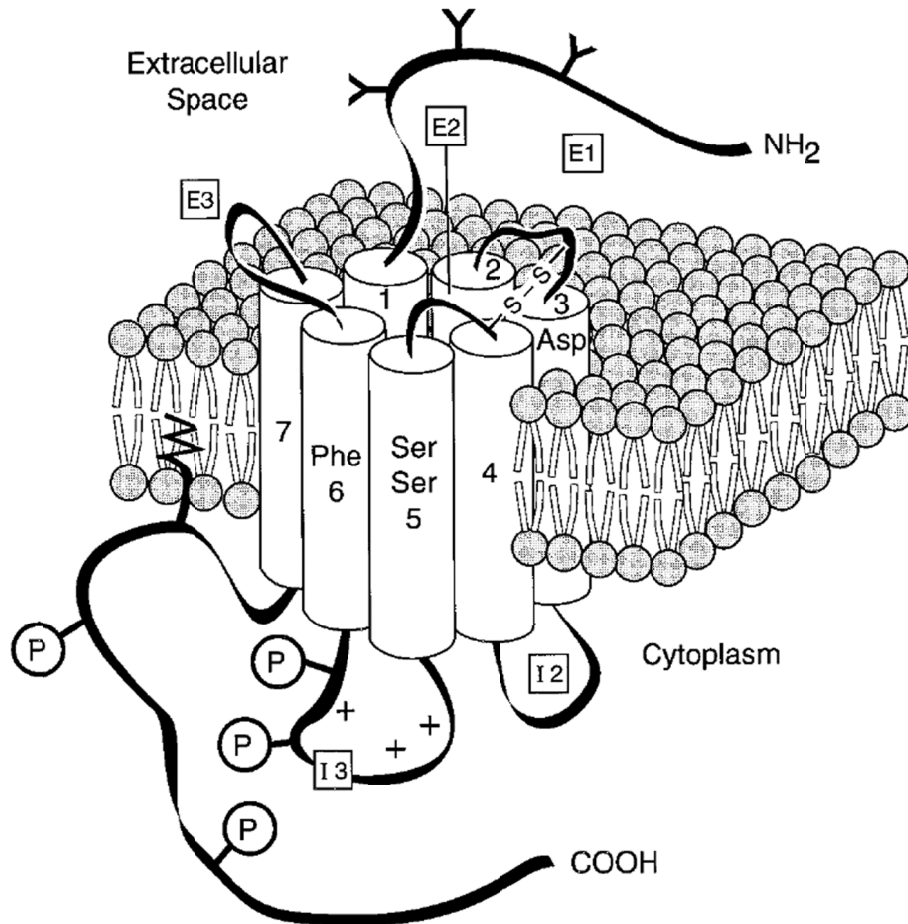
Figure 5: Dopamine receptor structure. Structural features of D_1-like receptors are represented. D_2-like receptors are characterized by a shorter COOH-terminal tail and by a bigger 3rd intracellular loop. Residues involved in dopamine binding are highlighted in transmembrane domains. Potential phosphorylation sites are represented on 3rd intracellular loop (I3) and on COOH terminus. Potential glycosylation sites are represented on NH_2terminal. E1-E3, extracellular loops; 1–7, transmembrane domains; I2-I3, intracellular loops.(from (122)).

Dopamine receptors are expressed in the central nervous system where they mediate the dopaminergic functions that were just mentioned. But they are also present in some peripheral tissues, as summarized in Table 6.

Table 6: Distribution and function of peripheral dopamine receptors. (from (122)).

Tissue	Receptor Type	Function
Blood vessels		
Adventitia	D_2-like	Inhibition of NE release
Media	D_1-like	Vasodilatation
Intima	D_2-like	Unknown
Adrenal gland		
Glomerulosa	D_1-like	Unknown
	D_2-like	Inhibition of aldosterone secretion
Medulla	D_1-like	Stimulation of E/NE release
	D_2-like	Inhibition of E/NE release
Kidney		
Glomerulus	D_1-like	Increase of filtration rate
Juxtaglomerular apparatus	D_1-like	Stimulation of renin secretion
Proximal tubule	D_1-like	Inhibition of Na^+ reabsorption
Ascending limb of loop of Henle	D_1-like	Inhibition of Na^+ reabsorption
Cortical collecting duct	D_1-like	Inhibition of Na^+ reabsorption
	D_2-like	Inhibition of vasopressin action
Sympathetic ganglia/ endings	D_2-like	Inhibition of NE release
Heart	D_4	Unknown

NE, norepinephrine; E, epinephrine.

Particularly interesting, from my perspective, is the suggested expression of dopamine receptors in the mesenteric organs, as reported by Mezey *et al.* (123). Additionally, the more recent paper by Rubí *et al.* (3) suggested a function for D2 in the β-cells. So I decided to investigate this matter in greater detail, to understand what role dopamine may have on insulin

secretion. I describe the rationale and the results of this research in the next

chapters.

CHAPTER

2. DOPAMINE SYNTHESIS IN THE ISLETS

2.1 Historical background

In this section, I provide a historical overview of the literature that pertains to the presence of dopamine in the pancreatic islets. Our interest in studying the role of dopamine in the islets was initially inspired by the work of Rubí *et al*. (3). They describe the inhibitory effect of exogenous dopamine on glucose stimulated insulin secretion (GSIS). But a careful review of the literature shows that while dopamine is known to inhibit insulin secretion, there is no consensus about where dopamine could originate to stimulate islets in a living mouse.

The first mention of biogenic amines in pancreatic islets dates back to 1963 by Falck and Hellman (124). In their report the authors present the result of a new method to detect catecholamines and tryptamines. They report that

> "No specific fluorescence was observed in the islets of rat
> and mouse. In the guinea-pig, cat, dog and horse, however,
> a moderate and sometimes rather strong fluorescence
> developed in some of the islet cells."

The publications that followed this first report offered contradicting results and conclusions, so after 50 years the controversy is still in place. In the first decade following Falck and Hellman's brief communication, the scientific community seemed to agree that mouse islets were devoid of biogenic amines,

therefore most of the studies were performed in golden hamster, guinea pig and rabbit (125-130). In 1968, islet cells were classified as "amine precursor uptake and decarboxylation" (APUD) cells based on cytochemical and ultrastructural similarities with other polypeptide hormone producing cells (131). It was observed that injection of L-dopa and dopamine produced a hyperglycemic response in mice, but in the whole animal setting the contribution of epinephrine and norepinephrine release from adrenergic nerve fibers could not be excluded (126). Dopamine was first detected in freshly isolated mouse islet homogenates in 1977 by Hansen and Hedeskov (132). They used a system that combined thin layer chromatography to separate the amines, and double radio-isotope labeling to quantitate them against a standard curve. They simultaneously detected dopamine, epinephrine, norepinephrine and serotonin in the islet homogenates from albino mice, but they could not exclude that dopamine was coming from fragments of adrenergic nerve fibers in the islets. While the work of Feldman's group expanded the knowledge on monoamines uptake and action in the islets of the golden hamster (133-135), they emphasized that islets from different species show great differences in their responses to experimental treatments (136). Therefore the knowledge gained on one particular species does not always apply to another species. Moreover, understanding of dopamine action in the islet was complicated because both stimulation and inhibition of insulin secretion had been reported: potentiated GSIS was reported in rat islets perfused with L-dopa (137), whereas lowered GSIS was showed in mice injected with L-dopa (138, 139). The work from Lundquist's group showed that radio-labeled dopamine could be

detected in mouse beta cell secretory granules, following the injection of radio-labeled L-dopa (138). They report a partial inhibition of glucose stimulated insulin secretion following the injection, but in this and further studies, they suggested that dopamine synthesis could have taken place in other tissues (140). In following studies, they concluded that the L-dopa induced inhibition of GSIS was independent from dopamine accumulation but rather related to a direct effect of L-dopa (139). However, aromatic L-amino-acid decarboxylase (AADC) and monoamine oxidases (MAO) activities were characterized in mouse islets homogenates (139, 141, 142), but no direct measurement of dopamine accumulation was done in those studies. Vesicular monoamine transporter type 2 (VMAT-2) has also been reported in rodent islets (143, 144). Despite the presence of dopaminergic machinery in the β-cells, it is not known where dopamine could originate to stimulate islets in a living mouse. Dopamine does not cross the blood-brain barrier, and although there are peripheral sources of dopamine in the body (123, 145-147), circulating dopamine levels in the plasma are too low to activate its receptors (147-149). While there is a high degree of innervation in the islets, there are no reports of dopaminergic neurons innervating them (150). There is not a consensus conclusion in the literature about the physiological source of dopamine, and its function in the pancreatic islets. Therefore I tested the hypothesis that islet β-cells synthesize dopamine from circulating L-dopa. While parts of this hypothesis have been previously proposed by different authors over the years to explain different observations, this hypothesis has not been rigorously tested in all its aspects in intact mouse islets.

The cartoon in Figure 6 summarizes the main steps involved in our overall hypothesis: the uptake of L-dopa into the β-cell by the L-aromatic amino acid transporter; the decarboxylation of cytosolic L-dopa by the AADC, which produce cytosolic dopamine; the accumulation of dopamine in the insulin granules by the VMAT-2, and its degradation by MAO-B; the co-secretion of dopamine and insulin during GSIS; the signaling of secreted dopamine via the activation of dopamine receptor D2-like and the reuptake of dopamine by the dopamine transporter (DAT).
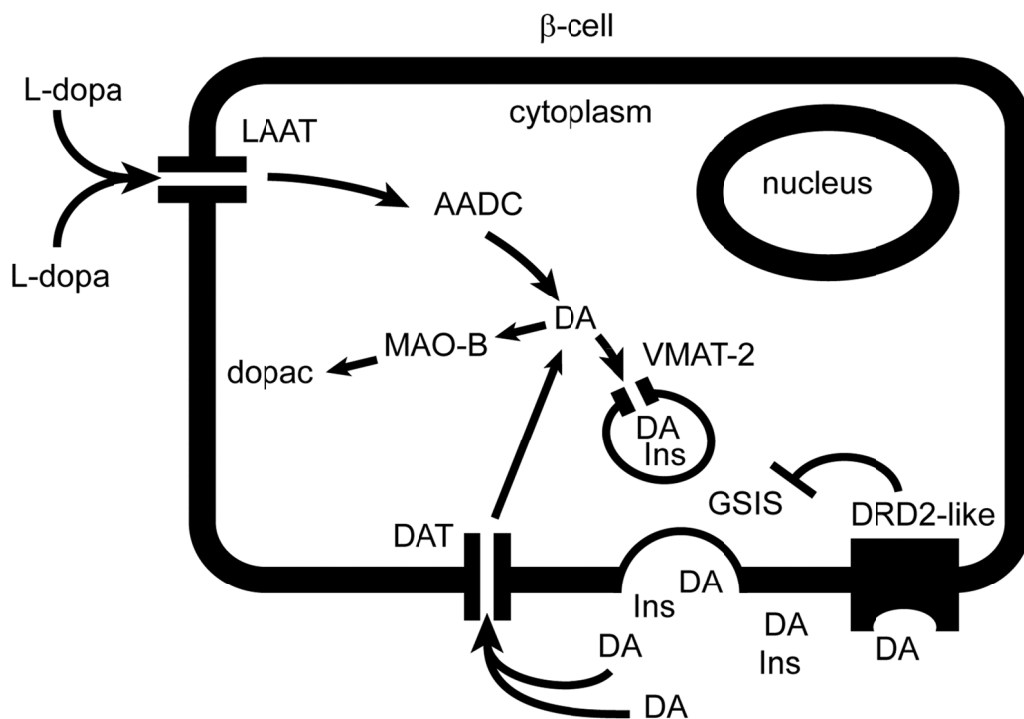
Figure 6: Diagram of the dopaminergic negative feedback in a β-cell.
DA = dopamine, Ins = insulin, dopac = dihydroxyphenylacetic acid.

In this chapter, I focus on the effects of L-dopa exposure in leading to dopamine accumulation in the secretory granules. I designed my experiments to

exclude as much as possible any external effect that could complicate the interpretation of the results. For this reason I chose to work with isolated intact islets instead of using the *in vivo* paradigm. This allowed me to study the interplay between dopamine synthesis and insulin secretion, without the contribution of other tissues and innervation.

2.2   Materials and methods

2.2.1   Islet isolation and culture

C57Bl/6 (Harlan Sprague Dawley, Inc) mice were used for these experiments. All animals were fed standard laboratory chow, and cared for according to the guidelines of the Vanderbilt Institutional Animal Care and Use Committee. 2-6 month-old mice were anesthetized by intraperitoneal injection of 0.05 ml of a ketamine (Bioniche Teoranta, Inverin, Co. Galway, Ireland) and xylazine (Lloyd laboratories, Shenandoah, IA, USA) mixture at a dose of 80 mg/ml and 20 mg/ml respectively. The pancreas was quickly removed and the animal was euthanized. The islets of Langerhans were isolated in Hanks' balanced salt solution (HBSS) following a modified version of the protocol from Lacy et al. (151). The isolated pancreas was rinsed in cold HBSS and minced using scissors. The tissue was collected in a 15 ml conical tube with 8 ml HBSS, and 6 mg of collagenase P (Roche) were added. The digestion proceeded for 10 minutes in a water bath at 34 ºC, with continuous shaking. Setting the water

temperature at 34 ºC instead that 37 ºC resulted in a more gentle and reproducible digestion of the tissue. Subsequently, the digested tissue was spun down for 15 seconds, until a soft pellet formed. The supernatant was discarded before resuspending the pellet in 8ml of cold HBSS. Two more rounds of centrifugation were necessary to remove any trace of collagenase. The final suspension was transferred in a 10 mm non-treated dish (Corning) and islets were handpicked under a dissecting microscope. This protocol for islet isolation yielded 150-300 islets per mouse. The islets were cultured overnight in islet medium (RPMI 1640 medium with glutamine (Invitrogen,Carlsbad, CA) supplemented with 10% heat inactivated fetal bovine serum, 100 units/ml penicillin, 100 µg/ml streptomycin, 11 mM glucose), at 37 ºC in humidified atmosphere with 5%CO_2. Islets for the dopamine assay were cultured overnight in islet medium with 2 mM glucose so that insulin secretion was kept at its basal rate, and dopamine accumulation was maximized.

2.2.2 <u>Dopamine content assay</u>

After being treated according to the experiment being performed, islets from a single mouse were transferred in a 1.5 ml tube containing ice cold phosphate buffered saline (PBS) (Mediatech Inc) and rinsed once. The lysis was performed in 28 µl of minimal lysis buffer (5 % glycerol, 1 % TritonX-100, 100 mM NaCl, 1 mM EDTA, 4 mM $Na_2S_2O_5$, 10 mM HCl) for 30 minutes on ice. The sample was snap frozen using a bath of ethanol and dry ice, and then thawed at room temperature. After 3 freeze/thaw cycles it was sonicated for 5 minutes.

Finally the sample was centrifuged at 13000 g for 10 minutes in a tabletop centrifuge, and the supernatant was collected for dopamine and protein determinations. I diluted 5 µl of sample in 20 ul of lysis buffer to measure the protein concentration in duplicate. I used the Pierce 660nm protein assay reagent in a 96-well plate format and read the absorbance at 660 nm. I used a serial dilution of BSA stock to generate the standard curve. The remaining sample was diluted to a final volume of 500 µl in minimal lysis buffer. This dilution it proved to be a critical step to be able to extract dopamine from the islet matrix. When I processed some undiluted samples, the dopamine extraction was reduced dramatically. I measured dopamine concentration using the Dopamine Research ELISA (Rocky Mountains Diagnostics, Inc.). The protocol has 4 phases. The first phase is the extraction phase where dopamine is extracted from the sample by using a cis-diol-specific affinity gel. In the next phase the gel bound dopamine is acylated and then eluted. Then the acylated dopamine is enzymatically derivatized. The derivatized samples and standards are then loaded in the ELISA plate. The unknown concentration is determined by comparison with the absorbance of a standard curve. The concentration range for the dopamine in the standard curve was 36 – 3600 pg. Each sample was split in half and processed in duplicate. I used a Spectramax M5 plate reader (Molecular Devices) to read the 96-well plates. The results of the dopamine concentration assay were normalized to the sample protein content, and expressed as (pg of dopamine)/(µg of protein). *n* represents the number of mice used to test each condition. Data are plotted as mean ± SEM.

2.2.3 Dopamine secretion assay

Islets from multiple mice were pooled and allowed to recover from the isolation procedure overnight in islet medium, at 37 ºC in 5% CO_2 humidified atmosphere. On the next day they were divided in groups of 215 islets in Krebs Ringer Bicarbonate HEPES Buffer (KRBH) at 37 °C in 5% humidified CO2. KRBH components were: 128.8 mM NaCl, 4.8 mM KCl, 1.2 mM KH2PO4, 1.2 mM MgSO4, 2.5 mM CaCl2, 5 mM NaHCO3, 10 mM HEPES, 0.1 % bovine serum albumin, pH 7.4. Each group was treated with 2.8 mM glucose +10 µM L-dopa for 40 min to increase the islet dopamine content. Each group was then transferred to 1.5 ml eppendorf tubes contatining KRBH + 2.8 mM glucose for 20 min, to let the dopamine content equilibrate. Then each group was transferred to the 1.5 ml eppendorf tube containing KRBH + the condition to be tested for the secretion experiments. Each group was incubated for 45 minutes. After incubation, the supernatant was collected, dopamine preservatives were added (1 mM EDTA, 4 mM $Na_2S_2O_5$, 10 mM HCl), and this supernatant was used to measure secreted dopamine. The standard curve for these measurements had a 12 pg – 1200 pg range. A small fraction of the same supernatant was used to measure secreted insulin. The islets were processed to measure total dopamine and insulin content. Data from each group were normalized to the respective islet dopamine content, and reported as the percentage of the islet dopamine content. n represents the number of experimental groups.

2.2.4 Insulin secretion assay

After being cultured overnight following the isolation procedure, the islets were equilibrated for 1 hour in Krebs Ringer Bicarbonate HEPES Buffer (KRBH) at 37 °C in humidified 5% CO_2 atmosphere. KRBH components were: 128.8 mM NaCl, 4.8 mM KCl, 1.2 mM KH_2PO_4, 1.2 mM $MgSO_4$, 2.5 mM $CaCl_2$, 5 mM $NaHCO_3$, 10 mM HEPES, 0.1 % bovine serum albumin, pH 7.4. During the equilibration period glucose concentration was 2.8 mM. Islets were then transferred in 1.5 ml tubes (4 islets per tube) containing KRBH + the condition to be tested. The tubes were incubated at 37 °C in a water-bath for 45 minutes. A fraction of the supernatant was collected to determine secreted insulin, while TritonX-100 was added to the remaining volume at a final concentration of 1 % to extract total islet insulin. The tubes were frozen overnight at -20 °C. Initially insulin concentration was measured by RIA in the Vanderbilt Hormone Assay Core. But later I measured the insulin concentration using the Insulin (Mouse) Ultrasensitive ELISA (ALPCO). Each condition was tested in triplicate. Insulin secretion results were always expressed as the percentage of secreted insulin relative to the total insulin content of the islets. *n* represents the number of mice used to test each condition.

2.2.5 Statistical analysis

Data analyses were performed using GraphPad Prism version 4.03 for Windows, GraphPad Software, San Diego California USA, www.graphpad.com.

Data are presented as mean ±SEM. Significance was evaluated by Student's *t* test, and defined as P < 0.05.

2.3 Examining dopamine accumulation in the islets

2.3.1 <u>Ths synthesis of dopamine from available L-dopa</u>

As described in section 2.1, the experiments presented in this section were designed to test the first part of our hypothesis focusing on whether dopamine is 1) naturally present in the islet cells, 2) produced by islet cells, and 3) co-secreted with insulin. This part of the hypothesis is independent from the other questions that pertain to how dopamine produces the inhibition of GSIS. Nonetheless it is a keystone component to demonstrate that a dopaminergic negative feedback regulates GSIS.

First, I measured the amount of dopamine, if any, present in the pancreatic islets of C57Bl6 mice. Due to the small size of our specimen (one islet can have from 100 to 10000 cells), I decided to use all the islets that could be isolated from a mouse for each dopamine measurement. I used the protocol described in 2.2.2 to extract and determine dopamine and protein content of the islet homogenates. I also wanted to be able to determine if the dopamine that I would detect was indeed coming from the islet cells, or was instead coming from residual acinar tissue (that has been shown to be enriched in dopamine itself (123)), or from the remnant fragment of adrenergic fibers in the islets. Therefore I

measured the amount of dopamine present in the islets at 4 time points: immediately after the isolation, after 1 hour, 2 hours and 24 hours of culture in islet medium.
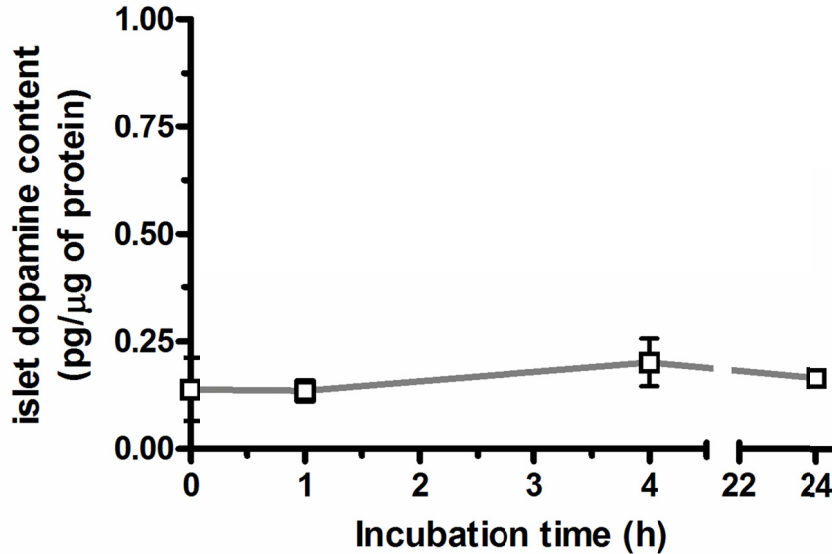
Figure 7: The dopamine content of isolated islets, as measured immediately after the isolation and after different time intervals in culture medium (n = 3-4). (from (152), copyright 2012, The Endocrine Society).

The rationale for this experiment was that during the time in culture, both the acinar cells and the severed adrenergic fibers undergo degradation, leaving just the dopamine content of the islets. As shown in Figure 7, dopamine was detectable in freshly isolated islets, and the average dopamine content of the islets did not change during up to 24 hours of culture, indicating that dopamine was actually stored in the islet cells. Since there is no statistically significant difference between the values obtained at different times, I pooled them together to estimate the average dopamine content of the islets:

0.161 ± 0.020 pg/µg of protein (n = 13). This value corresponds to approximately 0.5 pg of dopamine/islet. This result confirmed that islets cells contain dopamine.

With regard to the amount dopamine I measured in the freshly isolated islets, I found it to be much lower that what has been previously reported by Hansen and Hedeskov (132) or by Lundquist *et al.* (140). After converting our data to the same units, 0.161 ± 0.020 pg/µg of protein corresponds to 0.158 ± 0.020 µmol/Kg of islet wet weight (using the same conversion factors as (140), which assume the protein content to be 15% of the wet weight of a tissue), this value is 10 times lower of the 1.7 µmol/Kg of islet wet weight that has been reported in (140) and 100 time lower that the 16.8 ± 7.2 µmol/Kg of islet wet weight reported in (132). Even if Hansen and Hedeskov admittedly state that their value is much higher than expected, I still cannot identify a specific reason for the discrepancy between our estimate and the data from Lundquist *et al.*. However, I can present few possible explanations. First, the purity of the islet specimen is crucial, and if the islets contain acinar tissue, this would result in elevated dopamine content. Second, there can be variability within mouse strains: I used C57Bl6 male mice, Lundquist *et al.* used NMRI female mice, and Hansen and Hedeskov used albino male mice (Theiller's original strain, Tuck & Son, Rayleigh, Essex, UK). Third the animal feeding state, or the particular diet used, both can affect the dopamine content of the islets, since L-dopa levels in the plasma fluctuate with meals (153). Fourth the method used to extract and measure dopamine content, and the different normalization choice. I used an affinity gel and an ELISA and normalized our result to the protein content.

Lundquist *et al.* used alumina extraction and HPLC, and normalized their results to the protein content. Hansen and Hedeskov used thin layer chromatography and double isotope radioactive labeling technique, and normalized their result to the DNA content. As a final consideration, our estimate of the dopamine content of the islets is lower than the value reported for the striatum, but this is expected since that is the dopamine richest region of the brain (212.1 ± 19.8 pg/μg of protein (154)). Nonetheless, even if this amount may appear low, I will show in the next chapter that it is sufficient to exert a tonic inhibition on GSIS.

Next I wanted to know if islet cells can efficiently produce dopamine from its precursors. It has been reported previously that mouse islet cells express TH and AADC (142), therefore they could synthesize dopamine either starting from tyrosine or from L-dopa. I chose to use L-dopa as the precursor for our experiments for two practical reasons: more cells express AADC while only a few show TH expression (142), and TH activity is the rate limiting step in the dopamine synthesis process. So L-dopa can be processed by more islet cells, and would produce a more rapid response. I added 10 μM of L-dopa to the islet culture medium and I measured the amount of dopamine in the islet immediately after the isolation procedure, or after 30 minutes, 1 hour, 2 hours, 4 hours and 24 hours of culture. The results are shown in Figure 8. The incubation of isolated islets in medium supplemented with L-dopa produced a rapid and saturable increase in their dopamine content to an average value of 4.76 ± 0.48 pg/μg of protein (n = 28).
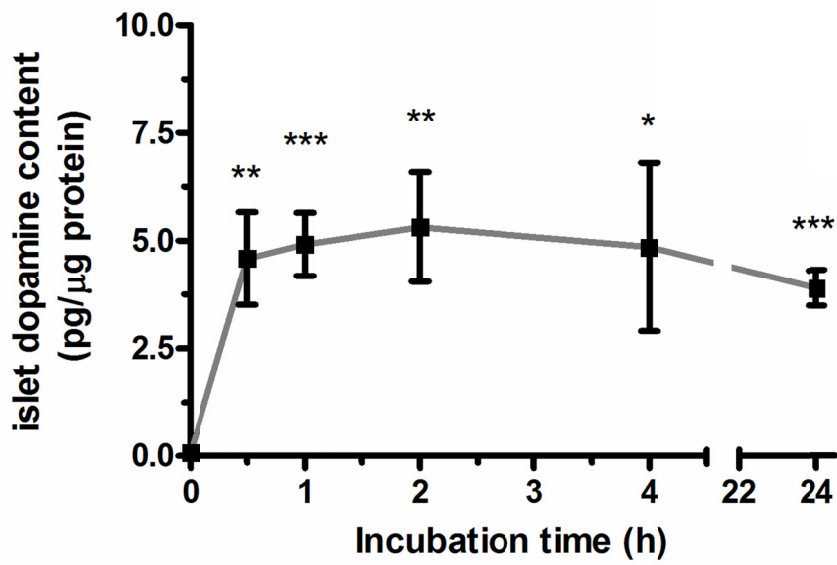
Figure 8: The effects of L-dopa on the dopamine content of pancreatic islets. The dopamine content was measured immediately after the isolation, or after different times in culture with islet medium + 10 μM L-dopa (n = 4-7). *, P < 0.05; **, P < 0.01; *** P < 0.001 *vs.* the incubation time = 0 h. (from (152), copyright 2012, The Endocrine Society).

After an incubation of 30 minutes the dopamine content had reached its maximum level, confirming that the islet cells synthesize and accumulate dopamine from available L-dopa. This fast response was expected based on the properties of the AADC enzyme in the islets described by Lindström (141). That work reported a Km ≈ 3.3 mM and a V_{MAX} ≈ 330 mmol/Kg of dry islet per hour for AADC in intact islets and he described the uptake of L-dopa by intact islets as being "well in excess of the decarboxylation rate and thus probably not rate limiting".

Next I performed a control experiment in which I verified that the L-dopa induced effect could be blocked by an inhibitor of AADC. Additionally I

measured the L-dopa induced increase of dopamine content of the islets *in vivo*.
The results are shown in Figure 9.
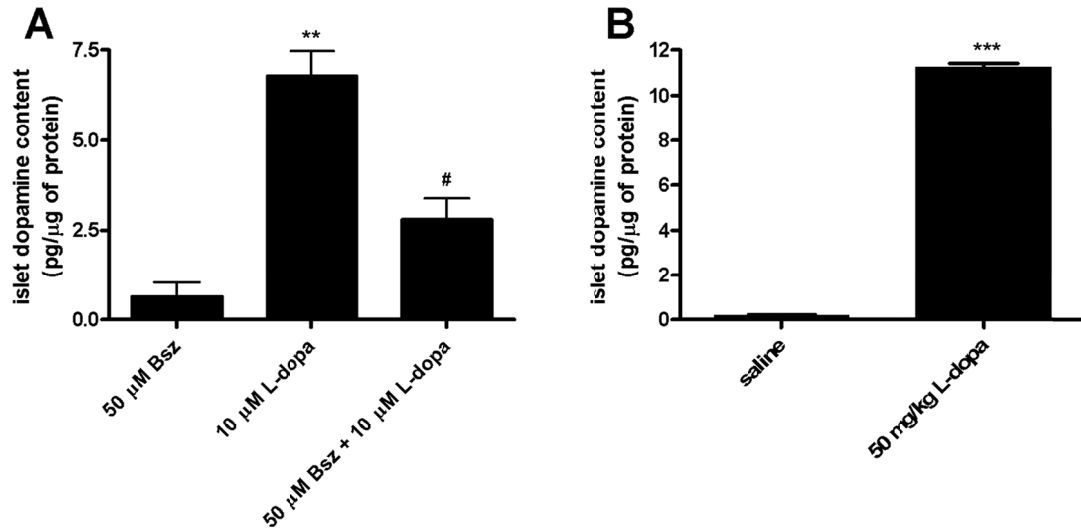
Figure 9: A: The dopamine content of pancreatic islets was measured after a 30
minutes incubation in presence of 50 µM benserazide, 10 µM L-dopa, and a
combination of 50 µM benserazide + 10 µM L-dopa (n = 2-3). ** P < 0.01 versus
50 µM benserazide; # P < 0.05 versus 10 µM L-dopa. D: The dopamine content
of pancreatic islets was measured immediately after isolation from mice that have
received an intraperitoneal injection of saline solution or 50 mg/kg of L-dopa 30
minutes prior to surgery (n = 2). *** P < 0.001 versus saline. Bsz = benserazide.
(from (152), copyright 2012, The Endocrine Society).

As anticipated, the inhibitor benserazide significantly reduced the

amount of dopamine in the islets. But more interestingly, injecting L-dopa

intraperitoneally resulted in a dopamine content of 11.29 ±0.14 pg/µg of protein

that is ~ 2-fold higher than our *in vitro* experiments. There are two likely

explanations for this difference. One is the lack of efficient perfusion of the islets

in culture compared to *in vivo* islets, which are provided with a rich vasculature

and therefore a better perfusion. The second reason could be that our

intraperitoneal injection may have produced a plasma concentration of L-dopa much higher than the 10 µM that was used for the *in vitro* experiments.

2.3.2 The secretion of dopamine from the islet cells

I showed in the previous section that the islets can produce and accumulate dopamine. Next I tested the hypothesis that dopamine is co-secreted with insulin to affect GSIS. In the first set of experiments I investigated the effects of L-dopa induced dopamine accumulation on GSIS from the intact pancreatic islets. Static incubation experiments show that increasing concentrations of L-dopa (0.1 µM, 1 µM, 10 µM, 100 µM) mixed with glucose stimulus (16.7 mM glucose) significantly inhibited GSIS (see Figure 10A).
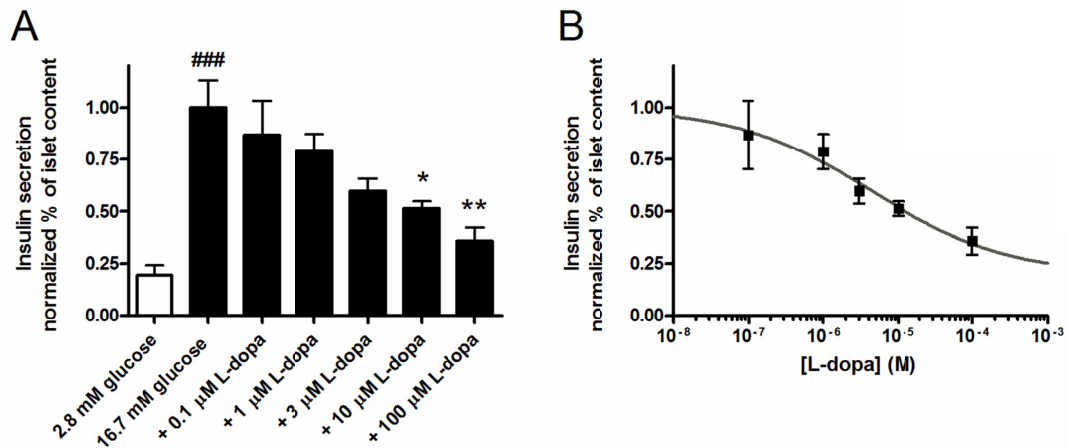
Figure 10: A: Insulin secretion measured at 2.8 mM glucose, 16.7 mM glucose, and 16.7 mM glucose plus increasing concentrations of L-dopa as indicated (n = 5-13). B: Sigmoidal dose response curve fit of insulin secretion stimulated by 16.7 mM glucose in presence of 0.1 µM, 1 µM, 3 µM, 10 µM, 100 µM L-dopa; $R^2 = 0.97$, — best-fit EC50 = 4.4 µM (n = 5-6). ### $P < 0.001$ *versus* 2.8 mM glucose; * $P < 0.05$, ** $P < 0.01$ *versus* 16.7 mM glucose.(from (152), copyright 2012, The Endocrine Society).

40

This effect was dose-dependent with an estimated EC_{50} = 4.4 µM (Figure 10B). I interpreted this result as a consequence of the fast uptake and conversion of L-dopa to dopamine, which makes the latter available for secretion during the 45 minutes incubation time that is used to measure insulin secretion. On the contrary, in non-stimulatory condition (2.8 mM glucose) L-dopa treatment did not change insulin basal secretion, as shown in Figure 11A. This is in agreement with the hypothesis that secretion needs to be triggered for dopamine to produce any effect.
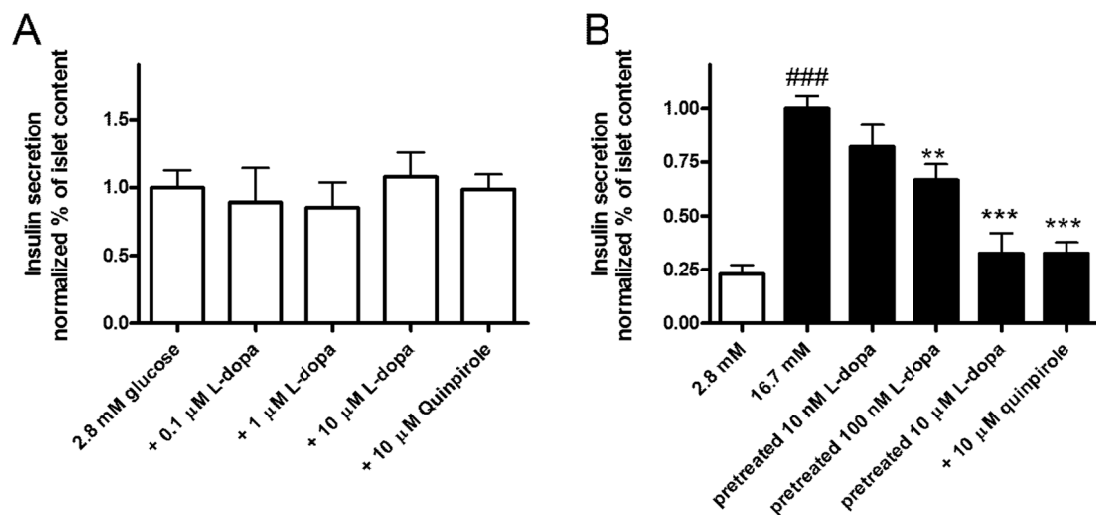
Figure 11: A: Insulin secretion measured at 2.8 mM glucose, and 2.8 mM glucose + 0.1 µM, 1 µM, 10 µM L-dopa, and 10 µM quinpirole (n = 4-12). B: Insulin secretion measured at 2.8 mM glucose, 16.7 mM glucose, 16.7 mM glucose after pre-treatment with 10 nM, 100 nM and 10 µM L-dopa, 16.7 mM glucose + 10 µM quinpirole (n = 4-11). ### $P < 0.001$ *versus* 2.8 mM glucose; ** $P < 0.01$, *** $P < 0.001$ *versus* 16.7 mM glucose.(from (152), copyright 2012, The Endocrine Society).

Based on the work of Rubí *et al. (155)* dopamine acts on D2-like receptors. Therefore quinpirole (a D2/D3/D4 agonist) should replicate the effects of dopamine on GSIS. I observed that the addition of 10 µM quinpirole the non-stimulatory condition did not change insulin secretion compared to the untreated islets Figure 11A. This confirms that dopamine effects can only be observed when secretion is stimulated.

At this point I wanted to rule out the possibility that L-dopa had a direct effect on GSIS, independent of dopamine accumulation. Therefore I performed insulin secretion experiments to measure GSIS in the presence of elevated islet dopamine content but in the absence of L-dopa. In this case, the islets were treated with three different concentrations of L-dopa for 60 minutes to increase their dopamine content. After this treatment they were used for the insulin secretion assay, using only the glucose stimulus (Figure 11B). The results show that pre-treatment with 100 nM and 10 µM L-dopa significantly inhibited GSIS, and addition of the D2/D3/D4 agonist quinpirole produced a comparable inhibition of GSIS. Also I observed that treatment with 10 nM L-dopa, which is comparable to 5 nM plasma concentration of L-dopa in the mouse (149, 156), produced a trend toward GSIS inhibition but did not reach statistical significance for the number of observations used (n=7). This result is at least in part due to the limitations of *in vitro* settings versus physiological situation. In the mouse, the islet is constantly exposed to L-dopa, while the *in vitro* experiments depend on an acute treatment. It is also known that L-dopa is quickly oxidized in aqueous solution, and for this reason ascorbic acid is often added as a preservative. In our

experiments, though, I could not add ascorbic acid because it affects GSIS directly (157). Thus, the effective concentration of L-dopa in the final solution may be diminished by oxidation, and this effect would particularly affect the results at lower L-dopa concentrations.

The data presented so far are in agreement with the working hypothesis that calls for dopamine secretion in order to produce inhibition of GSIS, and the results in Figure 11B clearly support it. But considering that dopamine, even if secreted, would be inactive at low glucose, as the quinpirole experiment showed, I cannot draw any conclusion about when dopamine is being secreted by the islet cells. According to the findings by Ericson *et al.* (138) dopamine accumulates in the insulin secretory granules of the β-cells. Based on that I hypothesized that dopamine is co-secreted with insulin. I wanted to have a direct measurement of dopamine secretion to clarify this part of the model. So I designed an experiment to measure both insulin secretion and dopamine secretion from the same islets.

The main challenge in this experiment was the small amount of dopamine that I anticipated to be secreted. To overcome this problem, I increased the number of islets to be used in each test. Also I treated the islets with 10 μM L-dopa for 40 minutes before the secretion experiment to maximally increase their dopamine content. While the increase in dopamine content would improve the detectability of dopamine secretion, it would also inhibit GSIS, as seen in Figure 11B. For this reason, glucose stimulation alone would not be a sufficient stimulus to test the co-secretion of dopamine and insulin. Therefore I

added 50 µM forskolin to force insulin secretion even in the presence of

dopamine induced inhibition of GSIS. The results of the experiment are shown in

Figure 12.
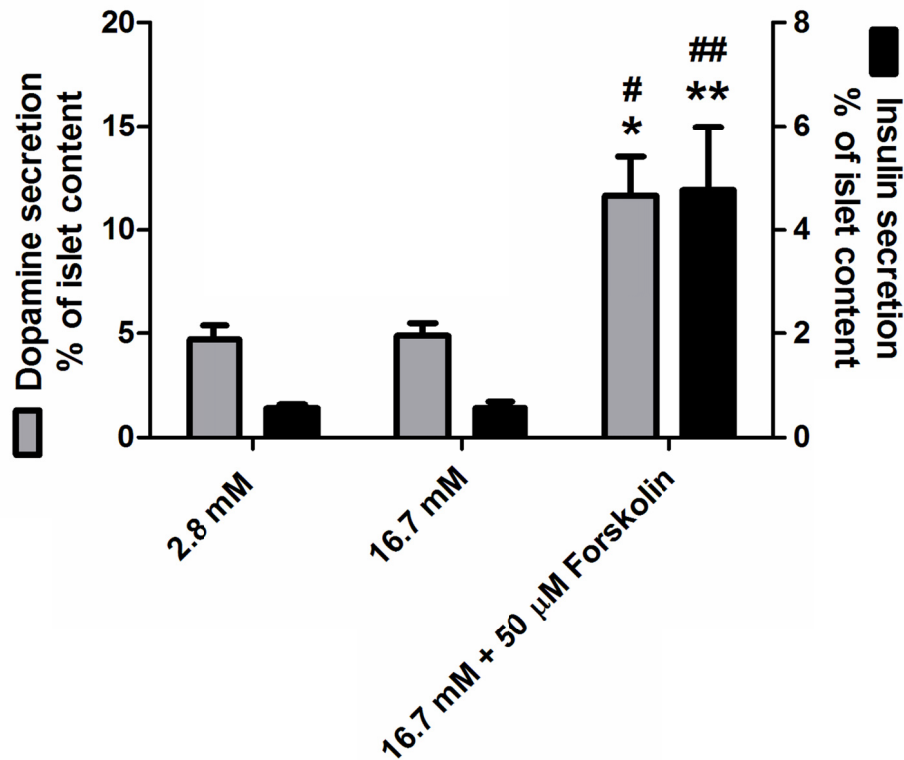
Figure 12: Dopamine secretion and insulin secretion from pancreatic islets measured at 2.8 mM glucose, 16.7 mM glucose, 16.7 mM glucose + 50 µm forskolin (n = 4-5). # P < 0.05, ## P < 0.01 *versus* 2.8 mM glucose; * P < 0.05, ** P < 0.01, *versus* 16.7 mM glucose. (from (152), copyright 2012, The Endocrine Society).

When stimulated with 2.8 mM glucose, the islets secreted 4.73 ±

0.65 % of their dopamine content (n = 5). Stimulation with 16.7 mM glucose

resulted in the secretion of 4.88 ± 0.61 % of islet dopamine content (n = 5). When

the islets were maximally stimulated with 16.7 mM glucose and 50 µM forskolin,

they secreted 11.7 ±1.9 % of their dopamine content (n = 6). The insulin

secretion from the same experimental groups of islets showed an inhibition of

GSIS, with no statistically significant difference between insulin secretion at 2.8

mM glucose versus 16.7 mM glucose (0.57 ± 0.07 % of islet insulin content, n =5,

and 0.57 ± 0.12 % of islet insulin content, n =5), consistent with Figure 11B.

Insulin secretion was maximally stimulated by 16.7 mM glucose + 50 µM

forskolin (4.8 ± 1.2 % of islet insulin content, n =4). I chose forskolin to overcome

the dopamine-induced inhibition of GSIS because it can stimulate insulin

secretion even in the absence of extracellular calcium influx, by elevating cAMP

(158). As I show in the next chapter, this would relieve the dopamine-induced

inhibition of GSIS because the inhibition itself correlates with a possible reduction

of calcium influx.

The design of this experiment proved to be very critical to obtain data

that could be easily interpreted. It took few rounds of puzzling results before I

could figure out the correct approach. In my first attempt, I tried to reduce the

number of islets necessary for the experiment, by applying a series of stimuli to

the same group of islets and collect the supernatant after each stimulus. The

result was that the amount of secreted dopamine would always be very high for

the first stimulus. I measured dopamine secretion over an interval of two hours

under the same condition (2.8 mM glucose), and observed that soon after the

L-dopa treatment, dopamine is constitutively secreted by the islet, until its content

returns to its basal level. This behavior can be explained by assuming that the

excess of newly produced dopamine saturates the insulin granule but also the

synaptic-like micro vesicles. These vesicles could be responsible for the secretion of dopamine in the absence of a glucose stimulus. Therefore I decided that the best strategy was to work in parallel with large groups of islets. In this way each group received the assigned stimulus at the same time after the dopamine loading step. Following this protocol a change in dopamine secretion would not be masked by the time dependent decrease in dopamine content.

2.4   Summary

In this chapter, I introduced the relevant literature that in the past 50 years has contributed to build our understanding of the role of dopamine in regulating insulin secretion from the pancreatic islet. Previous studies have shown that dopamine can inhibit GSIS in isolated islets (3), but there is no consensus on the availability or origin of any dopamine that can act on islets *in vivo*. Even when dopamine accumulation was qualitatively found in mouse β-cells following an L-dopa injection to the animal (138), the site of synthesis was not addressed. This has led to a conundrum since the islets are sensitive to dopamine, but the dopamine concentration in the plasma is too low (0.67 ± 0.21 nM in C57Bl6 mice) to trigger its receptor (148, 149), and dopaminergic innervation of the pancreas has not been reported. Thus, islet sensitivity to exogenous dopamine has not generally been considered physiologically relevant.

I tested the hypothesis that the islet itself produces dopamine from circulating L-dopa (149, 156), which has not yet been rigorously examined in a single species. In this chapter I addressed the question of dopamine synthesis

46

and secretion in mouse islet cells. By focusing our study on isolated mouse islets, I could measure dopamine accumulation due solely from synthetic activity of the islets (Figure 7 and Figure 8), excluding the contribution of other tissues (138). Our data show that freshly isolated islets contain dopamine at a level of ~ 0.5 pg/islet. This value should reflect as close as possible the *in vivo* condition of an islet in its native environment. When L-dopa was increased *in vitro*, I measured a rapid 30-fold increase in the islet dopamine content. Similarly, when circulating L-dopa levels were raised by exogenous administration *in vivo*, I saw a 50-fold increase in dopamine concentration, which corresponds to a robust inhibition of GSIS. I observed a dose-dependent inhibition of GSIS by combining L-dopa and glucose, but based on the results in Figure 11B I conclude that this effect was due to increased dopamine content, and not a direct pharmacological effect of L-dopa on GSIS. Neither L-dopa nor the dopamine receptor agonist quinpirole altered basal insulin secretion at low glucose concentration. This supports the hypothesis that dopamine only produces its effect when insulin is being secreted. Also it suggest that intracellular dopamine does not affect GSIS. Only when dopamine is secreted by the islet it shows its inhibitory effect. From these experiments I conclude that dopamine is physiologically present in the pancreatic islet of the mouse. It is produced by the islets and this production can be significantly boosted by increasing the availability of the precursor L-dopa.

Next I studied when dopamine is secreted by the β-cells in the islet. Based on findings by Ericson et al. using radiolabeled L-dopa (138), I hypothesized that dopamine is co-secreted with insulin, and I tested this concept

by simultaneously measuring dopamine and insulin secretion under different conditions. These results in Figure 12 show that dopamine secretion follows insulin secretion, which is a circumstantial evidence of the co-localization of the two substances in the same granules.

By the same time that our work was published, a study by Simpson *et al.* (159) was published, where they authors similarly study a dopamine-mediated autocrine inhibition in human islets. They used Nafion-coated carbon fiber microelectrodes to measure dopamine secretion by chrono-amperometry and voltammetry. They come to the same conclusion: dopamine is secreted from the islet in response to glucose. Moreover, they performed perfusion experiments under glucose stimulation and reported dopamine secretion peaks largely coincident with insulin secretion peaks. These independent experiments corroborate our conclusion that dopamine and insulin co-localize in the secretory granule of the β-cells.

Having established that β-cells synthesize and secrete dopamine during GSIS, I proceeded to investigate how dopamine inhibits GSIS. The results of those experiments are described in the next chapter that pertains to the identification of the specific receptor that dopamine is signaling through, and the intracellular changes that are associated with the dopamine-induced inhibition of GSIS.

CHAPTER

3. DOPAMINE SIGNALING IN THE ISLETS

3.1 Introduction

The material presented in this chapter summarizes our work done to
identify the specific dopamine receptor involved in the dopamine-induced
inhibition of GSIS. We know that dopamine signals through a family of five
G-protein coupled receptors named: D1, D2, D3, D4 and D5 (160). Additionally
Rubí et al. first showed expression of dopamine receptor D2 (DRD2) in the rat
β-cell tumor cell line INS1-E, and described the inhibition of cytoplasmic Ca^{2+}
activity and insulin secretion by dopamine (3). Two following studies reported
opposite roles for DRD2 in regulating insulin secretion showing both inhibition
and stimulation (161, 162). Hence there is still a controversy about the role of
DRD2 in mouse islets. I studied dopamine signaling in intact isolated islets of
C57Bl6 mice. Also I studied the intracellular changes that follow the activation of
the dopamine signaling cascade in the β-cells, focusing our attention to the
changes in the $[Ca^{2+}]_i$. I identified DRD3 as the mediator of dopamine signaling it
the β-cells. The results of these experiments, combined with the ones presented
in the previous chapter complete the picture of a dopaminergic negative
feedback that regulates GSIS in the mouse. They collectively show that β-cells
produce dopamine from L-dopa, secrete dopamine with insulin, detect the

secreted dopamine signal through their dopamine receptors, and react by decreasing their $[Ca^{2+}]_i$ thereby inhibiting GSIS.

3.2 Materials and methods

3.2.1 <u>NAD(P)H imaging</u>

Combined autofluorescence from nicotinamide adenine dinucleotide (NADH) and nicotinamide adenine dinucleotide phosphate (NADPH) is collectively indicated as NAD(P)H autofluorescence. Both dinucleotides are involved in the redox state of the β-cells as they transfer electrons to other molecules by transitioning from the reduced state (NADH and NADPH) to the oxidized state (NAD^+ and $NADP^+$) and vice versa. As they are both fluorescent only in their reduced form, they can be used to monitor the metabolism of the the β-cells during glucose stimulation (163), as shown in Figure 13. NAD(P)H autofluorescence can be excited using UV light with a wavelength of 360 nm, and the emission is in the 400 nm – 500 nm region. But, the use of the ultraviolet light is highly toxic to living cells. Instead, I used two-photon excitation to excite the NAD(P)H autofluorescence. With this technique a pulsed laser is used to increase the temporal density of the photons, and a high numerical aperture objective is used to concentrate the photons in a small focal spot. The result is a photon density high enough to produce the simultaneous absorption of two

infrared photons by the same molecule that would otherwise need an ultraviolet photon.
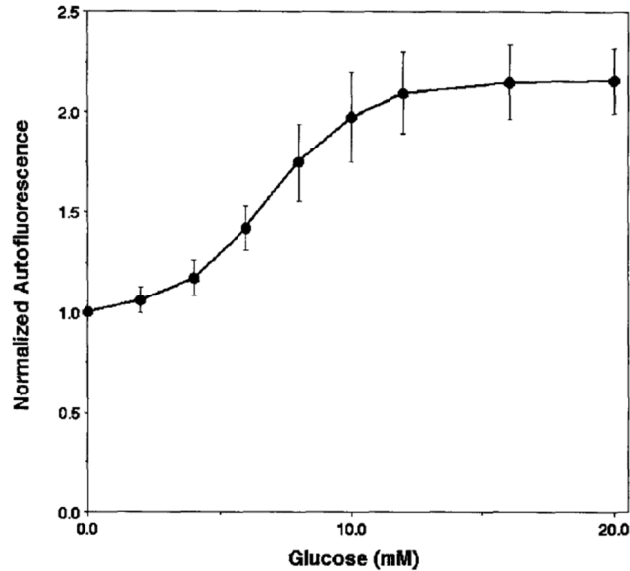
Figure 13: NAD(P)H autofluorescence dose response. Average of responses from 80 β-cells in intact islets. (reprinted from Methods in Enzymology, 307, D. W. Piston and S. M. Knobel, Quantitative imaging of metabolism by two-photon excitation microscopy,351-368, copyright (1999), with permission from Elsevier) (163).

I used a LSM710 laser-scanning confocal microscope (Zeiss Inc.) and a tunable Chameleon Ti:Sapphire laser (Coherent Inc.). The excitation wavelength was set to 710 nm and power was set to 60 mW entering the LSM710 (~5 mW at the sample). I used a Plan-Apochromat 20x/0.8 objective (Zeiss Inc.). Pixel size was 0.830 µm. NAD(P)H autofluorescence was collected through the LSM710 spectral detector with the bandpass filter set from 381 nm to 581 nm. The microscope stage was equipped with a temperature-controlled stage (Zeiss Inc.) to keep the islets at 37°C and 5 % CO_2 during the imaging experiments. Islets were transferred (10 islets per dish) to a 35 mm glass-

bottomed dish (Mat-Tek Corp.) containing freshly prepared imaging media (125 mM NaCl, 5.7 mM KCl, 2.5 mM $CaCl_2$, 1.2 mM $MgCl_2$, 10 mM HEPES, 0.1 % bovine serum albumin, pH 7.4) with 2 mM glucose and equilibrated 30 minutes prior to the experiment. NAD(P)H images were acquired at 2 mM, 8 mM and 16.7 mM glucose and a at 16.7 mM glucose + 3 mM sodium cyanide to have a maximum value for normalization of the results. This is based on the property of cyanide that blocks the mitochondrial electron transport chain, forcing the conversion of all $NAD(P)^+$ to NAD(P)H (164). After this initial group, different groups of islets from the same mouse were then used to image NAD(P)H autofluorescence in the experimental conditions to be tested. *n* represents the number of mice that all the conditions were tested on.

3.2.2 Calcium Imaging

Islets were labeled by incubation with 4μM Fluo-4 AM (Invitrogen) in imaging medium containing 2 mM glucose at room temperature for 45 minutes. The islets were then loaded in a simple microfluidic device on the microscope stage (165) and maintained at 37 °C under humidified 5 % CO_2. The islets were constantly perfused with fresh imaging buffer containing the drug to be tested. I used a Plan-Apochromat 20x/0.8 objective (Zeiss Inc.) and 488 nm excitation laser at 0.3 % of total power. The emission was collected from 492 nm to 622 nm. Pixel size was 0.830 μm. Images were acquired at a rate of 1 frame per second. *n* represents the number of islets.

3.2.3 MIN6 culture

Mouse MIN6 cells (166) were maintained in sodium bicarbonate buffered Dulbecco's modified Eagle's medium (DMEM) with the addition of 10% heat inactivated fetal bovine serum, 50 µM β-mercaptoethanol, 100 units/ml penicillin, and 100 µg/ml streptomycin. Cells were cultured at 37 °C in 5% CO_2 humidified atmosphere.

3.2.4 DRD2-mVenus live imaging

Islets and MIN6 cells were transduced using adeno-associated virus (AAV) particles for the expression of the fusion protein in which the long isoform of the human DRD2 ($DRD2_L$) is fused to the yellow fluorescent protein mVenus. AAV for the expression of mVenus alone was used as a control. The AAV particles were a generous gift from Dr. Jonathan Javitch (Columbia University). Briefly, the islets or cells were exposed to AAV for 18 hours and then cultured for 48 hours in regular medium to obtain maximal expression prior to imaging. The islets were imaged on the LSM710 confocal microscope (Zeiss Inc.) using a Fluar 40X oil objective, with NA=1.30. I used a 514 laser line to excite the mVenus fluorescence, and I collected the emission setting the bandpass from 518 nm to 613 nm. The pixel dwell time was 25.2 µs. To image whole islets, I acquired z-stack of images with a pixel size of 0.415 µm and 2 µm between each image in the stack. To image single cells in the islet, I changed the pixel size to 0.086 µm. For imaging experiments with MIN6 cells, I used a Nikon Eclipse Ti microscope equipped with a TIRF objective (ApoTirf 60X Oil DIC N2 NA = 1.49).

The widefield fluorescence images were acquired using a Xenon lamp excitation and a GFP ex/em filter set. For the TIRF images the excitation was provided by a 488 nm diode laser while the same emission filter was used (505 bp). The acquisition time was 1 frame/s and the pixel size was 0.086 μm. All the live fluorescence experiments were performed at 37 ºC under humidified 5 % CO_2.

3.2.5 Image analysis

Image analysis was performed using ImageJ (167). For each image, background was subtracted and regions of interest (ROIs) were drawn corresponding to the islets. The average intensity in these ROIs was calculated for each frame. The intensity plots from calcium imaging experiments were subsequently processed for frequency analysis using SpectralAnalysis v3.0, a freely available routine written for MATLAB(168). For the NAD(P)H images, the average intensity was then averaged between the islets from the same mouse and expressed as a percentage of the intensity obtained with cyanide.

3.2.6 SDS-PAGE and western blot

Islets were transferred to a tube and rinsed once in ice cold PBS. The tube was kept on ice and the lysis buffer was added. The lysis buffer had the following components: 150 mM NaCl, 1 % TritonX-100, 0.5 % sodium deoxycholate, 0.1 % SDS, 50 mM Tris pH 8.0, 5 mM EDTA, 1 mM EGTA, 5 mM NaF, 1 mM Na_3VO_4, 1 mM PMSF, and a cocktail of mammalian protease inhibitors (P8340 from Sigma). Lysis proceeded on ice for 45 minutes, followed

by sonication for 5 minutes. The sample was centrifuged at 14000 *g* for 30 minutes at 4 °C. The supernatant was collected, assayed for protein concentration and mixed with Laemli loading buffer. Mouse brain extract (B6928, Sigma) was used as positive control. The islet lysates and positive control were subjected to SDS/PAGE (10 %) and then transferred onto nitrocellulose membrane. The membranes were blocked for 1 hour at room temperature with Tris-buffered saline containing 0.1 % Tween-20 (TBS-T), 5 % BSA, and 5 mM sodium azide. For DRD2 immunoblotting, the membranes were incubated with the rabbit anti-D2 polyclonal antibody (AB5084P, Millipore) (1:1000) at 4 °C overnight. Secondary incubation was done with goat anti-rabbit IgG horseradish peroxydase conjugate antibody (W4011, Promega) diluted 1:5000. The specific control peptide (AG221, Millipore) was used to neutralize the rabbit anti-D2 antibody in the control experiment. The same protocol was used for immunoblotting of DAT, but with a 1:1000 dilution of mouse anti-DAT monoclonal antibody (mAb16, generous gift from Dr. Roxanne A. Vaughan at University of North Dakota). The secondary antibody was a goat anti-mouse IgG horseradish peroxydase conjugated, diluted 1:5000. In all of the experiments, signal was detected by chemiluminescence (ECL Plus system from GE Healthcare, and Kodak BioMax light film).

For the DRD3 immunoblotting, the islets were homogenized in Dounce homogenizer in lysis buffer without detergents. The homogenate was centrifuged at 7000 *g* for 5 min. The resulting pellet was dissolved in lysis buffer and defined as the nuclear fraction. The supernatant was centrifuged at 500000 *g* for 10

minutes. The resulting pellet was dissolved in lysis buffer and defined as the membrane fraction. The second supernatant was used as the cytosolic fraction. The primary antibody used for this experiment was a rabbit polyclonal antibody (ab42114, from Abcam inc.) at a 1:750 dilution. The secondary antibody was the same used for the DRD2 immunoblotting. The control peptide used in the neutralization experiment was a 19 amino acids D3 peptide (ab128688, from Abcam Inc.)

3.2.7 Design PCR strategy for genotyping DRD2-KO mice

During the course of our study I received breeding pairs of mice carrying a null-mutation in of the Drd2 gene from Dr. Claudia Schmauss (Department of Psychiatry/Neuroscience, Columbia University, New York). They were generated by gene targeting strategy as described in (169). In detail, a 2 kb restriction fragment of the Drd2 gene was replaced with the poly(A^+)less PGK-neo^r-cassette. This insertion replaces the majority of exon 2 and results in the null mutation by the introduction of a stop codon in the 5' end of the cassette.

When I received the mice, DNA extraction and following southern blotting was the only protocol available for genotyping these mice. The DNA region containing the Drd2 gene is GC-rich, therefore some polymerases can fail to amplify it. I tested different approaches using commercially available polymerases that are specifically designed to amplify GC-rich regions, as well as multiple primer pairs. I established a reliable PCR protocol that does not required

special polymerases, and that correctly identifies the wild type and the mutant allele in the genomic DNA.

The primer pair for the wild type allele amplifies a 515 bp product in the DNA region that is deleted in the mutant allele. The sense primer is: D2wt1 5'-AACTCAGAGAGCTGACCCTCCT-3'. The antisense primer is: D2wt2 5'-AGAACAAGCTGAGCATTGAGC-3'. Conversely the primer pair for the mutant allele amplifies a 673 bp product that includes part of the Neo^r cassette and part of the Drd2 gene. The sense primer is: D2KOc1 5'-ATGAACTGCAGGACGAGGCA-3'. The antisense primer is: D2KOc2 5'-AAATGGGTGGAGCCAAGAAAG-3'. I used Extract-N-Amp™ Tissue PCR Kit (Sigma) for the DNA extraction following the vendor's instruction. I added to each reaction mix 4 µl of tissue extract and 0.5 µl of each of the 4 primers (from 10 µM solution). The thermocycler sequence was: 95 °C for 2 minutes, 95 °C for 20 seconds, 60 °C for 10 seconds, 72 °C for 5 seconds, 72 °C for 3 minutes, and the steps from the second to the fourth are repeated 35 times. A wild type mouse (D2$^{+/+}$) produces a single 515 bp product, a homozygous mutant mouse (D2$^{-/-}$) produces a single 673 bp product, and a heterozygous mouse (D2$^{+/-}$) produces both products.

3.3   The intracellular effect of dopamine signaling in the β-cell

3.3.1   The effects of dopamine on the redox state of the β-cells

GSIS requires the metabolism of glucose via the mitochondrial respiration to produce the ATP. This is the first step in the chain of events that lead to insulin secretion, as it is described in section 1.1.3. Dopamine instead can produce reactive oxygen species (as hydrogen peroxide), semiquinones and quinones through the activity of MAO-B or via auto-oxidation (170, 171). These highly reactive species are cytotoxic in elevated concentrations and are thought to be the cause of dopamine and L-dopa neurotoxicity in culture (172, 173). Notably, it has been shown that dopamine can inhibit mitochondrial respiration (174). For these reason, I first tested the possibility that dopamine-induced inhibition of GSIS was just the direct result of impaired mitochondrial function in β-cell.

I used two photon excitation microscopy to excite autofluorescence from NAD(P)H, which increases with the metabolism of glucose during the production of ATP. Therefore, it can be used to monitor the redox state of the β-cell in the islets (163). The rationale for this experiment was that if dopamine is inhibiting the mitochondrial respiration, then it should prevent the glucose dependent increase in NAD(P)H autofluorescence. The results are shown in Figure 14.
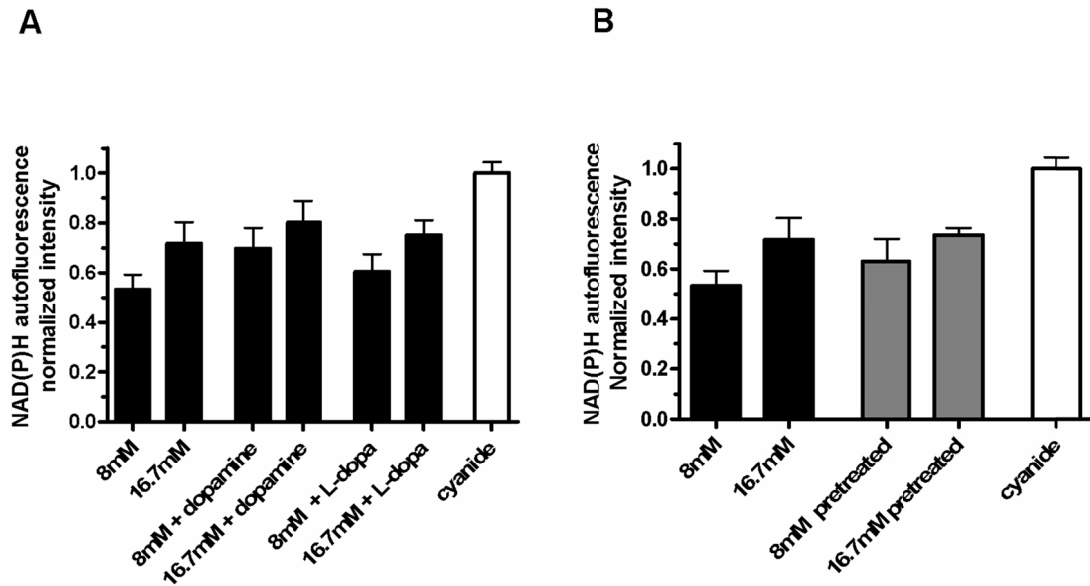
Figure 14: The effects of L-dopa and dopamine on the redox state of pancreatic islets. A: NAD(P)H autofluorescence from isolated islets was measured at 8mM glucose and at 16.7 mM glucose and with 10 µM dopamine or 10 µM L-dopa as indicated; results are normalized to the maximum signal obtained with 3 mM sodium cyanide (n =2-4). B: Islets were incubated with or without 10 µM L-dopa for 30 min prior to the experiment, then NAD(P)H autofluorescence was measured at 8 mM and 16.7 mM glucose (n = 3-4). (from (152), copyright 2012, The Endocrine Society).

I did not detect any statistically significant reduction of the NAD(P)H autofluorescence when I used L-dopa or dopamine mixed with glucose, at a concentration that gives maximal inhibition of GSIS (Figure 14A). Even when the islet dopamine content was increased by L-dopa treatment, the islets did not show decreased NAD(P)H autofluorescence during glucose stimulation (Figure 14B). I concluded that at the concentration I used, dopamine is not inhibiting mitochondrial respiration in the β-cells, and cytotoxicity is not the cause of the dopamine-induced inhibition of GSIS.

3.3.2 The effects of dopamine on the intracellular calcium dynamics

The next best candidate for our study was intracellular calcium. As discussed in section 1.1.3 the rise in $[Ca^{2+}]_i$ causes the exocytosis of insulin granules. Also, calcium channels CaV1.2 and CaV1.3 are possible downstream targets of dopamine receptors (175, 176). Moreover when Rubí *et al.* (3) looked at the effect of dopamine in rat INS1-1E cells, they observed that the 15 mM glucose-induced increase in $[Ca^{2+}]_i$ was reduced in presence of 10 µM dopamine. Therefore it is possible that endogenous dopamine causes the inhibition of GSIS by reducing the influx of Ca^{2+} in intact islets.

I imaged $[Ca^{2+}]_i$ in intact islets using the fluorescent indicator Fluo4-AM that, once in the cytoplasm, emits a fluorescence signal with an intensity that is proportional to $[Ca^{2+}]_i$ and to the concentration of the indicator itself. I used a confocal microscope for this experiment, because it is well suited to image thick specimens as the islets. Instead of measuring the Fluo4 fluorescence just before and after each treatment, I took advantage of the characteristic coordinated response of the β-cells in the islet. I stimulated the islets by increasing the glucose concentration in the imaging media from 2 mM to 8 mM. This treatment triggers the fast $[Ca^{2+}]_i$ oscillations that are exquisitely dependent on the electrical properties of the β-cells membrane. I imaged the $[Ca^{2+}]_i$ oscillations in the islet over time, before and after each treatment. I quantified the frequency of the oscillations instead of their amplitude, so that our data are independent from the concentration of Fluo4, and unaffected by focal drift and photobleaching that can occur during extended imaging time. Having established a robust method to

monitor the changes of the $[Ca^{2+}]_i$ dynamics, I measured the effects of L-dopa

and dopamine for a range of concentrations. Representative traces for these

experiments are shown in Figure 15.
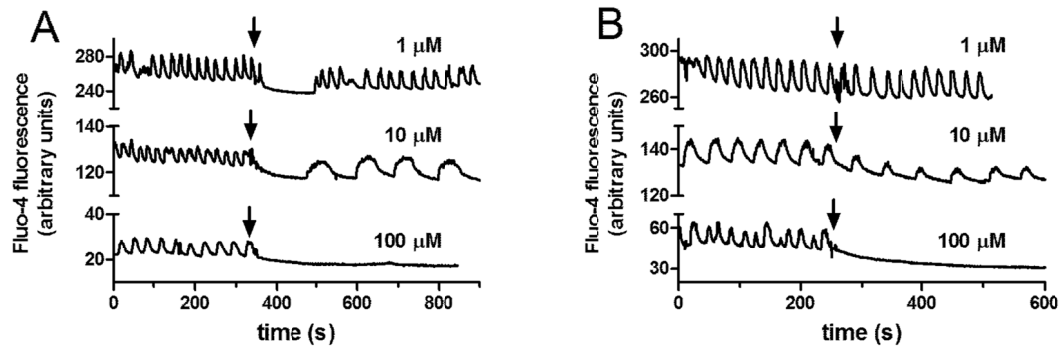
Figure 15: $[Ca^{2+}]_i$ oscillations in isolated islets. A: Representative patterns of $[Ca^{2+}]_i$ oscillations from a single islet before and after dopamine stimulus. The typical oscillation pattern, stimulated by increasing glucose concentration from 2 mM to 8 mM, is shown in the first 300s; the pattern changed after the addition of dopamine at the indicated concentration; the black arrows indicate the time when dopamine was added; the three plots are offset for an easier comparison. B: Representative patterns of $[Ca^{2+}]_i$ oscillations from a single islet before and after L-dopa stimulus. The oscillations were triggered by increasing glucose concentration from 2 mM to 8 mM. The black arrows indicate the time when L-dopa was added. (from (152), copyright 2012, The Endocrine Society).

From the traces in Figure 15 I can see that following the addition of

dopamine and L-dopa there is a transient phase that last ~ 120 seconds before

the islets come to a new steady oscillatory state. I measured the frequency of the

oscillations before adding the drugs, and after the transient phase. The summary

of the results is presented in Figure 16.
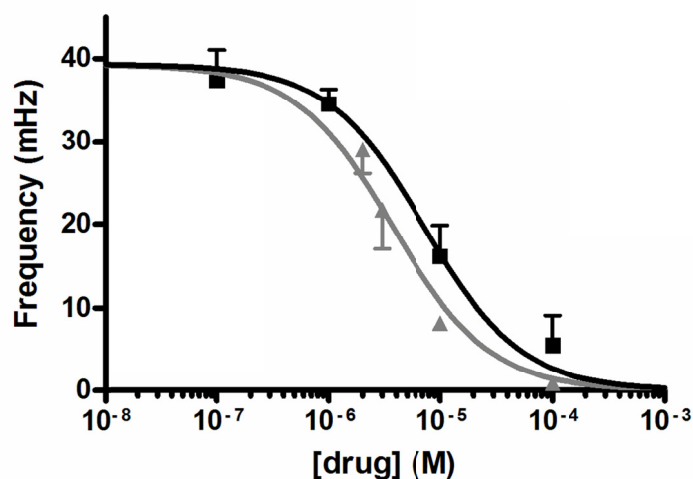
Figure 16: Sigmoidal dose response curve fit of $[Ca^{2+}]_i$ oscillation frequency in response to treatment with dopamine (▲) or L-dopa (■) in conjunction with 8 mM glucose stimulus; — best-fit EC_{50} = 3.8 μM, R^2 = 0.78 (n = 4-7); — best-fit EC_{50} = 7.2 μM, R^2 = 0.89 (n = 5-14); The difference between EC_{50} values is statistically significant with a $P < 0.05$. (from (152), copyright 2012, The Endocrine Society).

The $[Ca^{2+}]_i$ oscillations had a frequency of 39.3 ± 1.3 mHz (n = 58) (that is a period of 27.19 ±0.98 s) when stimulated with 8 mM glucose. As seen in Figure 15, I consistently observed a decrease in the $[Ca^{2+}]_i$ oscillation frequency when I stimulated the islets with 8 mM glucose + dopamine (▲) or L-dopa (■). Both L-dopa and dopamine diminished the frequency in a dose dependent manner. A sigmoidal fit of the data gives an estimated EC_{50} for L-dopa and dopamine of 7.2-μM and 3.8 μM respectively. According to our working model, L-dopa is being converted to dopamine during the stimulus and the resulting dopamine is producing the change in frequency $[Ca^{2+}]_i$ oscillation. Therefore I anticipated that, if there was any difference between the two EC_{50} values, L-dopa should have had the greater value, which was indeed the case.

I confirmed that L-dopa was not directly acting on the β-cells with the experiment in Figure 17. I treated groups of islets with 10 μM L-dopa for 30 minutes, to increase the dopamine content of the islets. Then I stimulated the islets with 8 mM glucose, and I measured the $[Ca^{2+}]_i$ oscillation. I repeated the same procedure with groups of untreated islets.
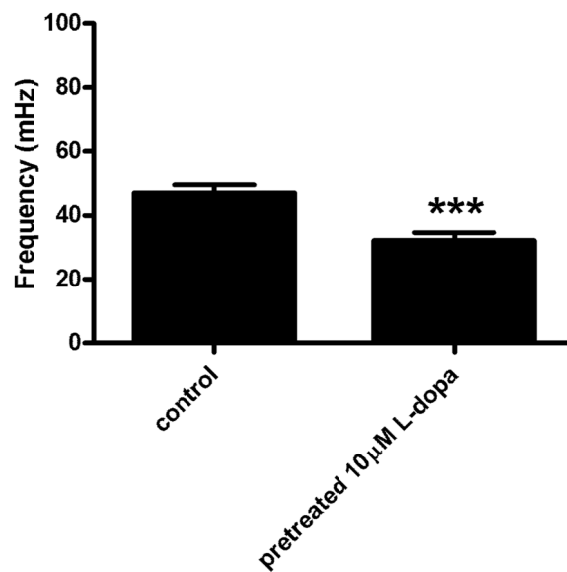
Figure 17: The $[Ca^{2+}]_i$ oscillation frequency of control islets *versus* islets with elevated dopamine content resulting from a pretreatment with L-dopa as indicated (n = 8); *** P < 0.001; (from (152), copyright 2012, The Endocrine Society).

As shown in Figure 17, the islets that had the elevated dopamine content responded to the glucose stimulus with significantly slower oscillations. Their frequency was 32.1 ± 2.5 mHz (n = 8), while the control group had oscillation with a frequency of 47.1 ±2.4 mHz (n = 8).

In Figure 18, I tested how this reduction in frequency correlated with the reduction in GSIS, which I showed in section 2.3.2. There was a significant correlation between the frequency of $[Ca^{2+}]_i$ oscillations at 8 mM glucose and the percentage of secreted insulin at 16.8 mM glucose. This suggests that dopamine changes the electrical properties (i.e. ionic conductances) of the β-cell membrane, thus leading to observed reduction in frequency. These are likely the same changes as those causing the inhibition of GSIS at 16.7 mM glucose. I propose that dopamine is acting on its receptor, resulting in a change in conductance of the calcium channels. I will discuss in chapter V how I plan to test this hypothesis with new experiments.
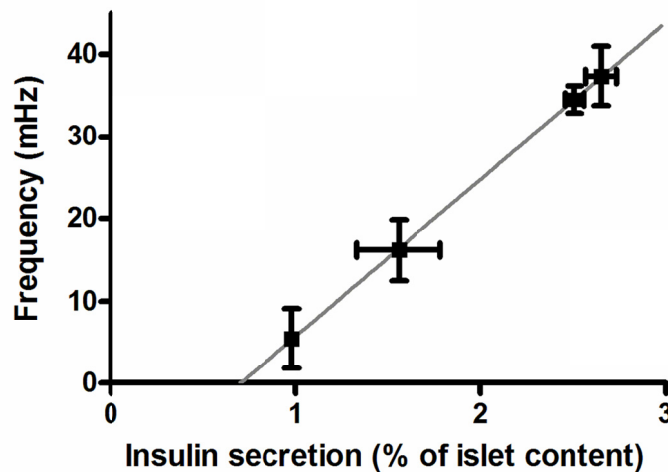
Figure 18: Plot of $[Ca^{2+}]_i$ oscillation frequency *versus* insulin secretion from two independents sets of experiments; the gray line (—) represents the linear fit of the data ($R^2 = 0.999$); Pearson's correlation coefficient r = 1 with P < 0.001; (from (152), copyright 2012, The Endocrine Society).

3.4   The identification of the dopamine receptor expressed in β-cells

3.4.1   The immunodetection of DRD2 and DAT

I have tested so far the parts of the hypothesis pertaining to the synthesis and secretion of dopamine. I also showed that this endogenous secretion affects the frequency of $[Ca^{2+}]_i$ oscillation, and ultimately inhibits GSIS. The question remains of which of the 5 dopamine receptors are expressed in β-cells, and more importantly which one(s) is mediating the effects of dopamine. Also, to complete the picture of the dopaminergic system that is regulating GSIS, I looked for the expression of the dopamine transporter (DAT). DAT would reuptake dopamine from the intracellular space, terminating the dopamine signaling and contributing to keep this signaling localized in the islet.

The work of Rubí *et al.* (3) is the only study showing that dopamine receptors are expressed in mouse β-cells. In detail, they show the expression of the dopamine receptor D2 (DRD2) in rat INS1-E cells, by SDS-PAGE and western blot; also they show immunostaining for DRD2 in dispersed mouse β-cells. From these experiments, they concluded that DRD2 is associated with insulin granules and not present on the plasma membrane.

Our first experiment was to test the expression of DRD2 in mouse islets. The results of the western blot are shown in Figure 19.
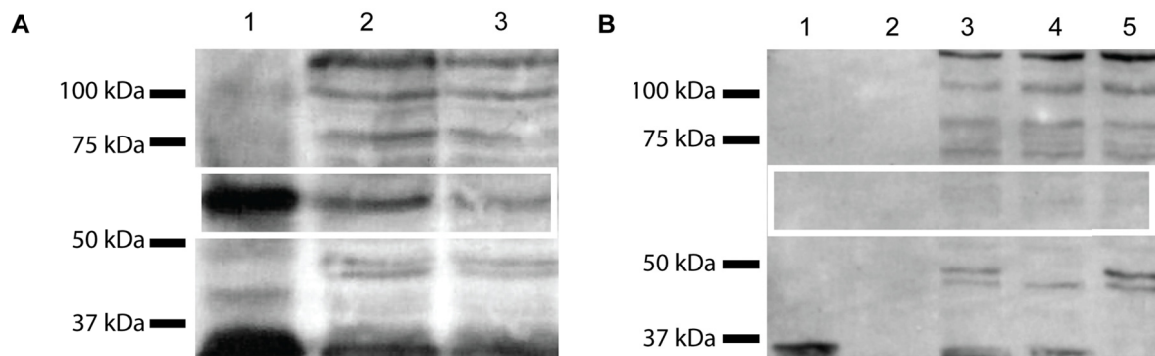
Figure 19: Immunoblot for DRD2. A: lane 1 = mouse brain extract (25 µg total protein); lane 2 = pancreatic islets lysate (54 µg total protein); lane 3 = pancreatic islets lysate (45 µg total protein); the white box overlay highlights the 58 kDa band present in all lanes. B: Control immunoblot for DRD2 using the blocking peptide for the primary antibody: lane 1 = mouse brain extract (20 µg total protein); lane 2 = empty; lanes 3-5 = pancreatic islets lysate (20 µg total protein); the white box overlay highlights the 58 kDa band missing in all lanes. (from (152), copyright 2012, The Endocrine Society).

I used the same antibody used by Rubí *et al.* (3) in their study (AB5084P, rabbit anti DRD2, Chemicon). A band of approximately 58 kDa was detected in the positive control (mouse brain extract) and in the islets lysate Figure 19A. This is in good agreement with the molecular weight reported in the literature for DRD2. Several other bands were present in the islet lysate lanes, so I performed another experiment to discriminate between specific and non-specific interaction and confirm that the 58 kDa band in the islet lane was indeed DRD2. I neutralized the primary antibody with its own immunogen, the 28 amino acids peptide from the third intracellular loop of DRD2. Under this condition the band at 58 kDa was not detectable in any lane while the other non-specific bands were still present Figure 19B. Similar western blot procedures using a DAT antibody showed a single band of 50-62 kDa representing DAT expression in the islets

(Figure 20). I showed with these experiments that DRD2 and DAT are present in the mouse islets, but the amount of non-specific bands in Figure 19A lead us to think that this antibody was not very specific in the islets. I reasoned that this could explain the unusual intracellular localization of DRD2 that was reported by Rubí *et al.* (3), since the same antibody was used. I addressed this question with the next experiment.
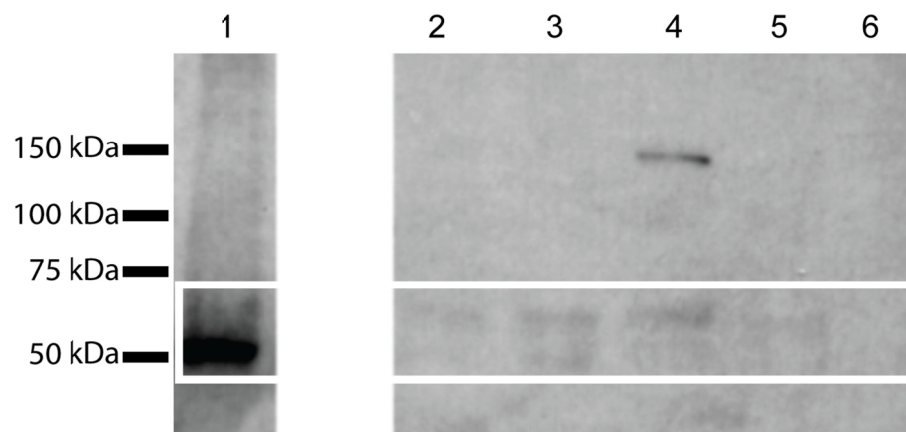
Figure 20: Immunoblot for DAT: lane 1 = mouse brain extract (10 µg total protein); lanes 2-5 = pancreatic islets lysate (76, 73, 46, and 24 islets respectively); lane 6 = empty. (from (152), copyright 2012, The Endocrine Society).

3.4.2 Live subcellular localization of DRD2$_L$-mVenus

I utilized an adeno-associated virus vector to express DRD2$_L$ (the long isoform of the receptor) tagged with the fluorescent protein mVenus to determine if dopamine receptors are present on the plasma membrane in islet cells. This transduction allowed us to image DRD2$_L$-mVenus distribution in live islet cells. 48

hours after the transduction, multiple cells per islet showed fluorescence (Figure 21A).
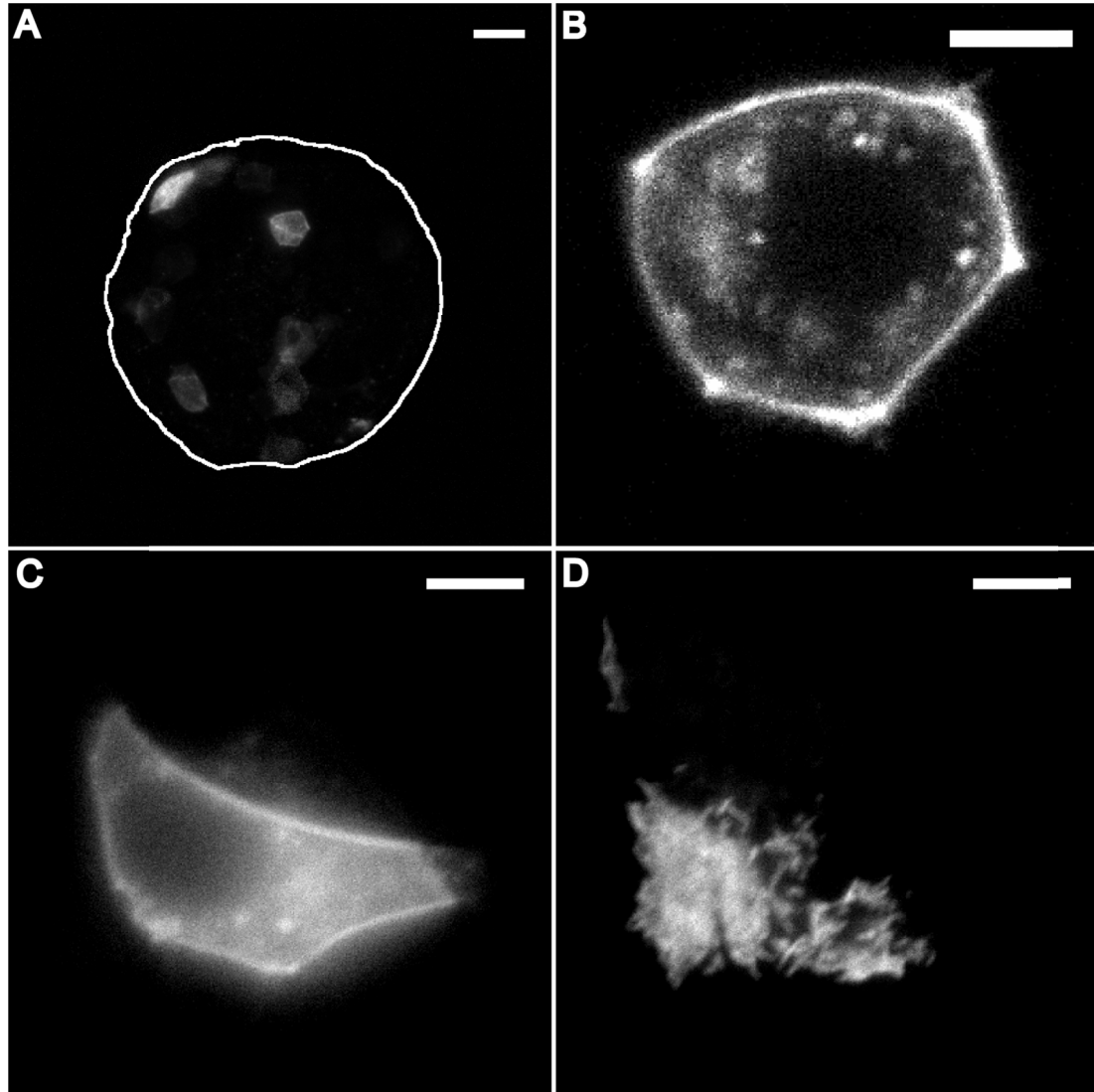
Figure 21: DRD2-mVenus images.A: Sum intensity projection of 47 confocal images of an islet expressing DRD2-mVenus (representative image of 33 cells from 7 islets); the white line indicates the islet outline; scale bar 20 μm. B: Confocal image of a single cell from the islet shown in A; scale bar 5 μm. C: Widefield fluorescence image of a MIN6 expressing DRD2$_L$-mVenus; scale bar 5 μm. D: TIRF image of the same field of view shown in C; scale bar 5 μm. (from (152), copyright 2012, The Endocrine Society).

When I imaged these islet cells at higher spatial resolution, they all showed fluorescence associated with their plasma membrane (Figure 21B), supporting the assumption that DRD2 is present on the plasma membrane of live islet cells. I confirmed this result performing (total internal reflected fluorescence) TIRF imaging on single MIN6 cells that were transduced with DRD2$_L$-mVenus (Figure 21C-D). The plasma membrane localization of DRD2$_L$-mVenus appeared as a bright contour line when a cell is imaged with a widefield microscope (Figure 21C). This was similar to what was observed in the islet with a confocal microscope. The membrane localization of the DRD2$_L$-mVenus was confirmed by TIRF microscopy by the presence of fluorescence in all the cellular regions that are in contact with the coverslip (Figure 21D). AAV vectors containing EGFP alone were used as a control (Figure 22).
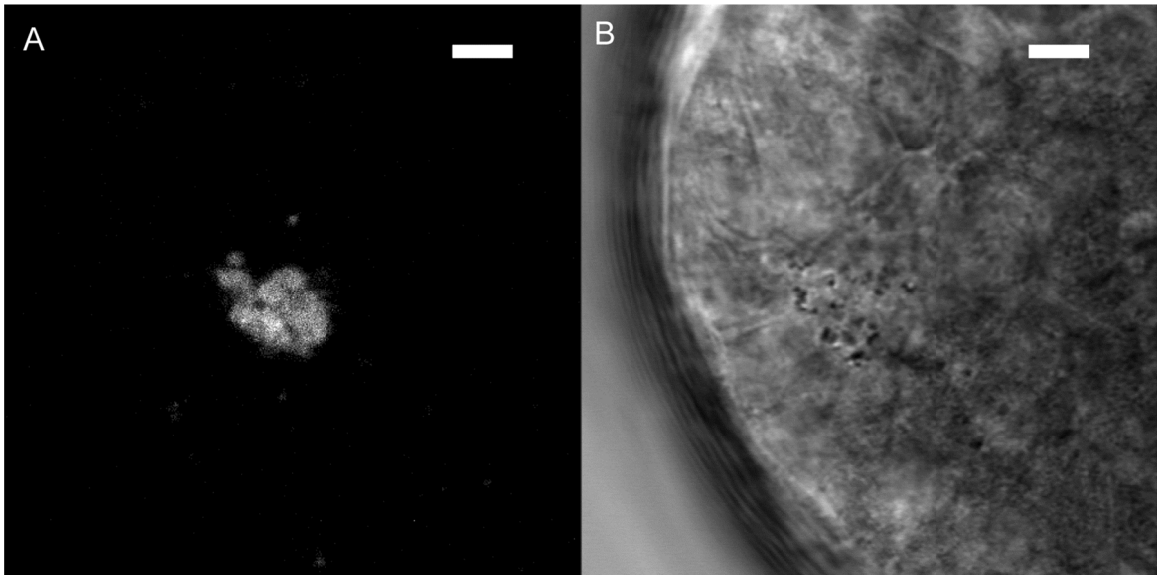
Figure 22: mVenus images.A: Confocal image of a single cell in an islet expressing mVenus. B: Differential interference contrast image corresponding to the field of view in A. Scale bar 5 μm.

The islet cells transduced with EGFP showed diffuse fluorescence with no membrane labeling (Figure 22). Since I am overexpressing this receptor, I expect to observe a percentage of abnormal trafficking that may not reflect the natural localization of the protein. But the fact the majority of the signal is associated with the cell membrane lead us to conclude that the receptor is normally trafficked to the plasma membrane. The perinuclear distribution that can still be observed can be interpreted as immature peptide that has yet to be translocated to the plasma membrane. More experiments can definitively answer the question about DRD2 localization in β-cells, but these results strongly suggest that the intracellular localization presented by Rubí *et al.* (3) is not the conclusive answer.

3.4.3 Functional consequences of Drd2 gene deletion in islets

During the course of our study I received transgenic mice carrying a global null-mutation of the Drd2 gene. The details of the gene targeting strategy are described in (169). The mice lack the majority of exon 2 of the Drd2 gene and they have a stop codon that prevents the translation of the rest of the truncated gene. The homozygous mutant mouse (D2$^{-/-}$) was a good model to further test our hypothesis: I could isolate islets that lacked the DRD2. These islets should have enhanced GSIS, according to our hypothesis of a dopaminergic negative feedback. Also they should be insensitive to dopamine and L-dopa treatment. The results of the insulin secretion experiments are shown in Figure 23.
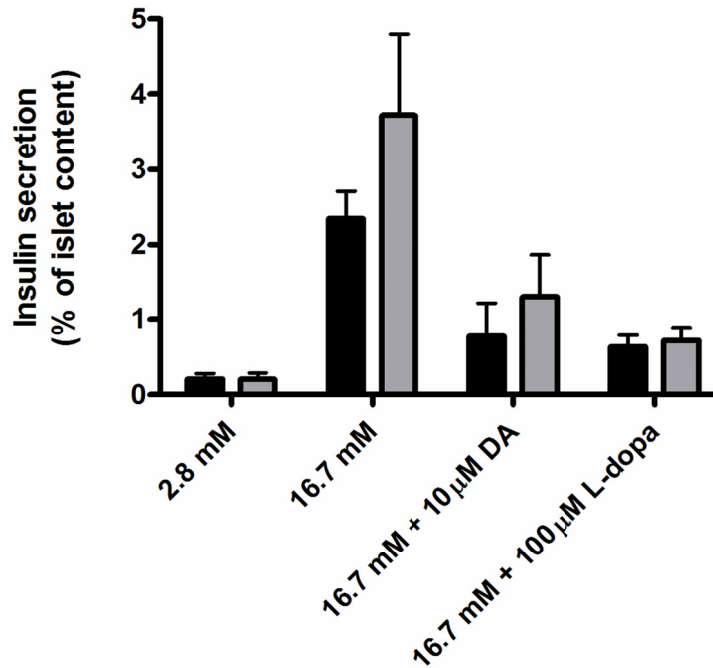
Figure 23: Insulin secretion measured at 2.8 mM glucose, 16.7 mM glucose, and 16.7 mM glucose plus 10 µM dopamine (DA) or 100 µM L-dopa (n=4). The black bars indicate wild type islets ($D2^{+/+}$). The gray bars indicate mutant islets ($D2^{-/-}$). The differences between $D2^{+/+}$ and $D2^{-/-}$ are not statistically significant.

Surprisingly, the $D2^{-/-}$ islets did not show a GSIS that was significantly higher than the control $D2^{+/+}$ islets. More importantly, they were still sensitive to both dopamine and L-dopa, showing GSIS inhibition in response to both treatments. The simplest interpretation of these results was that DRD2 was not mediating the effect of dopamine in mouse islets.

3.4.4 Examining the expression and the function of DRD3 in the islets

Since I excluded that DRD2 mediates the effect of dopamine, I tested the possibility that another member of the D2-like group of dopamine receptor, DRD3, was expressed in the islets and was responsible for these effects. In the region of the brain where it is expressed, DRD3 is usually expressed at lower level compared with DRD2. For this reason I decided to perform subcellular fractionation on the islet lysate, so that I had a plasma membrane enriched fraction to better detect low level of the receptor. The results of the western blot are shown in Figure 24.
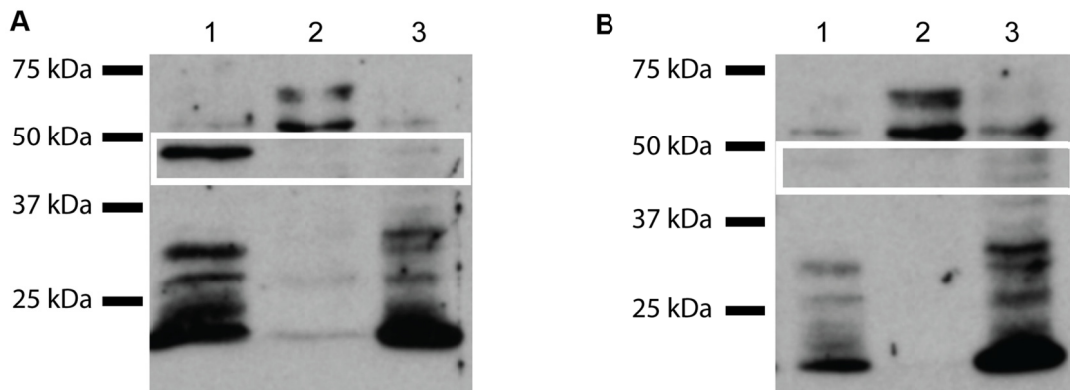
Figure 24: Immunoblot for DRD3. A: lane 1 = islet membrane fraction (18 µg); lane 2 = islet cytosolic fraction (18 µg); lane 3 = islet nuclear fraction (18 µg); white box overlay highlights the 48 kDa band present in the islet membrane fraction. B: Control immunoblot for DRD3: lane 1 = islet membrane fraction (18 µg); lane 2 = islet cytosolic fraction (18 µg); lane 3 = islet nuclear fraction (18 µg): white box indicates the absence of the 48 kDa band in the islet membrane fraction. (from (152), copyright 2012, The Endocrine Society).

I detected a band of approximately 48 kDa corresponding to DRD3 in the membrane fraction of the islet lysate (Figure 24A), and I confirmed the

specificity of this signal by neutralization of the antibody with its specific

immunogen peptide, resulting in the disappearance of the band (Figure 24B).

Since I demonstrated the presence of both DRD2 and DRD3 in the islets, I used

selective antagonists for each receptor isoform to confirm the results I obtained

from the D2$^{-/-}$ islets, and to test if DRD3 is the receptor involved in the

dopaminergic signaling in the islets. The first test was to measure insulin

secretion with each antagonist, and in the presence of dopamine (Figure 25).

Figure 25: Effect of DR antagonists on insulin secretion measured at 2.8 mM glucose (white bar), 16.7 mM glucose (black bar), and 16.7 mM glucose + 10 µM dopamine (gray bar). The selective antagonist for DRD2 (L-741,626), or for DRD3 (GR 103691) were added to the three stimuli as indicated (n = 6-8). + P < 0.05, +++ P < 0.001 *versus* the respective untreated control. (from (152), copyright 2012, The Endocrine Society).

Clearly the DRD2 antagonist (L-741,626) did not change the insulin secretion at 2.8 mM glucose and at 16.7 mM glucose when compared with the untreated control islets. Also, the DRD2 antagonist did not block the effect of 10 μM dopamine added to the 16.7 mM glucose. In contrast, the DRD3 antagonist (GR 103691) produced a statistically significant 2 fold increase in insulin secretion at 16.7 mM glucose, and it abolished the inhibitory effect of 10 μM dopamine. Additionally, I tested the effects of the DRD3 antagonist on the frequency of the $[Ca^{2+}]_i$ oscillations of the islets (Figure 26).
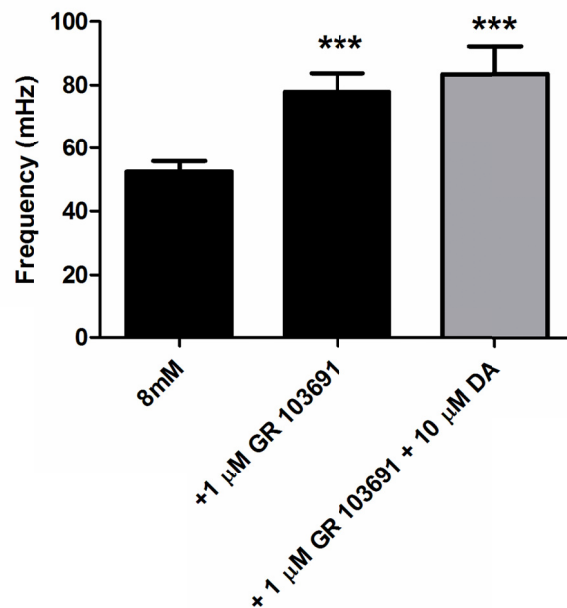
Figure 26: The $[Ca^{2+}]_i$ oscillation frequency of control islets *versus* islets treated with the DRD3 antagonist (GR 103691) or a mixture of the DRD3 antagonist and dopamine as indicated (n = 9-14); *** $P < 0.001$. (from (152), copyright 2012, The Endocrine Society).

As expected, the antagonist produced a significant increase in the frequency compared to the untreated islets. Also, when dopamine was added to the islets in the presence of the antagonist, there was no observed effect.

The results of these two experiments not only demonstrate that DRD3 is the receptor mediating the dopamine signaling in the β-cell, but they also show that the dopaminergic negative feedback is active in untreated islets. In fact, the blockade of DRD3 significantly increased GSIS and the frequency of the $[Ca^{2+}]_i$ oscillations in such islets.

In their study, Simpson *et al.* (159) present the results of similar experiments, performed on human islets. Based on the effects haloperidol on GSIS, they conclude that DRD2 mediates the dopaminergic inhibition. I think that their conclusion is questionable. A simple, but naïve, explanation is that contrary to mouse islets, human islets express only DRD2 and that isoform is mediating the dopaminergic inhibition. However, there is no evidence to exclude that DRD3 is also expressed in human islets, since they looked only for DRD2 expression. Moreover they used haloperidol to antagonize DRD2, and they measured an increase in GSIS. But haloperidol is not a selective DRD2 antagonist, in fact it has similar K_i for DRD2, DRD3 and DRD4 (~ 2.1, ~ 7, and ~ 2.3 nM respectively (177)). Therefore their results could be explained equally well by hypothesizing that DRD3 is the receptor mediating the dopamine effect in human islets.

3.4.5 Preliminary test of DAT activity in the islets

Since I showed that DAT is expressed in the islets, I tested the effect of a selective inhibitor (GBR 12909) on insulin secretion. In our hypothesis of the dopaminergic negative feedback, DAT is responsible for terminating the dopamine signaling. Therefore, I expected that the inhibition of DAT would produce an increase in the extracellular dopamine concentration and consequently an increased inhibition of GSIS. Furthermore I expected that the DAT inhibition would exacerbate the effect of exogenous dopamine, because there will be no uptake of dopamine that could possibly reduce its extracellular concentration. Figure 27 shows the results of these experiments.
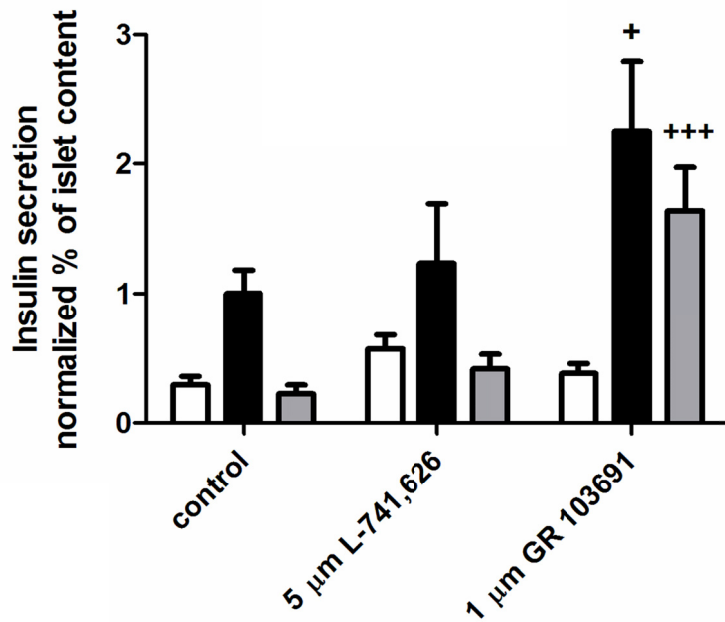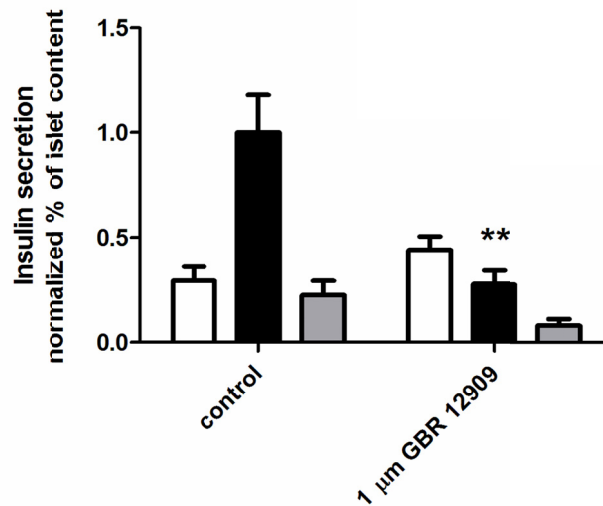

Figure 27: The effect of DAT blocker on insulin secretion measured at 2.8 mM glucose (white bar), 16.7 mM glucose (black bar), and 16.7 mM glucose + 10 µM dopamine (gray bar). The selective inhibitor of DAT (GBR 12909) was added to the three stimuli as indicated (n = 7-8). ** $P < 0.01$ *versus* the respective untreated control.

In support of our hypothesis, the selective inhibitor produced a significant inhibition of GSIS. When it was added in the presence of dopamine, the GSIS showed an accentuated inhibition, but it did not reach the statistical significance for the number of observation used (n=8).

Once again our conclusion on the role of DAT and the effect of its inhibition are conflicting with the conclusion of Simpson *et al.* (159). I used the same inhibitor (GBR 12909) at a higher concentration than they did (1 µM *versus* 500 nM). I used 4 islets/ml for our static incubations, and they used 50-250 islets/ml in their static incubations. I observed an inhibition of GSIS, while they report an enhanced GSIS in response to the DAT inhibitor. They reasoned that while it is commonly accepted that DAT inhibitors increase extracellular dopamine, this effect is lost in the islets because of their high degree of perfusion by the vasculature. According to their discussion, this should enhance the diffusion of dopamine away from the cultured islet tissue. Given the much higher islet concentration in their experiments, this effect should have been even more apparent in our experiments. Instead, I observe the opposite outcome, the inhibition of GSIS. If the diffusion of dopamine is to explain their data, I find it difficult to attribute it to perfusion, as in both labs, these were static incubations. One possible explanation, other than a species dependent difference, is the quality of the human islets they received. Having worked with human islets, we know how unpredictable their quality is. An over-digested batch would have loosely connected cells, which could better explain their result. But I can only speculate on this aspect. Further experiments are necessary to characterize the

function of DAT in the islets, and the resulting data should elucidate the truth underlying these currently contradictory results.

3.5 Summary

In this chapter, I further tested the hypothesis of a dopaminergic negative feedback loop that regulates the GSIS from the islet. I tested various steps that follow the secretion of dopamine from the β-cells and that have a role in GSIS. I confirmed that neither dopamine nor L-dopa are interfering with the metabolism of glucose. I did so by monitoring the glucose-induced increase in the autofluorescence from NAD(P)H. Then, I measured the changes in $[Ca^{2+}]_i$ dynamics that both dopamine and L-dopa produce during GSIS. Instead of measuring the absolute $[Ca^{2+}]_i$, I monitored its oscillations over time. This provided us with a robust measure that is independent from other experimental variables like: photobleaching, focal drift, the concentration of the calcium indicator, fluctuations in the illumination power. For both drugs I measured a dose dependent decrease in the frequency of the $[Ca^{2+}]_i$ oscillations, that correlates very well with the observed decrease in GSIS. I excluded that L-dopa directly affected the $[Ca^{2+}]_i$ oscillations, instead it worked as an external source to build up dopamine. The excess of dopamine, in turn, acted on the dopamine receptor to produce the changes in $[Ca^{2+}]_i$. Thus I came to test the most controversial question: which of the 5 dopamine receptor is expressed and functional in the pancreatic islet? In two other works (3, 159), the authors both concluded that DRD2 is the isoform present in mouse and human islets. Our data

instead clearly show that while DRD2 is present in the islets, DRD3 is the isoform that is mediating the dopaminergic signaling. I demonstrated this by using islets from knock-out mice lacking DRD2 and showing that they still responded to dopamine. I used isoform-specific dopamine receptor antagonists for DRD2 and DRD3 on wild type islets, and I showed that only the antagonism of DRD3 abolished the effects of dopamine, enhanced GSIS in untreated islets, and increased the frequency of $[Ca^{2+}]_i$ oscillations. Finally, I verified that DAT is also expressed in the islets, and I indirectly tested its activity using the DAT inhibitor (GBR 12909). Based on our working hypothesis, the inhibition of dopamine reuptake should result in increased extracellular dopamine, and that in turn produces a stronger inhibition of GSIS. This is indeed the result I measured. Simpson *et al.* (159) report the opposite outcome for the same experiment. While I question the logic of their interpretation of those results, I currently cannot find a good explanation to reconcile this conflict. More experiments will be necessary to solve this controversy.

CHAPTER

4. QUANTITATIVE FLUORESCENCE AND SINGLE MOLECULE IMAGING

4.1   Introduction

During the course of the research in the Piston lab, I had the opportunity to participate in a wide range of collaborative projects, to which I could contribute the microscopy expertise gained in the lab. These were also excellent opportunities to face different scientific questions, and come up with creative solutions. A number of these collaborative studies have already been published (178-181). In this chapter I present part of the results of one of these collaborations, because it exemplifies how significant information can be gained from quantitative analysis of confocal images. Also it used a strategy to perform single molecule tracking that can be translated to future studies aiming at studying the dynamics of dopamine receptors and dopamine transporter in the islet. The results of this study were published in the work by Chang *et al.*(182).

4.2   Materials and Methods

4.2.1   Cell culture and treatments

The immortalized serotonergic neural cell line, RN46A, was provided by Dr.Scott R. Whittemore (University of Miami School of Medicine). Cells were cultured in DMEM/F12 (1:1; Invitrogen) supplemented with 10% FBS and incubated in a humidified atmosphere with 5% CO_2 at 37°C. Although RN46A cells endogenously express functional SERT proteins, an increase in SERT expression can be obtained by incubating cells in DMEM/F12 (1:1) containing a 1% B27 supplement (Invitrogen) plus 1 µM serotonin (5-HT) for 24 h before single molecule labeling experiments.

4.2.2   Labeling RN46A cells with ligand-conjugated quantum dots

For single quantum dot (Qdot) labeling of SERT proteins, biotinylated IDT318 ligand was first incubated with RN46A cells followed by three washes to remove unbound ligand. Streptavidin-conjugated quantum dots (SAv-Qdots) (Invitrogen) were then added to detect the biotinylated moiety of antagonist-associated linker. To minimize the possibility of cross-linking of ligands and the overlap of quantum dots trajectories, we adapted the Qdot-based, single molecule labeling protocol of Triller and colleagues (183), where the ligand concentration (0.5 µM) is set well below saturation (saturation concentration: ≥ 10 µM). In addition, low concentrations (0.5 nM) of SAv-Qdots were used to detect

ligand binding at the lowest recommended concentration as studied by Triller and

colleagues (183). For experiments involving cholesterol depletion, cells were

incubated with 5 µM methyl-β-cyclodextrin (MβCD) (Sigma) at 37°C for 30 min

before two-step Qdot-SERT labeling. The MβCD cholesterol depletion protocol

we used does not result in overt changes in RN46A cell morphology, though

more prolonged incubations (90 min) of RN46A cells with 10 µM MβCD at 37°C

produce cell rounding paralleled by a decrease in SERT mobility. To avoid

endocytosis and to achieve successful quantification in dual-channel imaging, all

optical live-cell images were taken immediately after Qdot labeling. Endocytosis

from longer labeling experiments could be readily detected by an accumulation of

larger clusters of Qdots within the endosomes.

4.2.3 Microscopy

For high speed line-scanning confocal microscopy, images were

obtained on a Zeiss LSM 5-Live confocal system and collected with a Zeiss

63X/1.4 NA oil-immersion objective lens. Excitation was provided by a 488 nm

100-mW diode laser. Frame rate was 10 Hz. Imaging was performed at 37°C.

Single Qdot emission was collected using a long pass 650 filter. Line scan

images with scan format of 512x128 pixels were processed using Zeiss LSM

Image Examiner.

4.2.4 Data analysis of single quantum dot imaging

Real-time tracking of single Qdot labeled SERT proteins was obtained using a Zeiss 5-Live line-scanning confocal microscope. Individual recording of each sample was performed at 37°C for 1 min at a scanning speed of 1 frame/100 ms. Raw data files were extracted to generate stacks of individual 16 bit TIF images for single molecule tracking. Positions (*x* and *y* coordinates) and trajectories of the single Qdot-labeled SERT proteins were determined by Matlab routines developed by Jaqaman *et al.*(184). Single Qdots undergo fluorescence intermittency, which can contribute to the trajectory assessment and may cause difficulty in tracking. To effectively decrease Qdot blinking probability, we decreased excitation laser power through setting the signal-to-noise limit just above 6. In addition, as suggested by Dahan and colleagues (185), segment linking was processed to obtain trajectories as long as possible and blinking tolerance was limited to no more than 10 consecutive frames. Segment linking for complete trajectory generation was performed via the method described by Cohen and colleagues (186). Mean squared displacement (MSD) values, velocity, least-square fitting, and numerical distribution functions were processed using Matlab and Sigmaplot programming routines (187).

Although a complete understanding of the diffusion processes of membrane transporters is still lacking, temporary lateral confinement of a diffusing protein due to local environmental constraints such as interaction with lipid rafts or cytoskeletal corrals, can be best described as anomalous sub-diffusion (188). For a stochastic process of anomalous diffusion, monitored

continuously, others have previously established that such movements can be described as Lévy processes (189, 190). We investigated the distribution of instantaneous velocity (instantaneous movement over one time interval) of single SERT proteins in RN46A cells and found that the distribution follows a non-Gaussian distribution. The statistical distribution of instantaneous velocities of single SERT proteins is well fit to the Lévy probability distribution function. In all of our analyses the R^2 values of the fit of instantaneous velocity are higher than 95%, indicating high reliability of our fits.

4.3   Serotonin transporter, quantum dots, and fast imaging

The technical challenge at the base of this collaboration project was to image a single fluorescent particle at a high frame rate, to quantitate its dynamic properties over time. The establishment of a robust protocol for this imaging mode allowed interrogating the biological model during various treatments to study complex intracellular mechanisms. The protein of interest was the human serotonin transporter (SERT) that has been studied as a determinant of neuropsychiatric disease risk (191). The distribution of SERT across membrane micro-domains have been investigated with biochemical studies (192, 193), but they cannot resolve the changes in single molecule behavior which result in the macroscopic functions. The advantage of the single-molecule tracking allowed the characterization of the protein movement that reports on events affecting the function and the regulation of SERT.

4.3.1 The labeling of SERT with a single quantum dot

The SERT ligand ID318 (194, 195), which competes for serotonin uptake by SERT, and display antagonist binding properties, was used to tag SERT on the plasma membrane of RN46A cells. The ligand consisted of a SERT selective compound attached to a biotinylated polyethylene glycol (PEG 5000) linker via an alkyl spacer, as shown in Figure 28.
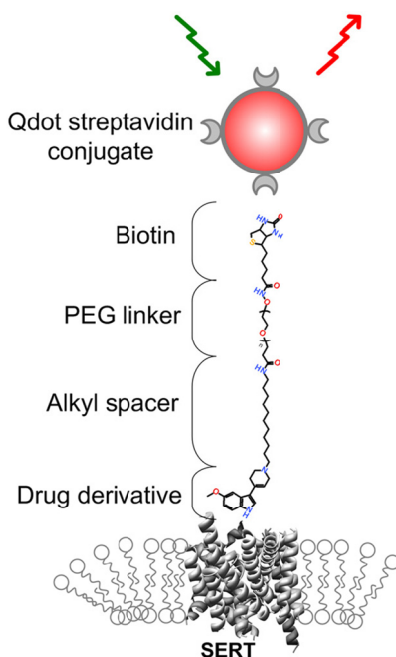
Figure 28: Schematic of a streptavidin-conjugated quantum dot binding the SERT ligand IDT318. (Modified from (182)).

This compound was used to specifically tag the SERTs on the cell membrane. In a second step the streptavidin-conjugate quantum dots were added, which bound to the biotin moiety realizing the fluorescent labeling of SERT. The average diameter of a quantum dot is ~20 nm that is well below the

spatial resolution of a confocal microscope (~250 nm). This implied that we could not distinguish a single quantum dot from a group of quantum dots, if they were closer than ~250 nm. In both cases we would see a bright spot with a diameter of ~250 nm. We circumvented this obstacle taking advantage of an intrinsic physical property of single quantum dots: under continuous illumination they interconvert between an ON state (in which they fluoresce) and an OFF state in which they are dark (196). We measured the fluorescence of quantum dots in Figure 29.
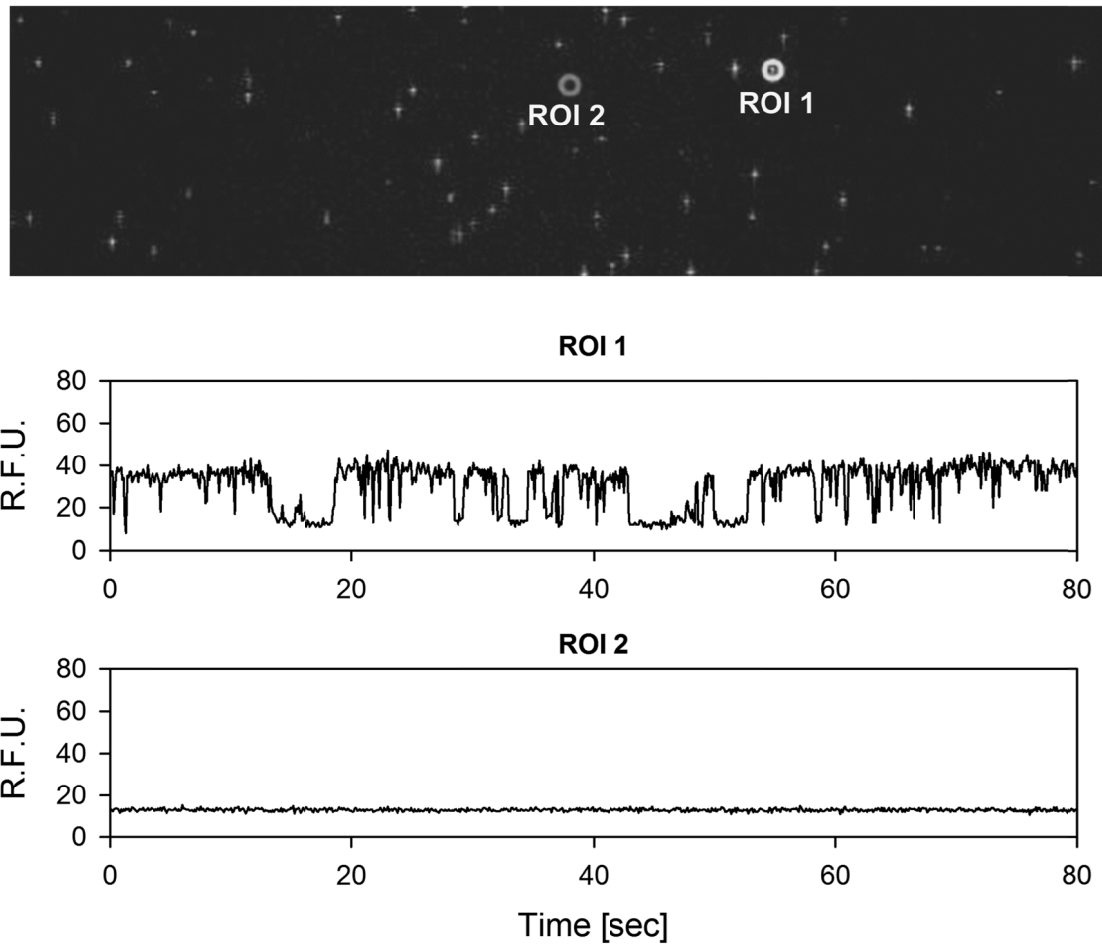
Figure 29: Single frame from a series of images of the fluorescence emitted by quantum dots. The region of interest (ROI) 1 encircles a single quantum dot, while the ROI2 encircle an area without quantum dots.

The quantum dot solution was imaged on the glass coverslip surface over time, and we could successfully identify single quantum dots displaying the characteristic intermittent fluorescence. This pattern is not detectable when multiple particles are measured. It can be seen in Figure 29 how the trace from ROI1 displays only 2 intensity levels, and the lower one coincides with the background intensity in the same image. The use of quantum dots to label SERT provided two advantages: 1) it allowed us to identify single particles, by looking at their intermittent fluorescence 2) it allowed us to use frame rate of 10 Hz and yet collect images with a good contrast, thanks to their brightness and photo-stability.

4.3.2 Tracking a single SERT

We labeled SERT on the neuronal cell line RN46A. We chose this cell line because it has a low expression level of SERT (197), and that made it easier to identify and track single SERT molecules over time. After extracting the trajectories of each individual SERT in an image, we proceeded computing the displacement over time and the mean squared displacement (MSD) for each trajectory. The displacement provided information on the type of movement of each particle (free *vs.* caged diffusion). The MSD is instead a function of the diffusion coefficient D, and it increases linearly with time in the case of free diffusion (MSD $\propto$ Dt). But the model that currently best describes the movement of a transporter in a membrane, and anchored to other structures, is the anomalous sub-diffusion (188, 198). In this model MSD $\propto t^{\alpha}$ ($\alpha<1$), and therefore

$D \propto 1/t^{1-\alpha}$. We chose to plot MSD/Δt *vs* Δt on a log-log scale, so that free diffusion appeared as a horizontal line, and anomalous sub-diffusion appeared as a line with a negative slope. In Figure 30 both the displacement and the MSD/Δt type of plot are displayed. In each plot there are two traces: one represents the movement of a SERT molecule in a control cell, and one represents the movement of a SERT molecule in a cell treated with methyl-β-cyclodextrin (MβCD) to disrupt the lipid rafts. The difference between the two situations is immediately visible. We can see that a SERT protein in a control cell (Figure 30A) shows a limited range of movement in comparison with the SERT protein in a cell that has been treated with MβCD. In this last case the movement is consistent with a free diffusion model (Figure 30B), while the in the untreated cell the movement is show the characteristic slope of anomalous sub-diffusion.
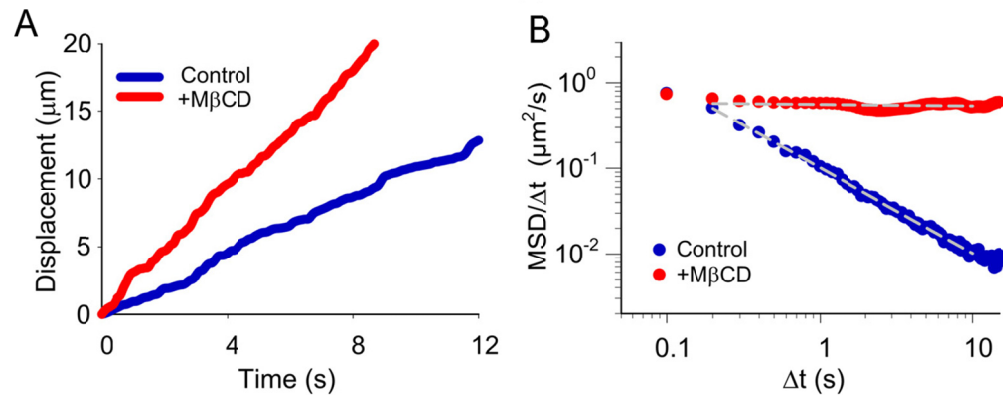
Figure 30: The displacement over time and MSD/Δt over Δt for two representative single SERT proteins. A: comparison of the displacement over time of two representative single SERT proteins. B: Plot of MSD/Δt over Δt for two representative single SERT proteins. (Modified from (182)).

When we extended this type of analysis to a high number of single

molecule trajectories (n > 50 from 3 independent experiments) we could better

characterize the two types of movement. The displacement plot showed a

distribution of slopes consistent with a movement two time faster for MβCD-

treated cells *versus* control (Figure 31A).
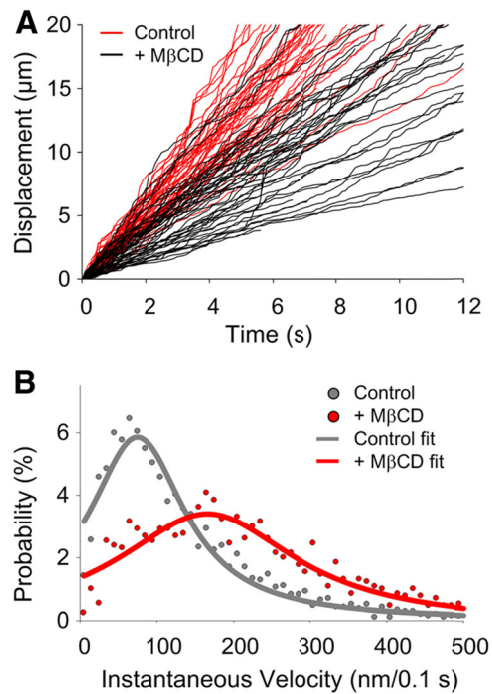
Figure 31: A: Displacement over time for SERT proteins (n = 52) in control cells, and in MβCD-treated (n = 51) cells. B: Comparison of the instantaneous velocities in control and MβCD-treated cells. (from (182)).

We fitted the single step displacements for each trajectory into a Lévy

probability distribution function to get a more accurate estimate of the

instantaneous velocity of each particle (Figure 31B). The result of the fits

returned an instantaneous velocity of 0.75 ± 0.06 µm/s (mean ± 95% confidence

limit) in untreated cells, and a significantly higher velocity of 1.74 ± 0.08 µm/s for

the MβCD-treated cells (P < 0.001). The analysis of the log-log plot of MSD/Δt

over Δt returned the interpretation, showing that SERT proteins in MβCD-treated

cells have a reduced constraint on lateral mobility (increased slope) when

compared to the ones in the control cells (Figure 32A, C).
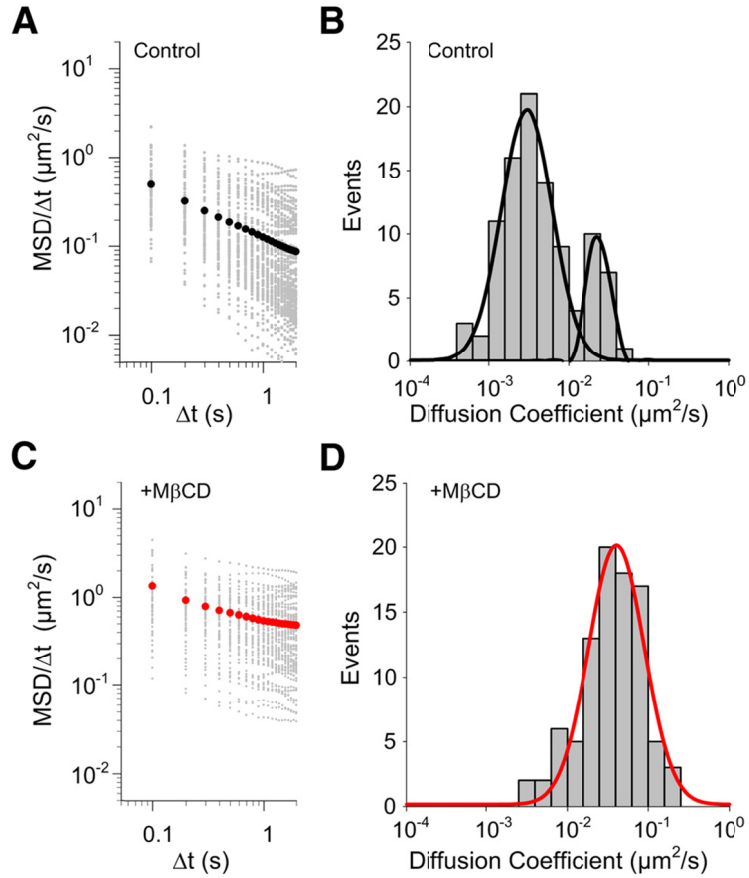
Figure 32: Characterization of the dynamic behavior of single SERT proteins.
A-B: Plot of MSD/Δt over Δt and distribution of diffusion coefficient in control cells
(n = 98). C-D: Plot of MSD/Δt over Δt and distribution of diffusion coefficient in
MβCD-treated cells (n = 91). The distribution were fit to double and single
Gaussian distributions. Black circles and red circle represent average MSD/Δt.
(from (182)).

The analysis of the distribution of diffusion coefficient in control cells

(Figure 32B), revealed that the majority of SERT proteins have a lower diffusion

coefficient ($10^{-3} \sim 10^{-2}$ µm^2/s), and a small fraction of them has a higher diffusion coefficient ($10^{-2} \sim 10^{-1}$ µm^2/s). On the contrary, in MβCD-treated cells, the distribution revealed the presence of a single population with a higher diffusion coefficient ($10^{-2} \sim 10^{-1}$ µm^2/s) matching the value of the minority population observed in the control (Figure 32D).

4.3.3 Correlation of SERT motor behavior with transporter function

The same analytical approach was used to quantitate the effect of various pharmacological treatments, in order to test if mobility restrictions contribute to physiologically relevant features of SERT regulation. It has been shown that activation of PKG by cGMP induce an increase in serotonin uptake rates (199). So we measured the effect of the cell-permeant cGMP analog (8-Br-cGMP) on SERT mobility. The treatment induced a significant increase in the instantaneous velocity that went from 0.75 ± 0.06 µm/s to 1.60 ± 0.03 µm/s (P < 0.001) (Figure 33A). It also increased the subpopulation of SERT proteins displaying a higher diffusion coefficient (Figure 33B). Interestingly, this increased in velocity and diffusion coefficient, was associated with a 75 % of SERT protein still displaying confined lateral diffusion (Figure 33C). Although the treatment induced faster movements of SERT, the protein appeared to be still confined to its membrane microdomain. As we thought that the effect of 8-Br-cGMP treatment was to induce phosphorylation of SERT and its increase in uptake rate, we treated the cells with a p38 MAPK specific inhibitor (SB203580). The treatment greatly reduced the effect of 8-Br-cGMP (Figure 33D).
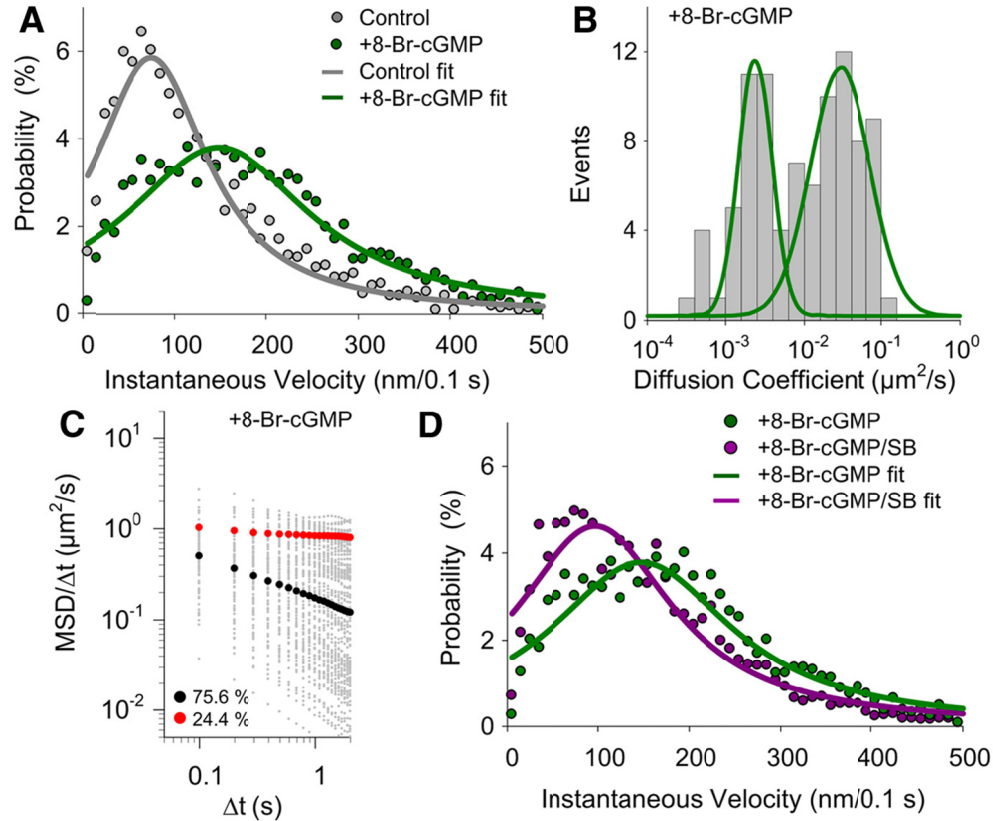
Figure 33: Velocity and diffusion coefficients of SERT in 8-Br-cGMP-treated cells. A: Fit for the instantaneous velocity of SERT in control and 8-Br-cGMP-treated cells. B. Distribution of diffusion coefficients of SERT proteins in 8-Br-cGMP-treated cells (n = 90). C. Log-log plot of MSD/Δt over Δt of SERT in 8-Br-cGMP-treated cells (n = 90), black circles and red circle represent average MSD/Δt for each sub-population indicated. D: Fit for instantaneous velocity of SERT in 8-Br-cGMP-treated cells with or without SB203580. (from (182)).

We reproduced the effect of 8-Br-cGMP treatment by using a natural stimulus of the p38 MAPK dependent SERT activation: IL-1β. In fact it has been shown that IL-1β acts via the IL-1 receptor to produce the p38 MAPK dependent SERT activation (200). The treatment with IL-1β produced an increase in the SERT instantaneous velocity similar to the one induced by 8-Br-cGMP (Figure

34A), and similarly it increased the sub-population of SERT that displayed higher

diffusion coefficients but maintaining the confined lateral diffusion (Figure 34B).
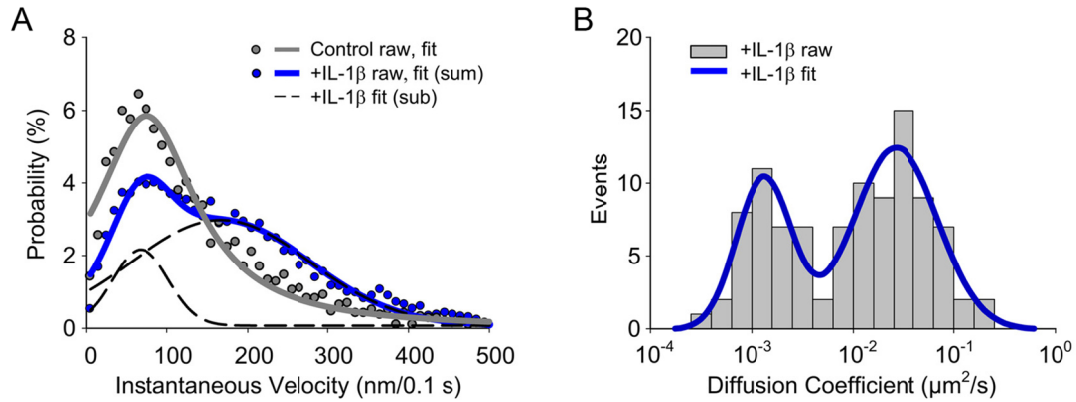
Figure 34: Velocity and diffusion coefficients of SERT in IL-1β-treated cells. A: Fit for the instantaneous velocity of SERT proteins in IL-1β-treated and in control cells. 79% of the population display higher velocities. B: Distribution of diffusion coefficient of SERT proteins in IL-1β-treated and control cells (n = 99). (from (182)).

A possible mechanism that would explain this p38 MAPK-dependent

increase in SERT instantaneous velocity, associated with the confined diffusion

typical of a protein residing in a lipid raft domain, is the liberation of SERT from

juxtamembrane cytoskeletal networks. These networks are thought to constraint

the movements of raft-localized transporters (199). We tested this hypothesis by

treating the cells with cytochalasin D (CytoD) to disrupt the actin filaments. CytoD

significantly increased the instantaneous velocity of 95% of the SERT population

(1.51 ± 0.06 µm/s *vs* 0.75 ± 0.06 µm/s for untreated cells) (Figure 35A). When

IL-1β was added to cells that were pretreated with CytoD, it did not produce any

further increase in velocity (Figure 35A). Together this data supports the

hypothesis that SERT activation by IL-1β treatment results in the liberation of the

transporter from the cytoskeleton anchors, while leaving the transporter

embedded in lipid raft domains.
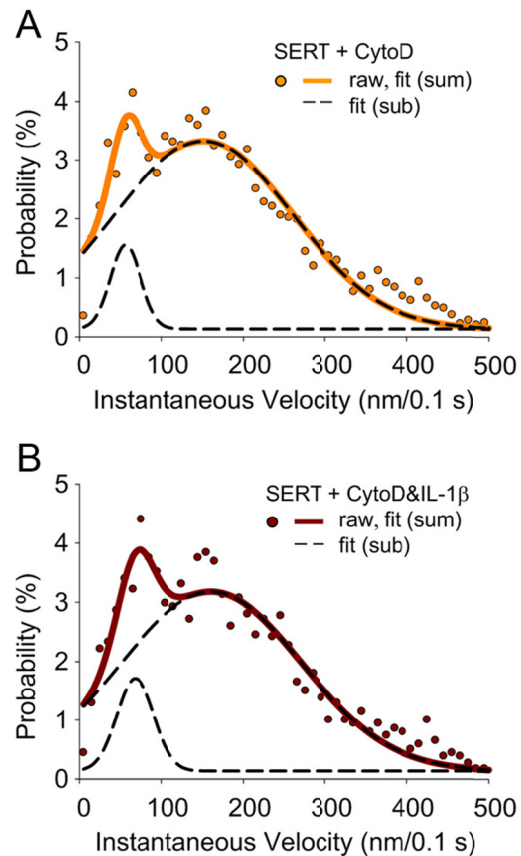
Figure 35: The effects of Cytochalasin D on the instantaneous velocity of SERT. A: Instantaneous velocities of SERT proteins in cells treated with Cytochalasin D. B: instantaneous velocities of SERT proteins in cell that were treated with IL-1β after being treated with Cytochalasin D. (from (182)).

4.4   Conclusion

In this chapter we presented the results of experiment done in

collaboration with Jerry C. Chang. While they addressed a biological question

that was unrelated with the core of our research, the imaging approach and the

analysis technique could be applied to the detection of other transporter (i.e. DAT) and membrane proteins (provided that a specific ligand or antibody is associated to the quantum dots). The experiment in this chapter described the movement of the endogenous SERT in the plasma membrane of RN46A cells. Taking advantage of the intermittent nature of the fluorescence of individual quantum dots, we could identify single SERT on the cell membranes and image them at high speed (frame rate was 10 Hz) over time. By plotting the MSD/Δt *vs* Δt, two population of SERT were identified: the majority that had lower diffusion coefficient and a confined lateral diffusion, and a smaller percentage that displayed higher diffusion coefficient. The treatment with MβCD that extracts cholesterol from the plasma membrane and disrupts lipid rafts, resulted in a total shift of the SERT population to the higher diffusion coefficient, and the MSD/Δt *vs* Δt displayed a slope indicative of free lateral diffusion. The treatment with IL-1β is known to produce the p38 MAPK activation of SERT, with consequent increase in the serotonin uptake rate. This treatment produced an increase in the instantaneous velocity of SERT that yet was still showing the confined lateral diffusion of the lipid raft milieu. We confirmed, by treating the cells with Cytochalasin D, that the increased mobility of SERT during the IL-1β treatment was caused by the disruption of the cytoskeleton anchors that regulates SERT activity. This disruption increased the instantaneous velocity, in association with the increased uptake rate, but did not cause SERT to diffuse out of the lipid raft. This also suggested that lipid raft integrity is independent from the cytoskeleton anchors.

CHAPTER

5. CONCLUSION AND FUTURE DIRECTIONS

5.1   Conclusion

I described experiments that show the existence of a negative feedback regulation of glucose-stimulated insulin secretion (GSIS) from the pancreatic islet. This negative feedback relies on the endogenous synthesis of dopamine by the islet and the consequent co-secretion of dopamine and insulin during glucose stimulation. The presence of the dopamine receptor D3 (DRD3) in the islet cells, makes them sensitive to the secreted dopamine, and mediates the tonic inhibition of GSIS, by reducing the Ca^{2+} influx.

Our study was based on the literature from the past 50 years, which has contributed to build our hypothesis for the role of dopamine in regulating insulin secretion from the pancreatic islet. Previous studies showed that dopamine can inhibit GSIS in isolated islets (3), but there was no consensus on the availability or origin of any dopamine that can act on islets *in vivo*. This led to a conundrum since the islets are sensitive to dopamine, but the dopamine concentration in the plasma is too low (0.67 ± 0.21 nM in C57Bl6 mice) to trigger its receptor (148, 149), and dopaminergic innervation of the pancreas has not been reported. Thus, islet sensitivity to exogenous dopamine has generally not been considered to be physiologically relevant.

I first tested the hypothesis that the islet itself produces dopamine from circulating L-dopa, which was not previously rigorously examined. By focusing our study on isolated mouse islets, I measured dopamine accumulation from the endogenous synthetic activity of the islets. I estimated that freshly isolated islets contain dopamine at a level of ~ 0.5 pg/islet. This value should reflect as close as possible the *in vivo* condition of an islet in its native environment. When L-dopa was increased *in vitro*, I measured a rapid 30-fold increase in the islet dopamine content. Similarly, when circulating L-dopa levels were raised by exogenous administration *in vivo*, I saw a 50-fold increase in dopamine concentration, which corresponded to a robust inhibition of GSIS. I report a dose-dependent inhibition of GSIS by combining L-dopa and glucose in static incubation assays performed on isolated islets. Based on the results from secretion experiment with pre-treated islets, I conclude that this effect was due to increased dopamine content, and not a direct pharmacological effect of L-dopa on GSIS. However, neither L-dopa nor the dopamine receptor agonist quinpirole altered basal insulin secretion at low glucose concentration. This supports the hypothesis that dopamine must be secreted by the islet to produce its effect; also it reinforces the idea that dopamine can only produce an effect when insulin secretion is being stimulated. The conclusion I draw from these experiments is that dopamine is physiologically present in the pancreatic islet of the mouse. It is produced by the islets, and its production can be significantly boosted by increasing the availability of the precursor L-dopa.

Next, I examined the glucose dependence of dopamine secretion by the β-cells in islets. According to our hypothesis, dopamine is co-secreted with insulin. I tested this concept by simultaneously measuring dopamine and insulin secretion. I showed that dopamine secretion parallels insulin secretion, thus making the granular co-localization of the two substances very likely. At the same time that our work was published, a study by Simpson *et al.* (159) was published, where the authors measured dopamine secretion by chrono-amperometry and voltammetry, and came to the same conclusion: dopamine is secreted from the islet in response to glucose. Moreover, they performed perfusion experiments under glucose stimulation and reported dopamine secretion peaks largely coincident with insulin secretion peaks. These independent experiments corroborate our conclusion that dopamine and insulin co-localize in the secretory granule of the β-cells.

Having established that β-cells synthesize and secrete dopamine during GSIS, I proceeded to investigate how dopamine inhibits GSIS. First, I verified that neither dopamine nor L-dopa were interfering with the metabolism of glucose. I did so by monitoring the glucose-induced increase in the autofluorescence from NAD(P)H. Then, I looked at the frequency of $[Ca^{2+}]_i$ oscillations during GSIS, which changes upon exposure to either dopamine or L-dopa. In both cases, I measured a dose-dependent decrease in the frequency of the $[Ca^{2+}]_i$ oscillations, which correlated with the decrease in GSIS. This suggests that dopamine signaling is altering $[Ca^{2+}]_i$ influx to produce inhibition of GSIS. Finally, I identified the dopamine receptor that mediates this inhibition.

It has been shown by two different groups that the DRD2 isoform is present in mouse and human islet, and thus it has been assumed that this isoform mediates the dopamine effects on GSIS (3, 159). However, the results of our experiments clearly showed that while DRD2 is present in the islets, DRD3 is the isoform that mediates the dopaminergic signaling. I demonstrated this by using islets from mice containing a genetic deletion of DRD2 and showing that they still responded to dopamine during GSIS. Further, by using isoform-specific dopamine receptor antagonists for DRD2 and DRD3 on wild type islets, I showed that only the antagonism of DRD3 abolished the effects of dopamine on insulin secretion, enhanced GSIS in untreated islets, and increased their frequency of $[Ca^{2+}]_i$ oscillations. Finally, I verified that the dopamine transporter (DAT) is also expressed in the islets, and I indirectly tested its activity using the DAT inhibitor (GBR 12909). Based on our hypothesis, DAT removes dopamine from the extracellular space, terminating the dopaminergic signaling. Therefore, the inhibition of dopamine reuptake should result in increased extracellular dopamine, and that in turn produces a stronger inhibition of GSIS. This is indeed the result that I measured in the static incubations performed in the presence of GBR 12909. Yet, Simpson *et al.* (159) report the opposite outcome for the same experiment, proposing that the extracellular dopamine is quickly diluted in the assay buffer, and so the antagonism of DAT results in dopamine depletion of the islet with a consequent enhancement of GSIS. I currently cannot find a good explanation to reconcile these conflicting results, and more experiments on this topic are necessary to solve this controversy.

5.2 Future directions

5.2.1 <u>Studying the pathway downstream of DRD3 activation</u>

I showed that dopamine inhibits GSIS via DRD3 activation; thus, it would be reasonable to investigate the resulting intracellular pathway that produces such effect in β-cells. DRD3 couples to inhibitory G-proteins, as do the other members of the D2-like family of dopamine receptor (122). The signaling pathway for this family implies that upon dopamine binding, the $G_{\alpha i}$ subunit can inhibit adenylyl cyclase (AC), and the free $G_{\beta\gamma}$ complex can affect Ca^{2+} channels, K^+ channels, or phospholipase C (201). However, the specific cellular milieu determines which one of the targets is primarily affected. The experiments described so far show that DRD3 activation decreases the frequency of $[Ca^{2+}]_i$ oscillations, which is suggestive of a reduction of Ca^{2+} influx. This effect is fast, as the frequency shift takes place in about 120 seconds in the experimental setup used for our imaging experiments. In a previous study on INS1-E cells, dopamine was shown to not produce a decrease of intracellular cAMP (3). For all these reasons, I propose that DRD3 acts via $G_{\beta\gamma}$ to modulate Ca^{2+} influx through the plasma membrane voltage dependent calcium channels. Yet, the same effect can be obtained in two ways: $G_{\beta\gamma}$ can activate K^+ channels (K_{ATP} or GIRK), hyperpolarizing the membrane and thus reducing the activity of the Ca^{2+} channels; or $G_{\beta\gamma}$ can directly bind the α-subunit of the Ca^{2+} channels and

100

decrease the Ca^{2+} conductance. Our future experiments aim at identifying the pathway that is active in β-cells.

I will use isolated islet loaded with the calcium indicator Fluo-4 AM, and keep them at the same glucose concentration (8 mM) at which I observed the DRD3 effects. I will treat them with K^+ channel blockers (Tolbutamide for K_{ATP} and tertiapine-Q for GIRK) to keep the membrane depolarized and measure the rise in $[Ca^{2+}]_i$. I will repeat the experiment adding dopamine to the K^+ channel blockers, and measuring again the rise in the $[Ca^{2+}]_i$. If I will observe a difference in the rate of the increase of $[Ca^{2+}]_i$ (or possibly in its plateau level) I will interpret the result as a sign that $G_{βγ}$ is acting on Ca^{2+} channels. Otherwise I will conclude that $G_{βγ}$ likely acts on K^+ channels. In this last case, I could use the same strategy to tell if K_{ATP} or GIRK are the target. I will apply to the islet tolbutamide alone, or tertiapine-Q alone, to see in which case dopamine produces a difference in the $[Ca^{2+}]_i$. Consequently, I will separate out which K^+ channel family is the target of $G_{βγ}$ complex.

It is possible that the effect of $G_{βγ}$ is localized near the channels, and is thus too small to be detected by measuring the global $[Ca^{2+}]_i$ by this approach. Therefore, negative results from these experiments cannot be conclusive. In this case, I can perform more sensitive experiments to detect local $[Ca^{2+}]_i$ changes with targeted indicator dyes, or measure directly the interaction between $G_{βγ}$ and its target.

To measure the interactions directly, I are planning to utilize Förster resonance energy transfer (FRET) experiments in βTC3 cells. I will use

G_γ-mVenus fusion protein to tag the $G_{\beta\gamma}$ complex without altering its function (202), while rsTagRFP (203) will be fused to the N-terminus of the α_{1C}-subunit of the Ca^{2+} channels to tag the L-type Ca^{2+} channels without affecting their properties (204). The co-transfection of these constructs will allow measuring FRET if the $G_{\beta\gamma}$ binds the L-type Ca^{2+} channel. However since not all the tagged proteins will be interacting at the same time, our FRET signal will be masked in the background fluorescence of the non-interacting proteins. I plan to circumvent this problem using a lock-in approach to extract the small FRET signal from the high background fluorescence (205). Thanks to the photo-switching properties of rsTagRFP, the acceptor in these experiments can be turned on and off by excitation at 445 nm and 570 nm respectively, which allows us to cyclically modulate the acceptor state of this protein. Correspondingly, I will look for intensity peaks in the mVenus emission. This approach has been shown to improve detection of FRET efficiencies down to 0.1% (205). Negative results from this experiment do not exclude the interaction between the two proteins, as FRET can be prevented by an incorrect relative orientation of the two fluorescent proteins. In this case, alternative fusion protein configurations would be tested.

Alternatively, I can do fluorescence cross-correlation spectroscopy (FCCS) experiments to detect the interaction of the two proteins. This approach will require tagging the $G_{\beta\gamma}$ complex and the L-type Ca^{2+} channel with GFP and mCherry. The cross-correlation function that is obtained from the two auto-correlation functions for the two fluorescent species will detect any interaction between the two proteins.

The experimental approaches that I described so far rely on fluorescence detection to investigate the changes in the ion channel properties (either Ca^{2+} or K^+) caused by dopamine receptor activation. Patch-clamp electrophysiology is the preferred technique to study ion channels properties. Therefore I will perform some electrophysiology experiments to investigate the effects of dopamine. I will use flattened islets or betaTC3 cells to measure the calcium currents through the voltage gated calcium channel. These currents will be monitored during glucose stimulus (8 mM), and during the administration of increasing concentrations of dopamine. I expect to observe a dose dependent effect of dopamine on the currents. Alternatively, if the results show that there is no effect of dopamine on the calcium currents, I will measure potassium currents at non stimulatory glucose concentration. The approach will be again to measure the currents at various dopamine concentrations and to observe a dose dependent effect. If one of these planned experiments will show a dopamine dependent effect on the currents, I will try to confirm that the effect is mediated by the $G_{\beta\gamma}$ complex by applying a synthetic peptide to the patched cell. The peptide will bind to the $G_{\beta\gamma}$ complex, and I expect it to counterbalance the effect of dopamine on the ion currents.

If none of these approaches produce positive results, I will reconsider our initial assumption and instead investigate the effect of DRD3 activation on AC and PKA.

5.2.2 Studying the role of dopamine as a paracrine signal

Given the degree of similarity between the α-cells and the β-cells in the islets, I cannot exclude that α-cells also express DRD3. This hypothesis is very intriguing because it could explain the characteristic glucagon secretion pattern of the α-cells. They secrete glucagon at low glucose concentration (< 3 mM) and they stop secreting at high glucose concentration (> 5 mM). Yet it is not completely understood how this glucose-inhibition of glucagon secretion (GIGS) works. Experimental evidences show that the α-cells lose GIGS when they are dispersed from the islet, pointing at the possibility that a paracrine signal from other islet cells is responsible for the effect (19). Despite 40 years of research (10), an appropriate paracrine signal has not yet been identified, and many other hypotheses are being considered. Several likely paracrine candidates, such as insulin, zinc, GABA, and somatostatin, inhibit glucagon secretion when applied to isolated islets, but they do not show an effect when applied to dispersed α-cells (19). Moreover, α-cells respond to high glucose concentrations similarly to β-cells, by depolarizing the membrane and displaying elevated $[Ca^{2+}]_i$, yet they do not increase their secretion. Therefore the unknown inhibition mechanism is thought to act downstream of the increase in $[Ca^{2+}]_i$.

Based on this evidence, I plan to test the hypothesis that α-cells express DRD3, and that dopamine is a paracrine signal that produces GIGS. Since I showed that dopamine is co-secreted with insulin, this would explain the glucose-dependence of the glucagon inhibition. Since dopamine is secreted by the β-cells, this would explain why dispersed α-cells lose GIGS. Since DRD3 can

signal via $G_{\beta\gamma}$ complex, this could explain also the inhibitory effect downstream of the increase in $[Ca^{2+}]_i$. In fact it has been shown that $G_{\beta\gamma}$ can inhibit exocytosis independently of $[Ca^{2+}]_i$ (109, 206), by binding to the SNARE complex, thus competing with Ca^{2+}-dependent activation of the exocytotic machinery. I can test this hypothesis by performing static incubations to measure glucagon secretion from isolated islets. I would apply excess of dopamine at low glucose to see if this inhibits glucagon secretion. Conversely, I would apply dopamine receptor antagonists at high glucose to see if they increase glucagon secretion.

5.2.3 Subcellular localization of DRD3 and DAT

It has been suggested that DR are located on the insulin secretory granules in β-cells, so that they can be activated only during insulin secretion (3). This concept of localization poses a problem if I consider that the insulin granules also contain dopamine, the ligand for DR. I tried to investigate this subject by performing live-cell imaging experiments on islets that were transduced with DRD2-mVenus. I detected the majority of the receptor on the plasma membrane of the β-cells, but as I was not imaging the endogenous receptors, the results cannot be considered conclusive. I plan to perform a series of experiments using DRD3 antibodies to detect endogenous receptors in fixed intact islet. Based on our previous experiences, I anticipate having high level of non-specific binding of the primary antibody. So I will perform a series of control experiment to discriminate the specific signal from the non-specific one. The use of the antibody-specific antigen was very useful for our western blot experiment, so I

will use the same approach for the immunohistochemistry. Alternatively, I could

perform parallel experiments on wild type and DRD3-knock-out islets. I currently

do not have the DRD3-knock-out mice, but our collaborator Dr. Claudia

Schmauss at Columbia University has created this line of animals. Similarly, I

can investigate the localization of DAT in the islet, by comparing the results from

wild type and DAT-knock-out mice. In this case our collaborator Dr. Aurelio Galli

will provide the transgenic animals.

5.3   Significance

The summary of the presented results shows that a dopaminergic

negative feedback acting on insulin secretion is active in β-cells. Importantly,

blocking this dopaminergic feedback increases GSIS. Therefore DRD3, or one of

the steps downstream of its activation, is a potential target for new drugs to treat

type-2 diabetes. At the same time, the existence of a dopaminergic inhibition of

GSIS allows speculation regarding the high prevalence of abnormal glucose

tolerance in 50-80% of Parkinson patients (207). Prospective studies have

suggested that diabetes is not a preceding risk factor for Parkinson's disease, yet

the two diseases show a significant positive association, possibly explained by a

common underlying biological mechanism (208, 209). I reason that the

dopaminergic regulation of GSIS in the islets could be such underlying

mechanism. Since β-cells share the dopaminergic system with the dopaminergic

neurons of the substantia nigra, it is possible that the still unknown cause of

dopaminergic neuron loss underlying in Parkinson's disease could also cause the

specific loss of β-cell function that results in type-2 diabetes. Another interesting consideration can be made: the therapy for Parkinson's disease consists of administration of L-dopa and benserazide to increase dopamine concentration in dopaminergic neurons and prevent peripheral conversion of L-dopa and its consequent side effects (210). However, a few patients still experience hyperglycemia and hyperinsulinemia as side effects of the treatment (210, 211). Indeed, in our experiments benserazide did not completely halt the production of dopamine in the islets. I can speculate that if this holds true in patients, then the Parkinson's treatment regimen could partially inhibit GSIS and put a chronic stress on islet function that would exacerbate the association between type-2 diabetes and Parkinson's disease (207-210).

The expression of DAT in the pancreatic islet provides another possible link relating type-2 diabetes and Parkinson's disease. I can speculate that the brain and endocrine pancreas are responding to the same insult, and that both tissues suffer same type of damage (i.e., loss of dopaminergic cells). If substance(s) that enter neurons via DAT is one cause of Parkinson's disease, then the same substance(s) could have equally deleterious effects on islet cells (212-214).

Finally, the presence of DRD3 in the β-cells makes them an undesired target of antipsychotic drugs. This could be particularly important considering the number of studies showing associations between metabolic syndrome and atypical-antipsychotic therapy (215-219). The results on this subject are not of easy interpretation, as the atypical antipsychotic drugs act on multiple receptors.

Nonetheless some of their metabolic side effects could be independent from their action on the central nervous system, but instead may be related to direct action on insulin secretion. A better knowledge of their mechanism of action on the DRD3, and consequently on GSIS from the islet, could be helpful in designing antipsychotic drugs with fewer metabolic side effects, or improved therapeutic regimens that minimize these side effects with the current available drugs.

REFERENCES

1.   Unger RH, Dobbs RE, Orci L 1978 Insulin, glucagon, and somatostatin secretion in the regulation of metabolism. Annual review of physiology 40:307-343

2.   2011 National diabetes fact sheet: national estimates and general information on diabetes and prediabetes in the United States, 2011. Centers for Disease Control and Prevention

3.   Rubi B, Ljubicic S, Pournourmohammadi S, Carobbio S, Armanet M, Bartley C, Maechler P 2005 Dopamine D2-like receptors are expressed in pancreatic beta cells and mediate inhibition of insulin secretion. J Biol Chem 280:36824-36832

4.   Shankar E, Santhosh KT, Paulose CS 2006 Dopaminergic regulation of glucose-induced insulin secretion through dopamine D2 receptors in the pancreatic islets in vitro. IUBMB Life 58:157-163

5.   Motta PM, Macchiarelli G, Nottola SA, Correr S 1997 Histology of the exocrine pancreas. Microscopy research and technique 37:384-398

6.   Jansson L, Hellerstrom C 1983 Stimulation by glucose of the blood flow to the pancreatic islets of the rat. Diabetologia 25:45-50

7.   Lifson N, Kramlinger KG, Mayrand RR, Lender EJ 1980 Blood flow to the rabbit pancreas with special reference to the islets of Langerhans. Gastroenterology 79:466-473

8.   Langerhans P 1869 Beitrage zur mkorskischen Anatomie der Bauchspeicheldruse. Inaug Diss

9.   Langerhans P 1937 Contributions to the microscopyc anatomy of the pancreas. Bull Inst History Med 5:1-39

10. Gromada J, Franklin I, Wollheim CB 2007 Alpha-cells of the endocrine pancreas: 35 years of research but the enigma remains. Endocr Rev 28:84-116

11. Weir GC, Bonner-Weir S 1985 Pancreatic somatostatin. Advances in experimental medicine and biology 188:403-423

12. Floyd JC, Jr. 1980 Pancreatic polypeptide. Clinics in gastroenterology 9:657-678

13. Lonovics J, Devitt P, Watson LC, Rayford PL, Thompson JC 1981 Pancreatic polypeptide. A review. Arch Surg 116:1256-1264

14. Broglio F, Prodam F, Riganti F, Muccioli G, Ghigo E 2006 Ghrelin: from somatotrope secretion to new perspectives in the regulation of peripheral metabolic functions. Frontiers of hormone research 35:102-114

15. Hill JT, Mastracci TL, Vinton C, Doyle ML, Anderson KR, Loomis ZL, Schrunk JM, Minic AD, Prabakar KR, Pugliese A, Sun Y, Smith RG, Sussel L 2009 Ghrelin is dispensable for embryonic pancreatic islet development and differentiation. Regulatory peptides 157:51-56

16. Steiner DJ, Kim A, Miller K, Hara M 2010 Pancreatic islet plasticity: interspecies comparison of islet architecture and composition. Islets 2:135-145

17. Brissova M, Fowler MJ, Nicholson WE, Chu A, Hirshberg B, Harlan DM, Powers AC 2005 Assessment of human pancreatic islet architecture and composition by laser scanning confocal microscopy. J Histochem Cytochem 53:1087-1097

18. Kim A, Miller K, Jo J, Kilimnik G, Wojcik P, Hara M 2009 Islet architecture: A comparative study. Islets 1:129-136

19. Le Marchand SJ, Piston DW 2010 Glucose suppression of glucagon secretion: metabolic and calcium responses from alpha-cells in intact mouse pancreatic islets. J Biol Chem 285:14389-14398

20. Lernmark A 1974 The preparation of, and studies on, free cell suspensions from mouse pancreatic islets. Diabetologia 10:431-438

21. Ahren B 2000 Autonomic regulation of islet hormone secretion--implications for health and disease. Diabetologia 43:393-410

22. Marks V, Tan KS, Stagner JI, Samols E 1990 Intra-islet cellular interrelationships. Biochemical Society transactions 18:103-104

23. Serre-Beinier V, Mas C, Calabrese A, Caton D, Bauquis J, Caille D, Charollais A, Cirulli V, Meda P 2002 Connexins and secretion. Biology of the cell / under the auspices of the European Cell Biology Organization 94:477-492

24. Head WS, Orseth ML, Nunemaker CS, Satin LS, Piston DW, Benninger RK 2012 Connexin-36 gap junctions regulate in vivo first- and second-phase insulin secretion dynamics and glucose tolerance in the conscious mouse. Diabetes 61:1700-1707

25. Ravier MA, Guldenagel M, Charollais A, Gjinovci A, Caille D, Sohl G, Wollheim CB, Willecke K, Henquin JC, Meda P 2005 Loss of connexin36 channels alters beta-cell coupling, islet synchronization of glucose-induced Ca2+ and insulin oscillations, and basal insulin release. Diabetes 54:1798-1807

26. Rocheleau JV, Remedi MS, Granada B, Head WS, Koster JC, Nichols CG, Piston DW 2006 Critical role of gap junction coupled KATP channel activity for regulated insulin secretion. Plos Biol 4:e26

27. Henderson JR, Moss MC 1985 A morphometric study of the endocrine and exocrine capillaries of the pancreas. Q J Exp Physiol 70:347-356

28. Walker JN, Ramracheya R, Zhang Q, Johnson PR, Braun M, Rorsman P 2011 Regulation of glucagon secretion by glucose: paracrine, intrinsic or both? Diabetes, obesity & metabolism 13 Suppl 1:95-105

29. Cryer PE 2008 Glucagon and hyperglycaemia in diabetes. Clin Sci (Lond) 114:589-590

30. Kahn SE, Zraika S, Utzschneider KM, Hull RL 2009 The beta cell lesion in type 2 diabetes: there has to be a primary functional abnormality. Diabetologia 52:1003-1012

31. Lebovitz HE 1999 Type 2 diabetes: an overview. Clinical chemistry 45:1339-1345

32. Lemieux S, Prud'homme D, Nadeau A, Tremblay A, Bouchard C, Despres JP 1996 Seven-year changes in body fat and visceral adipose tissue in women. Association with indexes of plasma glucose-insulin homeostasis. Diabetes Care 19:983-991

33. 2010 Standards of medical care in diabetes--2010. Diabetes Care 33 Suppl 1:S11-61

34. Yki-Jarvinen H 1992 Glucose toxicity. Endocr Rev 13:415-431

35. 1995 U.K. prospective diabetes study 16. Overview of 6 years' therapy of type II diabetes: a progressive disease. U.K. Prospective Diabetes Study Group. Diabetes 44:1249-1258

36. Lebovitz HE 2001 Diagnosis, classification, and pathogenesis of diabetes mellitus. The Journal of clinical psychiatry 62 Suppl 27:5-9; discussion 40-41

37. Nathan DM, Buse JB, Davidson MB, Ferrannini E, Holman RR, Sherwin R, Zinman B 2009 Medical Management of Hyperglycemia in Type 2 Diabetes: A Consensus Algorithm for the Initiation and Adjustment of Therapy. Diabetes Care 32:193-203

38. Hughes SD, Quaade C, Johnson JH, Ferber S, Newgard CB 1993 Transfection of AtT-20ins cells with GLUT-2 but not GLUT-1 confers glucose-stimulated insulin secretion. Relationship to glucose metabolism. J Biol Chem 268:15205-15212

39. Johnson JH, Newgard CB, Milburn JL, Lodish HF, Thorens B 1990 The high Km glucose transporter of islets of Langerhans is functionally similar to the low affinity transporter of liver and has an identical primary sequence. J Biol Chem 265:6548-6551

40. Thorens B, Sarkar HK, Kaback HR, Lodish HF 1988 Cloning and functional expression in bacteria of a novel glucose transporter present in liver, intestine, kidney, and beta-pancreatic islet cells. Cell 55:281-290

41. Magnuson MA, Shelton KD 1989 An alternate promoter in the glucokinase gene is active in the pancreatic beta cell. J Biol Chem 264:15936-15942

42. Iynedjian PB, Pilot PR, Nouspikel T, Milburn JL, Quaade C, Hughes S, Ucla C, Newgard CB 1989 Differential expression and regulation of the glucokinase gene in liver and islets of Langerhans. Proc Natl Acad Sci U S A 86:7838-7842

43. Matschinsky FM 1990 Glucokinase as glucose sensor and metabolic signal generator in pancreatic beta-cells and hepatocytes. Diabetes 39:647-652

44. Detimary P, Van den Berghe G, Henquin JC 1996 Concentration dependence and time course of the effects of glucose on adenine and guanine nucleotides in mouse pancreatic islets. J Biol Chem 271:20559-20565

45. Ashcroft FM, Harrison DE, Ashcroft SJ 1984 Glucose induces closure of single potassium channels in isolated rat pancreatic beta-cells. Nature 312:446-448

46. Cook DL, Hales CN 1984 Intracellular ATP directly blocks K+ channels in pancreatic B-cells. Nature 311:271-273

47. Satin LS, Cook DL 1985 Voltage-gated Ca2+ current in pancreatic B-cells. Pflugers Archiv : European journal of physiology 404:385-387

48. Hoenig M, Sharp GW 1986 Glucose induces insulin release and a rise in cytosolic calcium concentration in a transplantable rat insulinoma. Endocrinology 119:2502-2507

49. Wollheim CB, Sharp GW 1981 Regulation of insulin release by calcium. Physiological reviews 61:914-973

50.   Rorsman P, Renstrom E 2003 Insulin granule dynamics in pancreatic beta cells. Diabetologia 46:1029-1045

51.   Kanno T, Rorsman P, Gopel SO 2002 Glucose-dependent regulation of rhythmic action potential firing in pancreatic beta-cells by K(ATP)-channel modulation. J Physiol 545:501-507

52.   Zhang M, Houamed K, Kupershmidt S, Roden D, Satin LS 2005 Pharmacological properties and functional role of Kslow current in mouse pancreatic beta-cells: SK channels contribute to Kslow tail current and modulate insulin secretion. The Journal of general physiology 126:353-363

53.   MacDonald PE, Wheeler MB 2003 Voltage-dependent K(+) channels in pancreatic beta cells: role, regulation and potential as therapeutic targets. Diabetologia 46:1046-1062

54.   Bergsten P 1995 Slow and fast oscillations of cytoplasmic Ca2+ in pancreatic islets correspond to pulsatile insulin release. American Journal of Physiology - Endocrinology And Metabolism 268:E282-E287

55.   Nunemaker CS, Bertram R, Sherman A, Tsaneva-Atanasova K, Daniel CR, Satin LS 2006 Glucose modulates [Ca2+]i oscillations in pancreatic islets via ionic and glycolytic mechanisms. Biophys J 91:2082-2096

56.   Bertram R, Previte J, Sherman A, Kinard TA, Satin LS 2000 The phantom burster model for pancreatic beta-cells. Biophys J 79:2880-2892

57.   Nunemaker CS, Wasserman DH, McGuinness OP, Sweet IR, Teague JC, Satin LS 2006 Insulin secretion in the conscious mouse is biphasic and pulsatile. Am J Physiol Endocrinol Metab 290:E523-529

58.   Lang DA, Matthews DR, Peto J, Turner RC 1979 Cyclic oscillations of basal plasma glucose and insulin concentrations in human beings. N Engl J Med 301:1023-1027

59.   Song SH, McIntyre SS, Shah H, Veldhuis JD, Hayes PC, Butler PC 2000 Direct measurement of pulsatile insulin secretion from the portal vein in human subjects. J Clin Endocrinol Metab 85:4491-4499

60.   Del Prato S 2003 Loss of early insulin secretion leads to postprandial hyperglycaemia. Diabetologia 46 Suppl 1:M2-8

61.   Efendic S, Luft R, Wajngot A 1984 Aspects of the pathogenesis of type 2 diabetes. Endocr Rev 5:395-410

62.   Matthews DR, Lang DA, Burnett MA, Turner RC 1983 Control of pulsatile insulin secretion in man. Diabetologia 24:231-237

63.   Lang DA, Matthews DR, Burnett M, Turner RC 1981 Brief, irregular oscillations of basal plasma insulin and glucose concentrations in diabetic man. Diabetes 30:435-439

64.   Mirbolooki MR, Taylor GE, Knutzen VK, Scharp DW, Willcourt R, Lakey JR 2009 Pulsatile intravenous insulin therapy: the best practice to reverse diabetes complications? Medical hypotheses 73:363-369

65.   Sima AA 2006 Pathological mechanisms involved in diabetic neuropathy: can we slow the process? Curr Opin Investig Drugs 7:324-337

66.   Bratusch-Marrain PR, Komjati M, Waldhausl WK 1986 Efficacy of pulsatile versus continuous insulin administration on hepatic glucose production and glucose utilization in type I diabetic humans. Diabetes 35:922-926

67.   Lagerstrom MC, Schioth HB 2008 Structural diversity of G protein-coupled receptors and significance for drug discovery. Nat Rev Drug Discov 7:339-357

68.   Civelli O 2005 GPCR deorphanizations: the novel, the known and the unexpected transmitters. Trends in pharmacological sciences 26:15-19

69.   Foord SM, Bonner TI, Neubig RR, Rosser EM, Pin JP, Davenport AP, Spedding M, Harmar AJ 2005 International Union of Pharmacology. XLVI. G protein-coupled receptor list. Pharmacol Rev 57:279-288

70.   Xiao SH, Reagan JD, Lee PH, Fu A, Schwandner R, Zhao X, Knop J, Beckmann H, Young SW 2008 High throughput screening for orphan and liganded GPCRs. Combinatorial chemistry & high throughput screening 11:195-215

71.   Hargrave PA, McDowell JH, Feldmann RJ, Atkinson PH, Rao JK, Argos P 1984 Rhodopsin's protein and carbohydrate structure: selected aspects. Vision research 24:1487-1499

72.   Hargrave PA, McDowell JH, Curtis DR, Wang JK, Juszczak E, Fong SL, Rao JK, Argos P 1983 The structure of bovine rhodopsin. Biophysics of structure and mechanism 9:235-244

73.   Nathans J, Hogness DS 1983 Isolation, sequence analysis, and intron-exon arrangement of the gene encoding bovine rhodopsin. Cell 34:807-814

74.   Fredriksson R, Lagerstrom MC, Lundin LG, Schioth HB 2003 The G-protein-coupled receptors in the human genome form five main families. Phylogenetic analysis, paralogon groups, and fingerprints. Molecular pharmacology 63:1256-1272

75.   Wess J 1997 G-protein-coupled receptors: molecular mechanisms involved in receptor activation and selectivity of G-protein recognition. Faseb J 11:346-354

76.   Hamm HE 1998 The many faces of G protein signaling. J Biol Chem 273:669-672

77.   Milligan G, Kostenis E 2006 Heterotrimeric G-proteins: a short history. Br J Pharmacol 147 Suppl 1:S46-55

78.   Neves SR, Ram PT, Iyengar R 2002 G protein pathways. Science 296:1636-1639

79.   Doyle ME, Egan JM 2007 Mechanisms of action of glucagon-like peptide 1 in the pancreas. Pharmacol Ther 113:546-593

80.   Jiang Y, Ma W, Wan Y, Kozasa T, Hattori S, Huang XY 1998 The G protein G alpha12 stimulates Bruton's tyrosine kinase and a rasGAP through a conserved PH/BM domain. Nature 395:808-813

81. Kieffer TJ, Heller RS, Unson CG, Weir GC, Habener JF 1996 Distribution of glucagon receptors on hormone-specific endocrine cells of rat pancreatic islets. Endocrinology 137:5119-5125

82. Hansotia T, Drucker DJ 2005 GIP and GLP-1 as incretin hormones: lessons from single and double incretin receptor knockout mice. Regulatory peptides 128:125-134

83. Winzell MS, Ahren B 2007 G-protein-coupled receptors and islet function-implications for treatment of type 2 diabetes. Pharmacol Ther 116:437-448

84. Ahren B 2009 Islet G protein-coupled receptors as potential targets for treatment of type 2 diabetes. Nat Rev Drug Discov 8:369-385

85. Drucker DJ, Nauck MA 2006 The incretin system: glucagon-like peptide-1 receptor agonists and dipeptidyl peptidase-4 inhibitors in type 2 diabetes. Lancet 368:1696-1705

86. Drucker DJ 2006 Incretin-based therapies: a clinical need filled by unique metabolic effects. The Diabetes educator 32 Suppl 2:65S-71S

87. Petit P, Loubatieres-Mariani MM 1992 Potassium channels of the insulin-secreting B cell. Fundamental & clinical pharmacology 6:123-134

88. Straub SG, Sharp GW 2012 Evolving insights regarding mechanisms for the inhibition of insulin release by norepinephrine and heterotrimeric G proteins. Am J Physiol Cell Physiol 302:C1687-1698

89. Krapivinsky G, Gordon EA, Wickman K, Velimirovic B, Krapivinsky L, Clapham DE 1995 The G-protein-gated atrial K+ channel IKACh is a heteromultimer of two inwardly rectifying K(+)-channel proteins. Nature 374:135-141

90. Krapivinsky G, Krapivinsky L, Wickman K, Clapham DE 1995 G beta gamma binds directly to the G protein-gated K+ channel, IKACh. J Biol Chem 270:29059-29062

91. Iwanir S, Reuveny E 2008 Adrenaline-induced hyperpolarization of mouse pancreatic islet cells is mediated by G protein-gated inwardly rectifying

potassium (GIRK) channels. Pflugers Archiv : European journal of physiology 456:1097-1108

92.   Samols E, Marri G, Marks V 1965 Promotion of Insulin Secretion by Glucagon. Lancet 2:415-416

93.   Clapham DE, Neer EJ 1997 G protein beta gamma subunits. Annual review of pharmacology and toxicology 37:167-203

94.   Yang SN, Berggren PO 2005 Beta-cell CaV channel regulation in physiology and pathophysiology. Am J Physiol Endocrinol Metab 288:E16-28

95.   Yang SN, Berggren PO 2006 The role of voltage-gated calcium channels in pancreatic beta-cell physiology and pathophysiology. Endocr Rev 27:621-676

96.   Newcomb R, Szoke B, Palma A, Wang G, Chen X, Hopkins W, Cong R, Miller J, Urge L, Tarczy-Hornoch K, Loo JA, Dooley DJ, Nadasdi L, Tsien RW, Lemos J, Miljanich G 1998 Selective peptide antagonist of the class E calcium channel from the venom of the tarantula Hysterocrates gigas. Biochemistry 37:15353-15362

97.   Llinas R, Sugimori M, Lin JW, Cherksey B 1989 Blocking and isolation of a calcium channel from neurons in mammals and cephalopods utilizing a toxin fraction (FTX) from funnel-web spider poison. Proc Natl Acad Sci U S A 86:1689-1693

98.   Randall A, Tsien RW 1995 Pharmacological dissection of multiple types of Ca2+ channel currents in rat cerebellar granule neurons. The Journal of neuroscience : the official journal of the Society for Neuroscience 15:2995-3012

99.   Tsien RW, Lipscombe D, Madison DV, Bley KR, Fox AP 1988 Multiple types of neuronal calcium channels and their selective modulation. Trends in neurosciences 11:431-438

100.   Yang SN, Berggren PO 2005 CaV2.3 channel and PKClambda: new players in insulin secretion. J Clin Invest 115:16-20

101. Catterall WA 2000 Structure and regulation of voltage-gated Ca2+ channels. Annual review of cell and developmental biology 16:521-555

102. Dolphin AC 2003 G protein modulation of voltage-gated calcium channels. Pharmacol Rev 55:607-627

103. Ammala C, Berggren PO, Bokvist K, Rorsman P 1992 Inhibition of L-type calcium channels by internal GTP [gamma S] in mouse pancreatic beta cells. Pflugers Archiv : European journal of physiology 420:72-77

104. Ivanina T, Blumenstein Y, Shistik E, Barzilai R, Dascal N 2000 Modulation of L-type Ca2+ channels by gbeta gamma and calmodulin via interactions with N and C termini of alpha 1C. J Biol Chem 275:39846-39854

105. Gauthier BR, Wollheim CB 2008 Synaptotagmins bind calcium to release insulin. Am J Physiol Endocrinol Metab 295:E1279-1286

106. Blackmer T, Larsen EC, Bartleson C, Kowalchyk JA, Yoon EJ, Preininger AM, Alford S, Hamm HE, Martin TF 2005 G protein betagamma directly regulates SNARE protein fusion machinery for secretory granule exocytosis. Nature neuroscience 8:421-425

107. Blackmer T, Larsen EC, Takahashi M, Martin TF, Alford S, Hamm HE 2001 G protein betagamma subunit-mediated presynaptic inhibition: regulation of exocytotic fusion downstream of Ca2+ entry. Science 292:293-297

108. Gerachshenko T, Blackmer T, Yoon EJ, Bartleson C, Hamm HE, Alford S 2005 Gbetagamma acts at the C terminus of SNAP-25 to mediate presynaptic inhibition. Nature neuroscience 8:597-605

109. Zhao Y, Fang Q, Straub SG, Lindau M, Sharp GW 2010 Noradrenaline inhibits exocytosis via the G protein betagamma subunit and refilling of the readily releasable granule pool via the alpha(i1/2) subunit. J Physiol 588:3485-3498

110. Carlsson A, Lindqvist M, Magnusson T, Waldeck B 1958 On the presence of 3-hydroxytyramine in brain. Science 127:471

111. Moore RY, Bloom FE 1978 Central catecholamine neuron systems: anatomy and physiology of the dopamine systems. Annual review of neuroscience 1:129-169

112. Ungerstedt U 1971 Stereotaxic mapping of the monoamine pathways in the rat brain. Acta Physiol Scand Suppl 367:1-48

113. Ben-Jonathan N, Hnasko R 2001 Dopamine as a prolactin (PRL) inhibitor. Endocr Rev 22:724-763

114. Barnes TD, Kubota Y, Hu D, Jin DZ, Graybiel AM 2005 Activity of striatal neurons reflects dynamic encoding and recoding of procedural memories. Nature 437:1158-1161

115. Mogenson GJ, Jones DL, Yim CY 1980 From motivation to action: functional interface between the limbic system and the motor system. Progress in neurobiology 14:69-97

116. Berridge KC, Robinson TE 1998 What is the role of dopamine in reward: hedonic impact, reward learning, or incentive salience? Brain research Brain research reviews 28:309-369

117. Williams GV, Goldman-Rakic PS 1995 Modulation of memory fields by dopamine D1 receptors in prefrontal cortex. Nature 376:572-575

118. Ehringer H, Hornykiewicz O 1960 [Distribution of noradrenaline and dopamine (3-hydroxytyramine) in the human brain and their behavior in diseases of the extrapyramidal system]. Klinische Wochenschrift 38:1236-1239

119. Seeman P, Weinshenker D, Quirion R, Srivastava LK, Bhardwaj SK, Grandy DK, Premont RT, Sotnikova TD, Boksa P, El-Ghundi M, O'Dowd B F, George SR, Perreault ML, Mannisto PT, Robinson S, Palmiter RD, Tallerico T 2005 Dopamine supersensitivity correlates with D2High states, implying many paths to psychosis. Proc Natl Acad Sci U S A 102:3513-3518

120. Bobb AJ, Castellanos FX, Addington AM, Rapoport JL 2005 Molecular genetic studies of ADHD: 1991 to 2004. American journal of medical

genetics Part B, Neuropsychiatric genetics : the official publication of the International Society of Psychiatric Genetics 132B:109-125

121. Pivonello R, Ferone D, Lombardi G, Colao A, Lamberts SW, Hofland LJ 2007 Novel insights in dopamine receptor physiology. European journal of endocrinology / European Federation of Endocrine Societies 156 Suppl 1:S13-21

122. Missale C, Nash SR, Robinson SW, Jaber M, Caron MG 1998 Dopamine receptors: from structure to function. Physiological reviews 78:189-225

123. Mezey E, Eisenhofer G, Harta G, Hansson S, Gould L, Hunyady B, Hoffman BJ 1996 A novel nonneuronal catecholaminergic system: exocrine pancreas synthesizes and releases dopamine. Proc Natl Acad Sci U S A 93:10377-10382

124. Falck B, Hellman B 1963 Evidence for the presence of biogenic amines in pancreatic islets. Cellular and Molecular Life Sciences 19:139-140

125. Falck B, Hellman B 1964 A Fluorescent Reaction for Monoamines in the Insulin Producing Cells of the Guinea-Pig. Acta Endocrinol (Copenh) 45:133-138

126. Hakanson R, Lundquist I, Rerup C 1967 On the hyperglycaemic effect of DOPA and dopamine. Eur J Pharmacol 1:114-119

127. Cegrell L 1968 The occurrence of biogenic monoamines in the mammalian endocrine pancreas. Acta Physiol Scand Suppl 314:1-60

128. Feldman JM, Lebovitz HE 1971 The nature of the interaction of amines with the pancreatic beta cells to influence insulin secretion. Journal of Pharmacology and Experimental Therapeutics 179:56-65

129. Quickel KE, Jr., Feldman JM, Lebovitz HE 1971 Inhibition of insulin secretion by serotonin and dopamine: species variation. Endocrinology 89:1295-1302

130. Wilson JP, Downs RW, Feldman JM, Lebovitz HE 1974 Beta cell monoamines: further evidence for their role in modulating insulin secretion. American Journal of Physiology -- Legacy Content 227:305-312

131. Pearse AG 1968 Common cytochemical and ultrastructural characteristics of cells producing polypeptide hormones (the APUD series) and their relevance to thyroid and ultimobranchial C cells and calcitonin. Proc R Soc Lond B Biol Sci 170:71-80

132. Hansen SE, Hedeskov CJ 1977 Simultaneous determination of the content of serotonin, dopamine, noradrenaline and adrenaline in pancreatic islets isolated from fed and starved mice. Acta Endocrinol (Copenh) 86:820-832

133. Mahony C, Feldman JM 1977 Species variation in pancreatic islet monoamine uptake and action. Diabetes 26:257-261 %R 210.2337/diabetes.2326.2334.2257

134. Zern RT, Foster LB, Blalock JA, Feldman JM 1979 Characteristics of the dopaminergic and noradrenergic systems of the pancreatic islets. Diabetes 28:185-189

135. Zern RT, Bird JL, Feldman JM 1980 Effect of increased pancreatic islet norepinephrine, dopamine and serotonin concentration on insulin secretion in the golden hamster. Diabetologia 18:341-346

136. Feldman JM 1979 Species variation in the islets of Langerhans. Diabetologia 16:1-4

137. Ahren B, Lundquist I 1985 Effects of L-dopa-induced dopamine accumulation on 45Ca2+ efflux and insulin secretion in isolated rat islets. Pharmacology 30:71-82

138. Ericson LE, Hakanson R, Lundquist I 1977 Accumulation of dopamine in mouse pancreatic B-cells following injection of L-DOPA. Localization to secretory granules and inhibition of insulin secretion. Diabetologia 13:117-124

139. Lundquist I, Panagiotidis G, Stenstrom A 1991 Effect of L-dopa administration on islet monoamine oxidase activity and glucose-induced insulin release in the mouse. Pancreas 6:522-527

140. Lundquist I, Ahren B, Hansson C, Hakanson R 1989 Monoamines in pancreatic islets of guinea pig, hamster, rat, and mouse determined by high performance liquid chromatography. Pancreas 4:662-667

141. Lindstrom P 1986 Aromatic-L-amino-acid decarboxylase activity in mouse pancreatic islets. Biochimica et biophysica acta 884:276-281

142. Teitelman G, Joh TH, Reis DJ 1981 Transformation of catecholaminergic precursors into glucagon (A) cells in mouse embryonic pancreas. Proc Natl Acad Sci U S A 78:5225-5229

143. Harris PE, Ferrara C, Barba P, Polito T, Freeby M, Maffei A 2008 VMAT2 gene expression and function as it applies to imaging beta-cell mass. J Mol Med 86:5-16

144. Raffo A, Hancock K, Polito T, Xie Y, Andan G, Witkowski P, Hardy M, Barba P, Ferrara C, Maffei A, Freeby M, Goland R, Leibel RL, Sweet IR, Harris PE 2008 Role of vesicular monoamine transporter type 2 in rodent insulin secretion and glucose metabolism revealed by its specific antagonist tetrabenazine. J Endocrinol 198:41-49

145. Eisenhofer G, Aneman A, Friberg P, Hooper D, Fandriks L, Lonroth H, Hunyady B, Mezey E 1997 Substantial production of dopamine in the human gastrointestinal tract. J Clin Endocrinol Metab 82:3864-3871

146. Eisenhofer G, Kopin IJ, Goldstein DS 2004 Catecholamine metabolism: A contemporary view with implications for physiology and medicine. Pharmacol Rev 56:331-349

147. Goldstein DS, Eisenhofer G, Kopin IJ 2003 Sources and significance of plasma levels of catechols and their metabolites in humans. J Pharmacol Exp Ther 305:800-811

148. Eldrup E 2004 Significance and origin of DOPA, DOPAC, and dopamine-sulphate in plasma, tissues and cerebrospinal fluid. Dan Med Bull 51:34-62

149. Keller NR, Diedrich A, Appalsamy M, Tuntrakool S, Lonce S, Finney C, Caron MG, Robertson D 2004 Norepinephrine transporter-deficient mice exhibit excessive tachycardia and elevated blood pressure with wakefulness and activity. Circulation 110:1191-1196

150. Miller RE 1981 Pancreatic neuroendocrinology: peripheral neural mechanisms in the regulation of the Islets of Langerhans. Endocr Rev 2:471-494

151. Lacy PE, Kostianovsky M 1967 Method for the isolation of intact islets of Langerhans from the rat pancreas. Diabetes 16:35-39

152. Ustione A, Piston DW 2012 Dopamine Synthesis and D3 Receptor Activation in Pancreatic beta-Cells Regulates Insulin Secretion and Intracellular [Ca2+] Oscillations. Mol Endocrinol

153. Eldrup E, Moller SE, Andreasen J, Christensen NJ 1997 Effects of ordinary meals on plasma concentrations of 3,4-dihydroxyphenylalanine, dopamine sulphate and 3,4-dihydroxyphenylacetic acid. Clin Sci (Lond) 92:423-430

154. Colebrooke RE, Humby T, Lynch PJ, McGowan DP, Xia J, Emson PC 2006 Age-related decline in striatal dopamine content and motor performance occurs in the absence of nigral cell loss in a genetic mouse model of Parkinson's disease. The European journal of neuroscience 24:2622-2630

155. Leblanc H, Lachelin GC, Abu-Fadil S, Yen SS 1977 The effect of dopamine infusion on insulin and glucagon secretion in man. J Clin Endocrinol Metab 44:196-198

156. Tjurmina OA, Armando I, Saavedra JM, Goldstein DS, Murphy DL 2002 Exaggerated adrenomedullary response to immobilization in mice with targeted disruption of the serotonin transporter gene. Endocrinology 143:4520-4526

157. Bergsten P, Moura AS, Atwater I, Levine M 1994 Ascorbic acid and insulin secretion in pancreatic islets. Journal of Biological Chemistry 269:1041-1045

158. Komatsu M, Schermerhorn T, Aizawa T, Sharp GW 1995 Glucose stimulation of insulin release in the absence of extracellular Ca2+ and in the absence of any increase in intracellular Ca2+ in rat pancreatic islets. Proc Natl Acad Sci U S A 92:10728-10732

159. Simpson N, Maffei A, Freeby M, Burroughs S, Freyberg Z, Javitch J, Leibel RL, Harris PE 2012 Dopamine-mediated autocrine inhibitory circuit regulating human insulin secretion in vitro. Mol Endocrinol 26:1757-1772

160. Beaulieu JM, Gainetdinov RR 2011 The Physiology, Signaling, and Pharmacology of Dopamine Receptors. Pharmacol Rev 63:A-AJ

161. Garcia-Tornadu I, Ornstein AM, Chamson-Reig A, Wheeler MB, Hill DJ, Arany E, Rubinstein M, Becu-Villalobos D 2010 Disruption of the dopamine d2 receptor impairs insulin secretion and causes glucose intolerance. Endocrinology 151:1441-1450

162. Wu W, Shang J, Feng Y, Thompson CM, Horwitz S, Thompson JR, MacIntyre ED, Thornberry NA, Chapman K, Zhou YP, Howard AD, Li J 2008 Identification of glucose-dependant insulin secretion targets in pancreatic beta cells by combining defined-mechanism compound library screening and siRNA gene silencing. J Biomol Screen 13:128-134

163. Piston DW, Knobel SM 1999 Quantitative imaging of metabolism by two-photon excitation microscopy. Methods Enzymol 307:351-368

164. Eng J, Lynch RM, Balaban RS 1989 Nicotinamide adenine dinucleotide fluorescence spectroscopy and imaging of isolated cardiac myocytes. Biophys J 55:621-630

165. Easley CJ, Benninger RK, Shaver JH, Steven Head W, Piston DW 2009 Rapid and inexpensive fabrication of polymeric microfluidic devices via toner transfer masking. Lab Chip 9:1119-1127

166. Miyazaki J, Araki K, Yamato E, Ikegami H, Asano T, Shibasaki Y, Oka Y, Yamamura K 1990 Establishment of a pancreatic beta cell line that retains glucose-inducible insulin secretion: special reference to expression of glucose transporter isoforms. Endocrinology 127:126-132

167. Rasband WS 1997-2009 ImageJ, U S National Institutes of Health, Bethesda, Maryland, USA, http://rsbinfonihgov/ij/

168. Uhlen P 2004 Spectral analysis of calcium oscillations. Sci STKE 2004:pl15

169. Jung MY, Skryabin BV, Arai M, Abbondanzo S, Fu D, Brosius J, Robakis NK, Polites HG, Pintar JE, Schmauss C 1999 Potentiation of the D2 mutant motor phenotype in mice lacking dopamine D2 and D3 receptors. Neuroscience 91:911-924

170. Graham DG 1978 Oxidative pathways for catecholamines in the genesis of neuromelanin and cytotoxic quinones. Molecular pharmacology 14:633-643

171. Chiueh CC, Miyake H, Peng MT 1993 Role of dopamine autoxidation, hydroxyl radical generation, and calcium overload in underlying mechanisms involved in MPTP-induced parkinsonism. Advances in neurology 60:251-258

172. Mytilineou C, Han SK, Cohen G 1993 Toxic and protective effects of L-dopa on mesencephalic cell cultures. Journal of neurochemistry 61:1470-1478

173. Tanaka M, Sotomatsu A, Kanai H, Hirai S 1991 Dopa and dopamine cause cultured neuronal death in the presence of iron. Journal of the neurological sciences 101:198-203

174. Ben-Shachar D, Zuk R, Glinka Y 1995 Dopamine neurotoxicity: inhibition of mitochondrial respiration. Journal of neurochemistry 64:718-723

175. Hernandez-Lopez S, Tkatch T, Perez-Garci E, Galarraga E, Bargas J, Hamm H, Surmeier DJ 2000 D2 dopamine receptors in striatal medium spiny neurons reduce L-type Ca2+ currents and excitability via a novel PLC[beta]1-IP3-calcineurin-signaling cascade. The Journal of neuroscience : the official journal of the Society for Neuroscience 20:8987-8995

176. Olson PA, Tkatch T, Hernandez-Lopez S, Ulrich S, Ilijic E, Mugnaini E, Zhang H, Bezprozvanny I, Surmeier DJ 2005 G-protein-coupled receptor

modulation of striatal CaV1.3 L-type Ca2+ channels is dependent on a Shank-binding domain. The Journal of neuroscience : the official journal of the Society for Neuroscience 25:1050-1062

177. Seeman P, Van Tol HH 1994 Dopamine receptor pharmacology. Trends in pharmacological sciences 15:264-270

178. Elliott AD, Gao L, Ustione A, Bedard N, Kester R, Piston DW, Tkaczyk TS 2012 Real-time hyperspectral fluorescence imaging of pancreatic beta-cell dynamics with the image mapping spectrometer (IMS). J Cell Sci

179. Pound LD, Sarkar SA, Ustione A, Dadi PK, Shadoan MK, Lee CE, Walters JA, Shiota M, McGuinness OP, Jacobson DA, Piston DW, Hutton JC, Powell DR, O'Brien RM 2012 The physiological effects of deleting the mouse SLC30A8 gene encoding zinc transporter-8 are influenced by gender and genetic background. PloS one 7:e40972

180. Benninger RK, Remedi MS, Head WS, Ustione A, Piston DW, Nichols CG 2011 Defects in beta cell Ca(2)+ signalling, glucose metabolism and insulin secretion in a murine model of K(ATP) channel-induced neonatal diabetes mellitus. Diabetologia 54:1087-1097

181. Chen SX, Osipovich AB, Ustione A, Potter LA, Hipkens S, Gangula R, Yuan W, Piston DW, Magnuson MA 2011 Quantification of factors influencing fluorescent protein expression using RMCE to generate an allelic series in the ROSA26 locus in mice. Disease models & mechanisms 4:537-547

182. Chang JC, Tomlinson ID, Warnement MR, Ustione A, Carneiro AM, Piston DW, Blakely RD, Rosenthal SJ 2012 Single molecule analysis of serotonin transporter regulation using antagonist-conjugated quantum dots reveals restricted, p38 MAPK-dependent mobilization underlying uptake activation. The Journal of neuroscience : the official journal of the Society for Neuroscience 32:8919-8929

183. Bannai H, Levi S, Schweizer C, Dahan M, Triller A 2006 Imaging the lateral diffusion of membrane molecules with quantum dots. Nature protocols 1:2628-2634

184. Jaqaman K, Loerke D, Mettlen M, Kuwata H, Grinstein S, Schmid SL, Danuser G 2008 Robust single-particle tracking in live-cell time-lapse sequences. Nature methods 5:695-702

185. Ehrensperger MV, Hanus C, Vannier C, Triller A, Dahan M 2007 Multiple association states between glycine receptors and gephyrin identified by SPT analysis. Biophys J 92:3706-3718

186. Bonneau S, Dahan M, Cohen LD 2005 Single quantum dot tracking based on perceptual grouping using minimal paths in a spatiotemporal volume. IEEE transactions on image processing : a publication of the IEEE Signal Processing Society 14:1384-1395

187. Vrljic M, Nishimura SY, Moerner WE 2007 Single-molecule tracking. Methods Mol Biol 398:193-219

188. Martin DS, Forstner MB, Kas JA 2002 Apparent subdiffusion inherent to single particle tracking. Biophys J 83:2109-2117

189. Zumofen G, Klafter J 1994 Reaction dynamics controlled by enhanced diffusion. Physical review E, Statistical physics, plasmas, fluids, and related interdisciplinary topics 50:5119-5122

190. Sokolov IM, Klafter J 2005 From diffusion to anomalous diffusion: a century after Einstein's Brownian motion. Chaos 15:26103

191. Murphy DL, Fox MA, Timpano KR, Moya PR, Ren-Patterson R, Andrews AM, Holmes A, Lesch KP, Wendland JR 2008 How the serotonin story is being rewritten by new gene-based discoveries principally related to SLC6A4, the serotonin transporter gene, which functions to influence all cellular serotonin systems. Neuropharmacology 55:932-960

192. Carneiro AM, Blakely RD 2006 Serotonin-, protein kinase C-, and Hic-5-associated redistribution of the platelet serotonin transporter. J Biol Chem 281:24769-24780

193. Magnani F, Tate CG, Wynne S, Williams C, Haase J 2004 Partitioning of the serotonin transporter into lipid microdomains modulates transport of serotonin. J Biol Chem 279:38770-38778

194. Chang JC, Tomlinson ID, Warnement MR, Iwamoto H, DeFelice LJ, Blakely RD, Rosenthal SJ 2011 A fluorescence displacement assay for antidepressant drug discovery based on ligand-conjugated quantum dots. Journal of the American Chemical Society 133:17528-17531

195. Adkins EM, Barker EL, Blakely RD 2001 Interactions of tryptamine derivatives with serotonin transporter species variants implicate transmembrane domain I in substrate recognition. Molecular pharmacology 59:514-523

196. Nirmal M, Dabbousi BO, Bawendi MG, Macklin JJ, Trautman JK, Harris TD, Brus LE 1996 Fluorescence intermittency in single cadmium selenide nanocrystals. Nature 383:802-804

197. Steiner JA, Carneiro AM, Wright J, Matthies HJ, Prasad HC, Nicki CK, Dostmann WR, Buchanan CC, Corbin JD, Francis SH, Blakely RD 2009 cGMP-dependent protein kinase Ialpha associates with the antidepressant-sensitive serotonin transporter and dictates rapid modulation of serotonin uptake. Molecular brain 2:26

198. Saxton MJ 2007 A biological interpretation of transient anomalous subdiffusion. I. Qualitative model. Biophys J 92:1178-1191

199. Steiner JA, Carneiro AM, Blakely RD 2008 Going with the flow: trafficking-dependent and -independent regulation of serotonin transport. Traffic 9:1393-1402

200. Zhu CB, Blakely RD, Hewlett WA 2006 The proinflammatory cytokines interleukin-1beta and tumor necrosis factor-alpha activate serotonin transporters. Neuropsychopharmacology : official publication of the American College of Neuropsychopharmacology 31:2121-2131

201. Beaulieu JM, Gainetdinov RR 2011 The physiology, signaling, and pharmacology of dopamine receptors. Pharmacol Rev 63:182-217

202. Ruiz-Velasco V, Ikeda SR 2001 Functional expression and FRET analysis of green fluorescent proteins fused to G-protein subunits in rat sympathetic neurons. J Physiol 537:679-692

203. Subach FV, Zhang L, Gadella TW, Gurskaya NG, Lukyanov KA, Verkhusha VV 2010 Red fluorescent protein with reversibly photoswitchable absorbance for photochromic FRET. Chemistry & biology 17:745-755

204. Grabner M, Dirksen RT, Beam KG 1998 Tagging with green fluorescent protein reveals a distinct subcellular distribution of L-type and non-L-type Ca2+ channels expressed in dysgenic myotubes. Proc Natl Acad Sci U S A 95:1903-1908

205. Mao S, Benninger RK, Yan Y, Petchprayoon C, Jackson D, Easley CJ, Piston DW, Marriott G 2008 Optical lock-in detection of FRET using synthetic and genetically encoded optical switches. Biophys J 94:4515-4524

206. Yoon EJ, Hamm HE, Currie KP 2008 G protein betagamma subunits modulate the number and nature of exocytotic fusion events in adrenal chromaffin cells independent of calcium entry. Journal of neurophysiology 100:2929-2939

207. Sandyk R 1993 The relationship between diabetes mellitus and Parkinson's disease. Int J Neurosci 69:125-130

208. Driver JA, Smith A, Buring JE, Gaziano JM, Kurth T, Logroscino G 2008 Prospective cohort study of type 2 diabetes and the risk of Parkinson's disease. Diabetes Care 31:2003-2005

209. Craft S, Watson GS 2004 Insulin and neurodegenerative disease: shared and specific mechanisms. Lancet Neurol 3:169-178

210. Sirtori CR, Bolme P, Azarnoff DL 1972 Metabolic responses to acute and chronic L-dopa administration in patients with parkinsonism. N Engl J Med 287:729-733

211. Van Woert MH, Mueller PS 1971 Glucose, insulin, and free fatty acid metabolism in Parkinson's disease treated with levodopa. Clin Pharmacol Ther 12:360-367

212. Horowitz MP, Greenamyre JT 2010 Gene-environment interactions in Parkinson's disease: the importance of animal modeling. Clin Pharmacol Ther 88:467-474

213. Sanyal J, Chakraborty DP, Sarkar B, Banerjee TK, Mukherjee SC, Ray BC, Rao VR 2010 Environmental and familial risk factors of Parkinsons disease: case-control study. Can J Neurol Sci 37:637-642

214. Vance JM, Ali S, Bradley WG, Singer C, Di Monte DA 2010 Gene-environment interactions in Parkinson's disease and other forms of parkinsonism. Neurotoxicology 31:598-602

215. 2004 Consensus development conference on antipsychotic drugs and obesity and diabetes. Diabetes Care 27:596-601

216. Girgis RR, Javitch JA, Lieberman JA 2008 Antipsychotic drug mechanisms: links between therapeutic effects, metabolic side effects and the insulin signaling pathway. Mol Psychiatry 13:918-929

217. Melkersson K, Dahl ML 2004 Adverse metabolic effects associated with atypical antipsychotics: literature review and clinical implications. Drugs 64:701-723

218. Miller LJ 2009 Management of atypical antipsychotic drug-induced weight gain: focus on metformin. Pharmacotherapy 29:725-735

219. Pramyothin P, Khaodhiar L 2010 Metabolic syndrome with the atypical antipsychotics. Curr Opin Endocrinol Diabetes Obes 17:460-466